Nucleation agents in the glass system

$BaO/SrO/ZnO/SiO_2$

Dissertation

(kumulativ)

zur Erlangung des akademischen Grades Doktor-Ingenieur

(Dr.-Ing.)

vorgelegt dem Rat der Chemisch-Geowissenschaftlichen Fakultät der

Friedrich-Schiller-Universität Jena

von M. Sc. Liliya Vladislavova

geboren am 15.08.1990 in Sofia

Gutachter:

1. Prof. Dr. Christian Rüssel,

(Friedrich-Schiller-Universität Jena, Germany)

2. Prof. Dr. Ruzha Harizanova,

(University of Chemical Technology and Metallurgy, Sofia, Bulgaria)

Tag der Verteidigung:19.09.2018

"If you were born without wings, do nothing to prevent them from growing."

Coco Chanel

Table of Contents

Abbreviations

CTE - Coefficient of Thermal Expansion

HT - High-Temperature

LT - Low-Temperature

NTE - Negative Thermal Expansion

ICSD - Inorganic Crystal Structure Database

XRD - X-Ray Diffraction

ZTE - Zero Thermal Expansion

DSC - Differential Scanning Calorimetry

LSM - Light Scanning Microscopy

SEM - Scanning Electron Microscope

n - Avrami parameter

m - Dimension growth constant

T_g - Glass transition temperature

T_{on} - Onset of crystallization

T_{off} - Offset of crystallization

T_p - Crystallization maximum

EDX - Energy-dispersive X-ray spectroscopy

EBSD - Electron backscatter diffraction

IQ - Image Quality

IPF - Inverse pole figure

Glass composition and their abbreviations

Name	Chemical composition in mol%							
	BaO	SrO	ZnO	SiO_2	ZrO_2	TiO_2	$PtCl_4$	Sb_2O_3
Base glass	8	8	34	50	-	-	-	-
Z3	8	8	34	47	3	-	-	-
Z5	8	8	34	45	5	-	-	-
Z6	8	8	34	44	6	-	-	-
T5	7.5	7.5	34	46	0	5	-	-
Z5T5	7.5	7.5	34	41	5	5	-	-
Z5T3	7.5	7.5	34	43	5	3	-	-
Z6T2	7.5	7.5	34	43	6	2	-	-
Z7T1	7.5	7.5	34	43	7	1	-	-
Z5T5	7.5	7.5	34	41	5	5	-	--
Z6Pt	8	8	34	43.99	6	-	0.01	-
10 ppm Pt	8	8	34	50	-	-	0.001	-
30 ppm Pt	8	8	34	50	-	-	0.003	-
50 ppm Pt	8	8	34	50	-	-	0.005	-
100 ppm Pt	8	8	34	49.99	-	-	0.01	-
50 ppm PtS	8	8	34	49.50	-	-	0.005	0.5
100 ppm PtS	8	8	34	49.49	-	-	0.01	0.5

1. Preface

Glass and glass-ceramics are a part of our everyday life. They are industrially manufactured and offer a wide range of properties. They have many advantages over classical materials, because different combinations of properties can be achieved such as high strength, translucency, zero porosity, high mechanical strength, high-temperature stability biocompatibility, bioactivity, low dielectric constant and low dielectric losses, low or even negative thermal expansion coefficient, etc. [1–6]. Materials, which possess zero thermal expansion, have found wide applications, e.g. as cooking panels or as telescope mirror blanks, due to their high thermal shock resistance and because they retain their shape under non-isothermal conditions. The space programs funded by NASA, SpaceX and others are another field in which the aforementioned characteristics of new materials are highly desirable. [1,7,8].

In the recent decade, materials with negative coefficients of thermal expansion (NTE) or close to zero-thermal expansion (ZTE) are attracting considerable interest. Although most materials expand during heating, crystalline phases which exhibit NTE, however, contract [9–12]. One of the most important classes of materials with NTE behaviour is based on glass ceramics containing lithium alumosilicates, such as β-quartz, eucryptite, spodumene or keatite [1,13–15]. These phases can be crystallized from glass and hence enable to tailor the thermal expansion by optimizing the temperature-time schedule used for the crystallization process [6,16]. Besides, other NTE phases, such as $BaAl_2B_2O_7$, ZrW_2O_8, $ZrMo_2O_8$, are also reported in the literature [17–19]. The latter, however, cannot be crystallized from glasses in concentrations for which zero thermal expansion can be achieved and therefore it is difficult to implement them into mass production industry, especially if large dimensions are required. $BaAl_2B_2O_7$ is not industrially produced as compact material, because its chemical durability is not sufficient for many applications.

Another crystalline phase recently reported to possess negative thermal expansion is the $Ba_{1-x}Sr_xZn_2Si_2O_7$ phase [20]. This compound is now intensely studied because of its complex behaviour. The pure $BaZn_2Si_2O_7$ occurs as a low- temperature (LT) phase or as a high-temperature (HT) phase [21–24]. The LT phase is stable up to 280 ºC and is monoclinic with the space group *C2/c*; the mean coefficient of thermal expansion (CTE) for the temperature range (100-300 °C) is very high at approximately $17.6 \cdot 10^{-6}$ K^{-1}. $BaZn_2Si_2O_7$ shows a phase transition which occurs above a temperature of 280 ºC and is accompanied by a high-volume expansion of around 2 % caused by a change in the structure from monoclinic below the phase transition to orthorhombic above the phase transition temperature. In the cases when the orthorhombic lattice is observed, the CTE is low and partially negative [21]. Recently, it was reported that a substitution of more than 10 % of Ba by Sr leads to the formation of a new phase which has a structure similar to the high-temperature phase of $BaZn_2Si_2O_7$ which, however, is stable at room temperature [12,20].

Hence the new $Ba_{1-x}Sr_xZn_2Si_2O_7$ phase is a promising candidate for industry applications. Thus, the aim of this work is to find a suitable nucleation agent and how this will affect the microstructure and the coefficient of thermal expansion. The main problem with the base glass composition $BaO/SrO/ZnO/SiO_2$ is that solely surface crystallization is obtained. Therefore in this thesis, the effect of the nucleation agents: ZrO_2, TiO_2 and a combination of both ZrO_2 and TiO_2 as well as Pt were intensively studied [25–27]. For the characterization of the glasses and glass-ceramics, intense studies on the crystallization kinetics were performed and Avrami parameters, as well as activation energies, were determined by using differential scanning calorimetry (DSC). The crystallization prediction using the Avrami parameters was followed by a detailed study on the microstructure using light scanning microscopy (LSM) and a scanning electron microscope (SEM) equipped with an EBSD detector. X-ray diffraction (XRD) was used to determine the phase composition of the obtained crystalline phase

2. Glass-ceramics with negative thermal expansion coefficient and applications

The glass-ceramics may combine the advantages of the glass and the specific properties of ceramics. The obtained materials may have high strength, translucency, zero porosity, high strength, high temperature stability, biocompatibility, bioactivity, low dielectric constant and low dielectric losses, low or even negative thermal expansion, etc. They experience some significant drawbacks such as relatively high prices due to the high required melting temperatures and long times needed for the preparation of the materials. Nevertheless, these problems are negligible when it comes to applications where other materials cannot compete. A solution can be easily achieved by applying mass production technologies to reduce the cost, additives which decrease the melting temperature and optimizing the production costs [28,29].

Most materials have the tendency to increase their volume when raising the temperature and contract during cooling. This effect is denoted as thermal expansion and is typical for almost all materials in our daily life, however, there is an exception- a class of materials exists which exhibit the opposite effect. Those materials contract during heating (negative thermal expansion) or do not change their dimensions while the temperature is changing (zero thermal expansion). These phenomena are not very common makes the materials, which possess these properties, extremely valuable. In Table 2.1, examples of such materials and their thermal expansions are presented.

Table 2-1 Examples of crystalline phases with negative or low thermal expansion

Formula/Name	CTE [$10^{-6}K^{-1}$]	Temperature [°C]	Ref.
SiO_2(β-quartz)	0	575-1000	[30]
Zn_2SiO_4(Willemite)	2.8	100-800	[11,31]
$LiAlSi_4O_{10}$(Petalite)	0.3	-	[3,11]
$LiAlSi_2O_6$(β-Spodumene)	0.9	20-1000	[3,11]
$BaAl_2B_2O_7$	-2.3	20-500	[32,33]
Fe36Ni(Invar)	0.1-1	<227	[34]
α-ZrW_2O_8	-9	152	[11,35]
β-ZrW_2O_8	-6	152-757	[11,35]

The mechanisms responsible for the NTE are not completely understood but the main reasons which explain this effects can be summarized in 4 categories; (1) shortening of bond lengths and phase changes; (2) Bridging atoms and RUMs (Rigid Unit Mode): (3) magneto volume effect; (4) electronic effects [1,11,36].

A typical example of a family of materials with a negative thermal expansion is the AM_2O_7 based group which corresponds to zeolites/zeolite-like materials. They are well known for their NTE in a wide temperature range. A well-known representative of this family is the ZrW_2O_8 which has a cubic structure and is characterized by a large isotropic negative thermal expansion coefficient over a wide temperature range. The origin of the NTE is due to the large-amplitude low-energy transverse vibration of the O atom in the middle of the W–O–Zr linkage. A transverse vibration of a bridging O in a framework in which metal (M)–O bond distances remain largely unchanged will cause contraction of the M–M distance and a negative coefficient of thermal expansion, a graphical example is given in Fig. 2.1. [2,11,36]

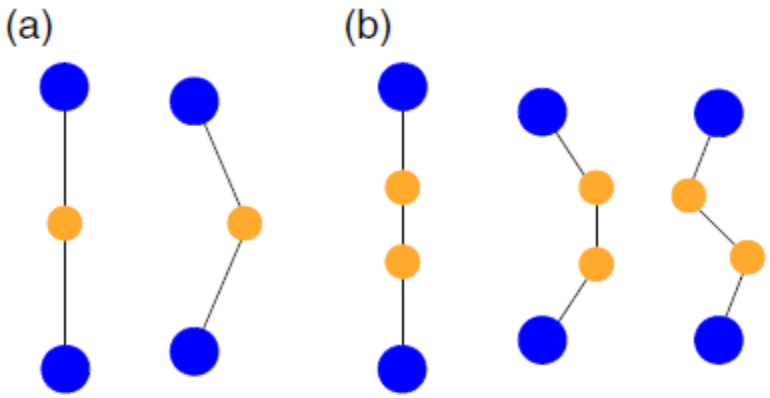

Fig. 2-1 Schematic of local vibrational modes responsible for negative thermal expansion: (a) single-atom and (b) diatomic linkages. The larger (blue) circles represent heavy (usually metal) atoms, whereas the smaller (orange) circles represent light atoms such as carbon, nitrogen, or oxygen [11].

Furthermore, another mechanism explaining the NTE can be found in the connection existing between the degree of covalency and the magnitude of the negative thermal expansion. This concept developed the RUM (Rigid Unit Modes) and the QRUM (Quasi RUM) model [11,37–40]. The idea behind them is to consider the polyhedra (SiO_2, ZrO_2, WO_4 and others) connected at their corners by shared oxygen ions in a rigid form. Thus, amplitude transverse vibrations of the oxygens can occur only through coupled oscillations of the tetrahedra and octahedra forming the structure. A schematic representation of this rotation motion is shown in Fig. 2.2 [11,37,40,41].

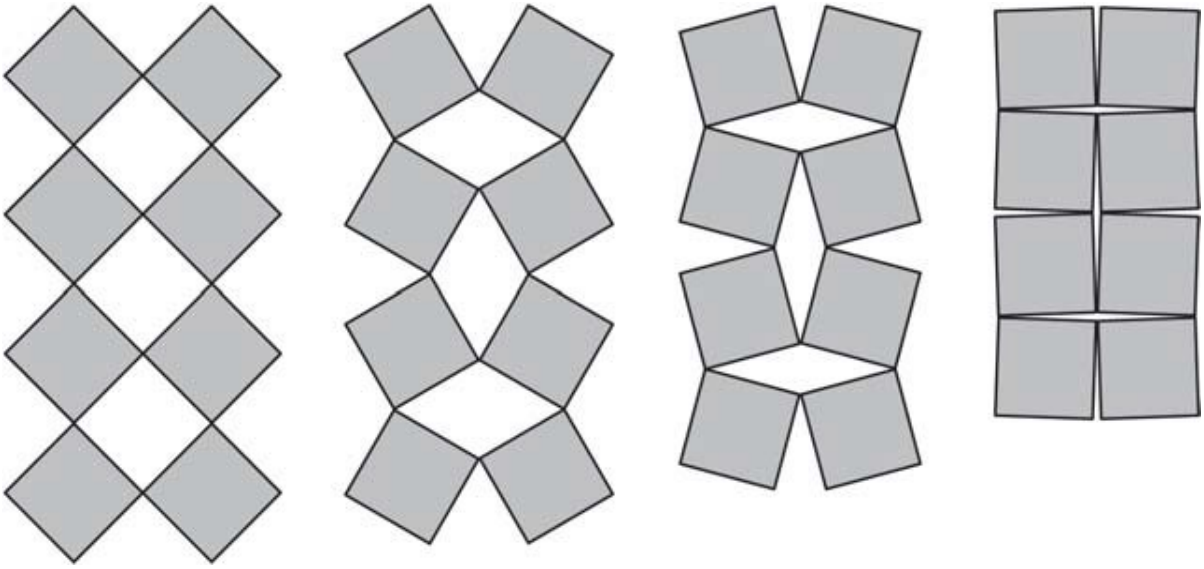

Fig. 2-2 Rotation of rigid structural units [39].

Another example for a phase which can be crystallized from oxide glasses and which has zero thermal expansion is $LiAlSiO_4$ (β-eucryptite). It is based on the Li_2O-Al_2O_3-SiO_2-system and is one of the most commonly studied and industrially produced systems. Additionally, from this system also β-quartz, spodumene, or keatite can be crystallized. This glass-ceramics are already in mass production for the preparation of kitchenware with low thermal expansion and are mainly produced by Corning Glass and SCHOTT AG. Another important application of this materials based on the above mentioned glass system are the laser gyroscopes for navigation purposes and mirrors for reflective optical systems in chip lithography [1,13,14,33]. Besides the alumosilicate phases mentioned above, other phases, such as ZrW_2O_8, $ZrMo_2O_8$, and $BaAl_2B_2O_7$ have also been reported in literature. Until now, these materials are not produced in industry, either due to an insufficient chemical durability ($BaAl_2B_2O_7$) or because the crystallization from glasses in quantities which allow adjusting a zero thermal expansion is not possible. This makes them difficult to fabricate at larger scale products.

3. The $Ba_{1-x}Sr_xZn_2Si_2O_7$ phase

The glass systems of BaO-ZnO-SiO_2, SrO-ZnO-SiO_2 and the BaO-SrO-ZnO-SiO_2 and their crystalline phases will be discussed in this chapter [12,42–44]. The $BaZn_2Si_2O_7$ is a well know phase since the 90's when it was first described by Lin et al. who reported structural analysis by X-ray diffraction [23]. The phase has fairly interesting properties and was considered being a proper candidate for seal materials due to the high CTE of the phase. At room temperature, the phase possesses a monoclinic space group *C2/c* and lattice constants a = 7.2750 Å, b = 12.7938 Å, c = 13.688 1 Å and β = 90.074° [22–24,45]. This is known as the low-temperature phase (LT-phase) and has a CTE varying from 13.4 to 17.6 10^{-6} K^{-1} [45]. The LT phase remains stable up to temperatures in the range of 250 – 280 °C, where a phase transition occurs. This transformation is followed by a high-volume increase of around 2 %. The phase transition is displacive which means it is not accompanied by real bond breaking and hence the kinetic hindrance is low [23,44]. As a matter of fact, we must mention that there is some weak ionic interaction between barium ions and oxygen which has to be altered to enable short distance movement of the barium ions. The HT-phase has a space group *Ccm21* and is orthorhombic with lattice constants a = 7.2718 Å, b = 13.0018(7) Å, c = 13.3860(7) Å and β = 90 °. The mean CTE of this phase is -3.2 to 2.3 10^{-6} K^{-1} [23,44]. The structures of the two polymorphs are shown in Fig. 3-1.

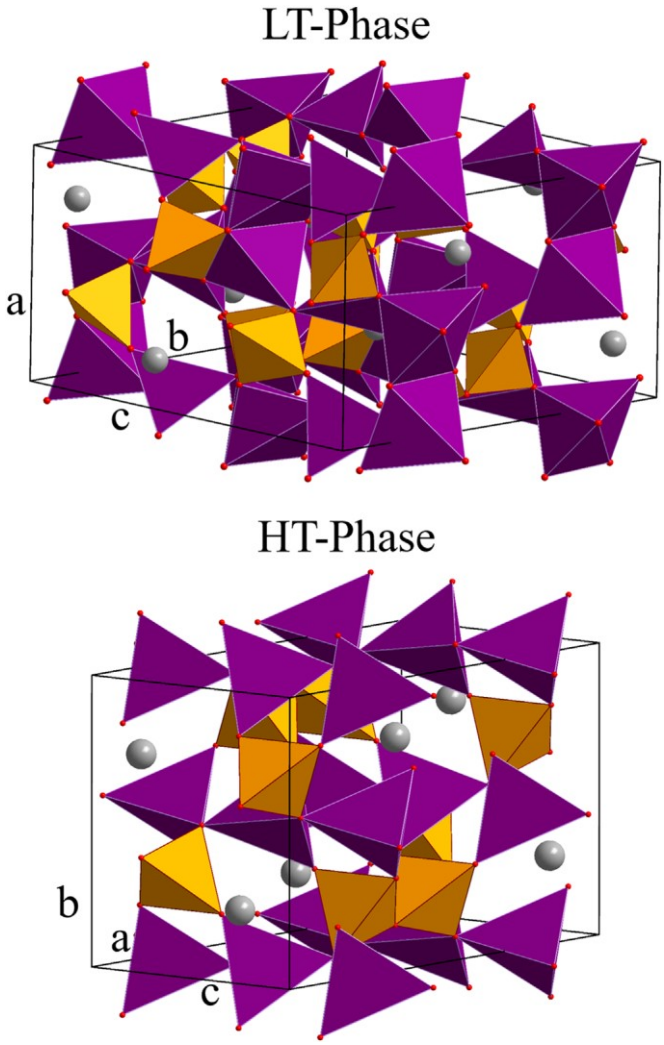

Fig. 3-1 Crystal structures of the HT-and the LT-Phase of $BaZn_2Si_2O_7$. The ZnO-polyhedra are shown in violet. The SiO_4–tetrahedra are presented in yellow and the Ba^{2+}- and Sr^{2+}-ions are illustrated as grey spheres[22].

The intriguing structure and the respective possible applications of the phase led to intensive studies over the last decades and showed that adding different ions with the same valence state and similar ionic radii may affect the transition low to high temperature phase. Substitutions of the Zn^{2+} ions were made with Co^{2+}, Mg^{2+} and Ni^{2+}, Cu^{2+}, resulting in a stabilization of the LT-phase to higher temperatures of up to 900 °C [48,49]. In addition the stabilization of the LT-phase can be achieved by replacing Si^{4+} by Ge^{4+} [48].

Breakthrough leading to a new family of materials with negative thermal expansion was achieved at the Otto-Schott-Institute by C. Rüssel and C. Thieme. During their intense work, substitution of the Ba^{2+} ions against Sr^{2+} was performed, which lead to the formation of a new solid solution $Ba_{1-x}Sr_xZn_2Si_2O_7$ [20]. If more than 10 % Ba ions are substituted against Sr, the formation of a new phase occurs with a structure almost identical to the HT – phase of $BaZn_2Si_2O_7$. In the structure of this new crystalline phase, silicon, as well as zinc, are fourfold coordinated. Two SiO_4 tetrahedra are bridged by oxygen. In analogy, also the Ba- and Sr- atoms are surrounded by 5 oxygens, forming a pyramid with a quadratic basal plane. The determination of the structure was performed via XRD and hence it could not be distinguished between Ba- and Sr-atoms. A clear comparison between the two phases can be made if cuts in different planes and directions are considered as shown in Fig. 3-2 [20]. This had to be done due to the different dimensions of the unit cells and lattice parameters of both phases. It can be seen that there are similar atomic arrangements in both phases for the b-c- planes in the case of $Ba_{1-x}Sr_xZn_2Si_2O_7$ and the a-c-planes for the crystal structure of the HT phase of the $BaZn_2Si_2O_7$. The differences in the crystal structures of both phases are only marginal so that both phases should exhibit similar thermal expansion properties [20]. The results obtained from the single crystal X-ray diffraction also show that the new crystals are highly isotropic. This is caused by the distortion of the SiO_4- and ZnO_4-tetrahedra, furthermore, the rotation of the ZnO_4 units will create a change in bond angles. This leads to a different thermal expansion in the different crystallographic directions $9.5 \cdot 10^{-6}$ K^{-1} (a-axis), $-32.1 \cdot 10^{-6}$ K^{-1} (b-axis), and $23.1 \cdot 10^{-6}$ K^{-1} (c-axis) (measured between 30 and 600 °C) [20]. Even though this behaviour is typical for crystals which have the negative thermal expansion (see chapter 2) this can be highly disadvantageous and may lead to destruction of the obtained materials.

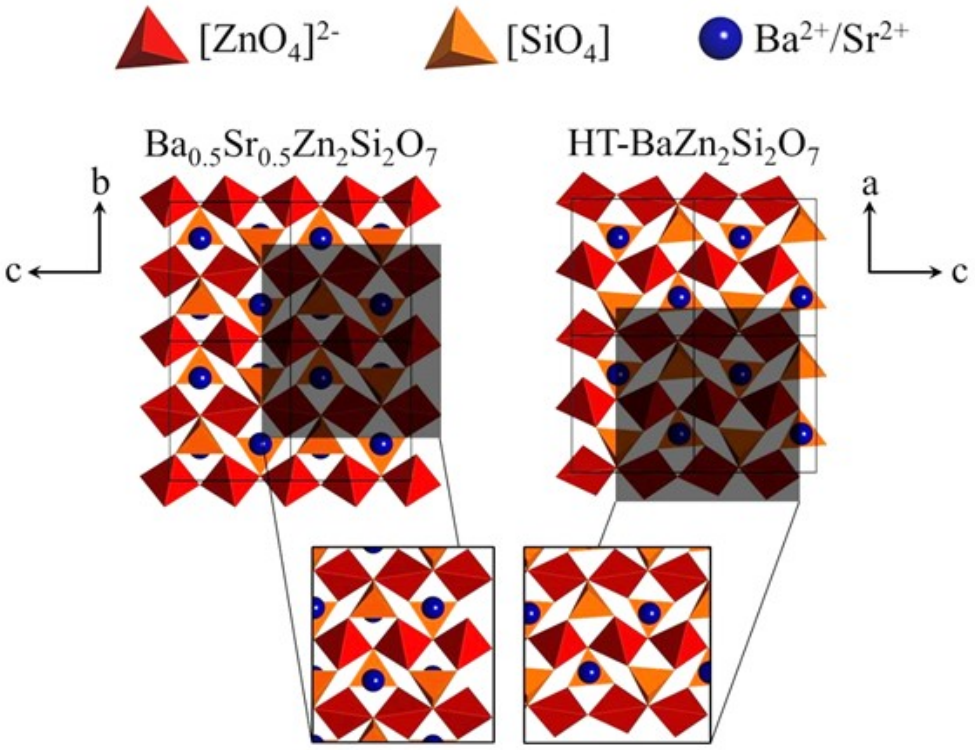

Figure.3-2 The crystal structure of the $Ba_{0.6}Sr_{0.4}Zn_2Si_2O_7$ phase at 20 °C. The left part of the image displays the crystal structure with different views. On the right side, a comparison between the crystal structures of $Ba_{0.6}Sr_{0.4}Zn_2Si_2O_7$ and HT-$BaZn_2Si_2O_7$ is displayed. The blue spheres are the Ba^{2+} and Sr^{2+}. In the case of $BaZn_2Si_2O_7$, the blue spheres only describe the positions of Ba^{2+} [20].

Further studies on the system showed that the overall coefficient of thermal expansion is strongly depending on several parameters. Variation in the Ba/Sr ratio can cause a shift in the CTE from 4.8 to 19.4 $10^{-6}K^{-1}$ [12]. A low concentration of Sr promoted the crystallization of LT- phase of $BaZn_2Si_2O_7$ which corresponds to high CTE. The increase of Sr stabilises the HT-phase of $BaZn_2Si_2O_7$ which exhibits low or almost negative CTE, but also increases the highly anisotropic behaviour. Another factor which may affect the overall coefficient of thermal expansion is the occurrence of other phases such as Zn_2SiO_4 (willemite) and SiO_2 (cristobalite) which have CTE 2.8 and 3.13 $10^{-6}K^{-1}$ (25 to 200 °C), respectively. The method of preparation also plays an important part in the obtained materials. It has been shown that sintering of a glass

and subsequent crystallization leads to glass-ceramics in which significant crack formation is observed. Nevertheless, crack-free materials with low thermal expansion, based on the $Ba_{1-x}Sr_xZn_2Si_2O_7$ phase were prepared via a sol-gel method and subsequent hot pressing [49].

All of these results show that the main advantage of the $Ba_{1-x}Sr_xZn_2Si_2O_7$ solid solutions is that they can easily be crystallized from silicate glasses in high volume fractions. For this purpose, the degree of crystallinity, the crystallite size and its distribution must be optimized by tailoring the glass composition and the temperature-time heat treatment schedule during crystallization as well as the microstructure of the obtained glass ceramics. This will be the main objective of this thesis.

4. Kinetic parameters

4.1 Nucleation and crystallization

There are two main mechanisms involved in the devitrification, nucleation (formation of a nucleus) and crystal growth. In order to obtain the desired microstructure, the size and quantity of crystallites have to be well controlled [6]. Obtaining transparent glass ceramics containing phases with a low coefficient of thermal expansion, like the already commercially available Zerodur®, is not an easy process [1,16]. Several challenges involving the microstructure of the system must be solved. To prepare transparent glass-ceramics one of the following requirements must be fulfilled (i) the crystallites of all species are much smaller than the wavelength of visible light and they are homogeneously distributed; (ii) the optical anisotropy (birefringence) within the crystals and refractive index difference between crystals and glass are very small. This means, a high quantity of very small crystals homogeneously distributed in the glass matrix is required [7].

Adding different components to the main systems may trigger nucleation. There are two types of nucleation mechanisms; homogeneous and heterogeneous [6,50]. Homogeneous nucleation is observed when the nuclei originate from their own melt and generally have a similar chemical composition. Good examples of glass compositions crystallizing via that mechanism are the lithium disilicate glasses where volume crystallization is possible without additives [51–53]. Unfortunately, the BaO/SrO/ZnO/SiO_2 system as well as related systems cannot nucleate homogeneously [25–27,54]. This means that a foreign interface has to be generated in order to enable heterogeneous nucleation. This can be made by adding different nucleation agents such as ZrO_2, TiO_2, Pt, Cr_2O_3, Ag and others, which under certain conditions are precipitated homogeneously in the glass. These crystals act as precursor and will trigger the growth of the desired crystal phase. This process can be controlled by finding the temperature and time of

nucleation, for which the higher number of nuclei is formed. In addition, it is good to mention that volume crystallization can be triggered by impurities originating from the raw materials and bubbles, but such parameter cannot be easily controlled. They do not affect the overall kinetic of the crystallization process and are very hard to predict [6,51].

After the nuclei are formed, crystal growth may occur. The glass-ceramics have the tendency to crystallize in the manner shown in Fig 4.1: (A) volume crystallization, (B) surface crystallization and (C) both surface and volume crystallization. Although a combination of these mechanism may exist, usually only one of them is predominant [6,51].

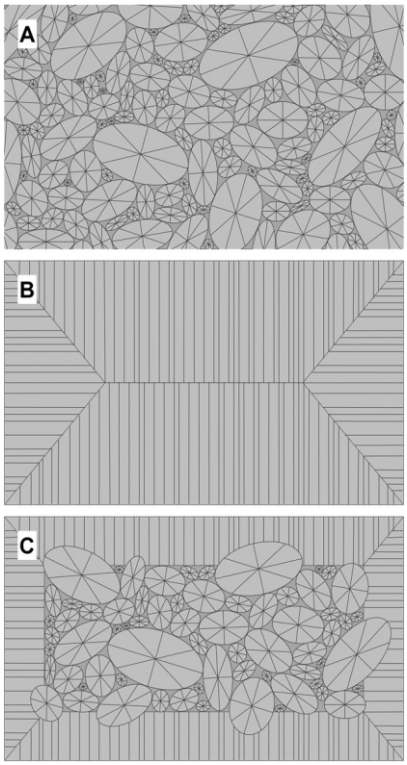

Fig. 4.1 Schematic cross sections of microstructures of crystallized glasses, which result from: A—volume (islands), B—surface (envelope) and C—combined volume and surface nucleation (coast-island).We note that a residual glassy matrix may occur, which results from a non-stoichiometric composition and trace elements [55].

4.2 The Avrami parameter

Developing a new glass ceramic is a hard and time-consuming task. One of the predominant aspects of obtaining the aimed microstructure to overcome the anisotropy of the phase is to find the proper nucleation agent/agents and the right quantities as well as the optimum time/temperature schedule. In order to make a fast assessment of the potential nucleation agents and the required concentration, calculating the kinetic parameters such as Avrami parameter (n), the dimensionality growth constant (m) and the activation energy are of main importance [15,26,56,57].

The Avrami parameter combines the process of growth and nucleation which are typical part of the overall crystallization process. Differential thermal analysis (DTA) and differential scanning calorimetry (DSC) have frequently been used to study the crystallization kinetics of glassy materials. They can be carried out isothermally or non-isothermally. One of the most commonly used methods for the determination of the Avrami parameter is the Ozawa equation which was devolved in the 1980's [58]. The position of the exothermic peak depends on the heating rate used for the measurements, the position of the peak shifting to higher temperatures for higher heating rates. The value of n (Avrami parameter) is determined by equation 1.

$$-n = \left| \frac{d\left[\ln(-\ln(1-x))\right]}{d(\ln \beta)} \right|_{T} \qquad \text{Eq. 4.1}$$

Where x is the volume fraction crystallized at the temperature T at a heating rate (β). The determination of the Avrami parameter is schematically shown in Fig. 4.2 to better illustrate the principle.

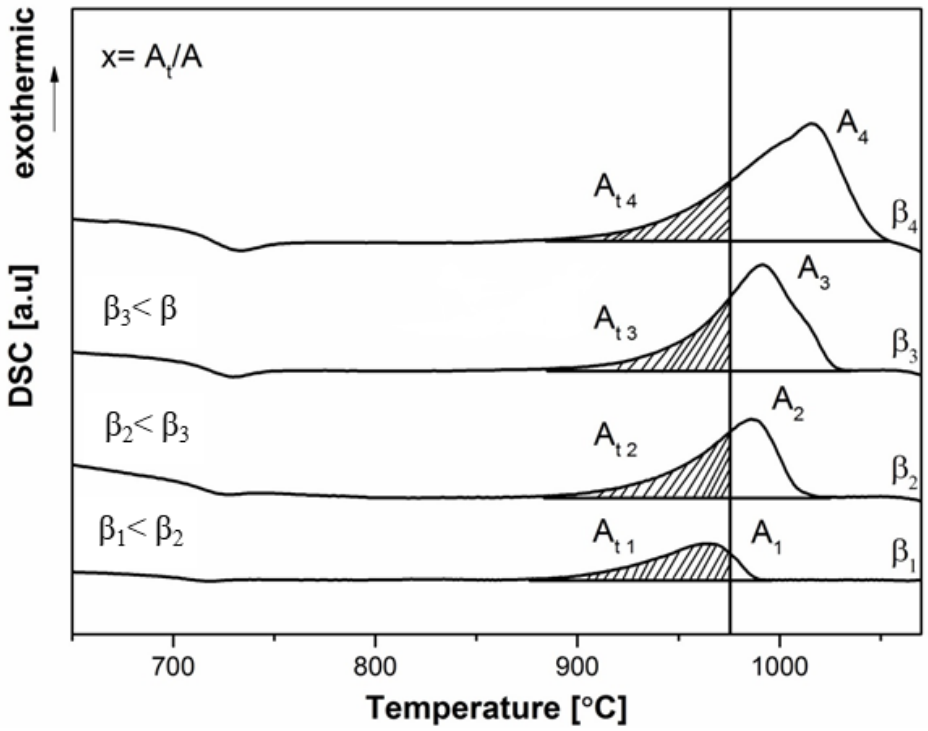

Fig. 4-1 Graphical representation of the determination of the Avrami parameter using the Ozawa equation.

Where x is the ratio of the partial area A_t (up to a chosen temperature), to the total area A_n under the peak. The value of x is determined for every heating rate until statistical significance is achieved, (ln-(ln(1-x))) versus lnβ is plotted and n is calculated from the slope of the straight line. In addition to obtain more accurate result, the calculated area under the exothermic peak has to be in the range from $0.2 \leq x \leq 0.8$. Another important factor is that the peak of crystallization has to be well defined and if two crystalline phases are precipitated at the same time, the method will not be accurate. However, if the two peaks are split and the offset of the first peak does not overlap with the onset of the second peak, the method can be used, and prediction of the crystallization mechanism should be enabled. In this case, it is good to keep in mind that the kinetics of crystallization and nucleation if two or more crystalline phases are formed is rather complicated and other method are more suitable [15,57–60].

4.3 Activation energies

The obtained data of the DSC analysis can be used also for determination of the activation energies [15,43,57,59,60].

One of the most commonly used methods is Kissinger's method for which the activation energy can be determined by Eq. 4.2 [15,43,57,61].

$$\ln\left[\frac{\beta}{T_p^2}\right] = \frac{-E_a}{RT_p} + const \qquad \text{Eq. 4.2}$$

Where T_p is the temperature attributed to the maximum crystallization peak, E_a is the activation energy and R is the gas constant. The method was originally proposed for DTA but furthers proved to be not very accurate because of the assumption that the maximum rate of the reaction occurs at the peak temperature. This proved to be generally incorrect for the DTA measurements, because the maximum rate occurs somewhat before the temperature maximum is reached. However this misconception was debunked from Ozawa who proved that the use of DSC can give more accurate result [43,57–59,61].

Furthermore, Ozawa developed another equation for calculating the activation energies known as the Ozawa equation (Eq. 4.3) [43,57,58].

$$\ln[\beta] = \frac{-E_a}{RT_p} + const \qquad \text{Eq. 4.3}$$

The values of the activation energies are taken from the slope of the plot and have a dimension [kJ mol^{-1}]. Both equations are quite similar and the basic difference between them is less than 6 %. Although the method is mathematically proven and widely implied, many scientists consider that these methods can be used only for surface crystallization and not when nuclei are formed during the measurements and volume crystallization is occurring. Crystallization and

nucleation are complex processes and hence, additional constants which represent the type of crystallization and their dimensionality have to be added, to accurately describe and take into account the complexity of the nucleation process [45,58].

Matusita and Sakka proposed a solution of this problem by adding two additional constants. This can be seen in Eq. 4.4 for the base equation of Kissinger, or as it is more commonly known, the modified Kissinger equation [15,43,57,62].

$$\ln\left[\frac{\beta^n}{T_p^2}\right] = \frac{-mE_a}{RT_p} + const \qquad \text{Eq. 4.4}$$

In Eq. 4.4, the already mentioned parameters are the same as in the Kissinger equation, the additional parameters are: n is the Avrami parameter (Eq. 4.1) and m is the dimensionality of crystal growth, which depends on the Avami parameter. The values of m were taken from a Table 4.1 which was published by Donald [57]. For example for bulk crystallization, the Avrami parameter is n = 3 and m = 2, while if surface crystallization is present the parameters are n=1, m=1 (then the equation is reduced to the original Kissinger equation, Eq. 4.2) [57]. Unfortunately, not many scientists acknowledge the usefulness of the proposed constants and ignore the Matusita and Sakka equation, which sometimes can lead to a misinterpretation of the results. Also the already mentioned parameters can give a good approximation for the accepted microstructure but further investigation is always necessary [57,62].

Table 4.1 Numerical values for m and n used in the determination of activation energies for crystallization [57].

Crystallization mechanism	*n*	*m*
Bulk crystallization with a constant number of nuclei (i.e. a well nucleated sample with the number of nuclei being independent of the heating rate)		
Three-dimensional growth of crystals	3	3
Two-dimensional growth of crystals	2	2
One-dimensional growth of crystals	1	1
Bulk crystallization with a constant number of nuclei (i.e. a well nucleated sample with the number of nuclei being independent of the heating rate) with crystal growth rate proportional to $t^{-0.5}$ (diffusion controlled)		
Three-dimensional growth of crystals	1.5	1.5
Two-dimensional growth of crystals	1	1
One-dimensional growth of crystals	0.5	0.5
Bulk crystallization with an increasing number of nuclei (i.e. an as-quenched sample with the number of nuclei inversely proportional to the heating rate)		
Three-dimensional growth of crystals	4	3
Two-dimensional growth of crystals	3	2
One-dimensional growth of crystals	2	1
Bulk crystallization with an increasing number of nuclei (i.e. an as-quenched sample with the number of nuclei inversely proportional to the heating rate) with crystal growth rate proportional to $t^{-0.5}$ (diffusion controlled)		
Three-dimensional growth of crystals	2.5	1.5
Two-dimensional growth of crystals	2	1
One-dimensional growth of crystals	1.5	0.5
Surface crystallization	1	1

5. Publications

5.1 The effect of ZrO_2 on the crystallization of a glass in the system $BaO/SrO/ZnO/SiO_2$: surface versus bulk crystallization

Liliya Vladislavova, Christian Thieme, and Christian Rüssel

Journal of Materials Science (2017) 52:4052–4060

DOI: 10.1007/s10853-016-0667-0

Authors	Liliya Vladislavova	Christian Thieme	Christian Rüssel
Conception of the research approach	X	X	X
Planning of examinations	X	X	X
Data collection	X		
Data analysis and interpretation	X	X	X
Writing the manuscript	X	X	X
Credits	1		

J Mater Sci (2017) 52:4052–4060

The effect of ZrO_2 on the crystallization of a glass in the system BaO/SrO/ZnO/SiO_2: surface versus bulk crystallization

Liliya Vladislavova[1], Christian Thieme[1,2], and Christian Rüssel[1,*]

[1] Otto-Schott-Institut, Jena University, Fraunhoferstr. 6, 07743 Jena, Germany
[2] Fraunhofer Institute for Microstructure of Materials and Systems IMWS, Walter-Hülse-Straβe 1, 06120 Halle, Germany

Received: 26 November 2016
Accepted: 8 December 2016
Published online: 21 December 2016

ABSTRACT

Recently discovered solid solutions with the composition $Ba_{1-x}Sr_xZn_2Si_2O_7$ ($0.1 \leq x \leq 0.9$) exhibit low or negative thermal expansion in a wide temperature range above room temperature. Materials which have low or negative thermal expansion find applications such as gyroscopes, telescope mirrors, and cook panels. In contrast to other low expansion materials described in the past two decades, these solid solutions can be crystallized from a glass. Due to the high anisotropy of the coefficient of thermal expansion, the obtained materials show a strong tendency to micro-cracking which makes them not yet suitable for industrial application. Studying the crystallization kinetics and finding suitable nucleation agents are the main keys to obtain a crack-free material. In the present article, the effect of one of the most commonly used nucleation agents, which is ZrO_2, is investigated. For the characterization of the glasses and glass–ceramics, X-ray diffraction was used in order to determine the obtained crystalline phases and scanning electron microscopy was applied to characterize the microstructure. By applying different heating rates in a differential scanning calorimetry device, it was possible to calculate the activation energy using the equations of Ozawa and Kissinger, and to determine the Avrami parameters, which provide further information on the crystallization process. Using ZrO_2 concentrations of up to 5 mol% resulted in sole surface crystallization, while at a ZrO_2 concentration of 6 mol% also bulk nucleation occurs.

Introduction

During heating, most solids expand [1–3]. Only a few known materials exhibit a negative thermal expansion, i.e., show smaller volume at higher temperatures. Among these are aluminosilicates, such as beta-quartz and beta-eucryptite [4–6]. These phases have found wide applications, e.g., as cooktop panels and as telescope mirror blanks, due to their high resistivity to changing temperatures and because they keep their

Address correspondence to E-mail: ccr@uni-jena.de

DOI 10.1007/s10853-016-0667-0

shape with high accuracy also under non-isothermal conditions [4].

Other materials which show negative thermal expansions are ZrW_2O_8, $ZrMo_2O_8$, and related compounds which nowadays are among the most frequently studied negative thermal expansion materials exhibiting a coefficient of thermal expansion (CTE) as low as -8.7×10^{-6} K^{-1} [4–7]. By contrast, alkaline earth silicates, especially barium silicates usually show very high coefficients of thermal expansion [8]. The compound $BaZn_2Si_2O_7$ has more complex behavior; it shows a high CTE up to 280 °C, and then it transforms to a high-temperature phase. This phase transition is accompanied by a high volume increase of around 2% [9]. Below the phase transition temperature, $BaZn_2Si_2O_7$ is monoclinic with the space group C2/c and the mean CTE is about 17.6×10^{-6} K^{-1} [9, 10]. At temperatures >280 °C, $BaZn_2Si_2O_7$ is orthorhombic with the space group $Ccm2_1$ and possesses a very low and partially negative CTE [11]. The low-temperature phase can be stabilized to temperatures as high as 800–950 °C by the partial or total substitution of Zn by Co, Mg, or Ni. By contrast, it was recently shown that also the stabilization of the high-temperature phase down to room temperature is possible [12]. This has been achieved by the partial substitution of Ba by Sr. The crystal structure of the compound $Ba_{0.6}Sr_{0.4}Zn_2Si_2O_7$ was measured using single-crystal X-ray diffraction (XRD), and the thermal expansion was determined as a function of the temperature and the crystallographic direction using high-temperature powder diffraction in combination with Rietveld refinement [13]. The high-temperature phase is also stable at room temperature, if Zn is partially replaced by Co, Mg, Ni, Cu, or Mn. In addition, also a part of the Si can be substituted by Ge and the high-temperature phase is still stable at room temperature [14]. All compounds which possess the structure of high-temperature $BaZn_2Si_2O_7$ show small or negative CTE, i.e., a new family of low expansion materials, whose chemical composition can be varied in a large extend, was found [11, 13].

It has already been proved that, despite of the strongly anisotropic thermal expansion of the unit cell, also sintered materials can be prepared which show zero thermal expansion. These materials up to now have been prepared from sinter active powders using a sol–gel method and subsequent hot pressing [15]. It has also been shown that sintering of a glass and subsequent crystallization has led to glass–ceramics with very different CTEs depending on the ratio Ba/Sr [16].

In contrast to compounds such as ZrW_2O_8, $Ba_{1-x}Sr_xZn_2Si_2O_7$ might be a serious alternative to low thermal expansion materials based on lithium aluminosilicates, because the desired phase can be crystallized from glasses. In comparison to aluminosilicates, the manufacturing process should be much easier, due to the much lower melting temperatures.

Crystallizing the desired phase from a glass has several advantages. One of them is controlling the crystal growth velocity and the degree of crystallinity which should enable to reduce the production costs. An appropriate way should be the addition of an effective nucleation agent to the base system. In the present study, the effect of different concentrations of ZrO_2, which in many previously studied systems acts as nucleation agent, is investigated [17].

Experimental procedure

The glasses in the base system of $BaO/SrO/ZnO/SiO_2$ with different concentration of ZrO_2 were melted in a platinum crucible in an inductively heated furnace. For the preparation of the batch, the following raw materials were used: $BaCO_3$ (Merck, >98.5%), $SrCO_3$ (VEB Laborchemie Apolda, >99%), ZnO (Carl Roth GmbH + Co KG, >99%), SiO_2 (Carl Roth GmbH + Co KG, >99%), and ZrO_2 (Tosoh > 99%). The homogenized batch (for 400 g of glass) was melted for 1 h at a temperature ranging from 1300 to 1400 °C. Subsequently, the melting temperature was increased to 1400 or even 1450 °C, depending on the ZrO_2 concentration. This temperature was kept for 2 h while the melt was stirred with 60 min^{-1}. This led to a homogeneous glass batch. Then the stirrer was removed, and the glass was soaked for 10–15 min and subsequently cast in a pre-heated mold and then placed in a furnace at a temperature of 680–700 °C. The furnace was switched off, and the sample was allowed to cool; the cooling rate was approximately 3 K/min. The chemical compositions of the respective samples are summarized in Table 1.

In order to confirm the non-crystallinity of the obtained glasses and the phase composition of the crystallized glasses, XRD was implemented using powdered samples and a Rigaku Miniflex 300 diffractometer with Ni-filtered Cu Kα radiation. The

Table 1 Chemical compositions of the studied samples in (mol%)

Sample	Chemical composition in mol%				
	BaO	SrO	ZnO	SiO_2	ZrO_2
$z = 0$	8	8	34	50	0
$z = 3$	8	8	34	47	3
$z = 5$	8	8	34	45	5
$z = 6$	8	8	34	44	6

scanned 2θ-range was from 10° to 60° with a scan speed of 1°/min.

Differential scanning calorimetry (DSC) was performed with a Linseis DSC Pt 1600 for determining the characteristic temperatures such as the glass transition temperature (T_g), the onset of crystallization (T_{on}), the offset of crystallization (T_{off}), and the crystallization maximum (T_p) for all studied glasses. In order to minimize the effect of surface crystallization, glass pieces with 5 mm in diameter, 3 mm in height, and a total mass of 0.21 g were used. The glass cylinders were inserted into a Pt crucible and heated at different heating rates (2, 5, 10, 15, and 20 K/min).

The densities were determined with a helium pycnometer Micromeritics AccuPyc 1330. The crystal morphology was studied on carbon-coated samples using a scanning electron microscope (SEM) JEOL 7001 F. The volume crystallization was also characterized by a Laser Scanning Microscope Axio Imager Z1 m PASCAL5 equipped with a heating stage Linkam HS1500. The samples were heat treated in an external muffle furnace at different nucleation temperatures followed by a crystallization step. All the samples were polished from both sides.

Results and discussion

All the prepared glasses were transparent, homogeneous, and bubble- and striae-free. In Fig. 1, XRD patterns of samples with different ZrO_2 concentrations—all thermally treated at 940 °C for 1 h—are shown. This temperature, which is near the crystallization maximum of all the investigated samples, was chosen in order to achieve widely crystallized samples. The patterns of the respective glass compositions are fairly similar and do not exhibit noticeable differences. There are no traces of additional crystalline phases, such as ZrO_2. All the registered peaks are consistent with the theoretical lines

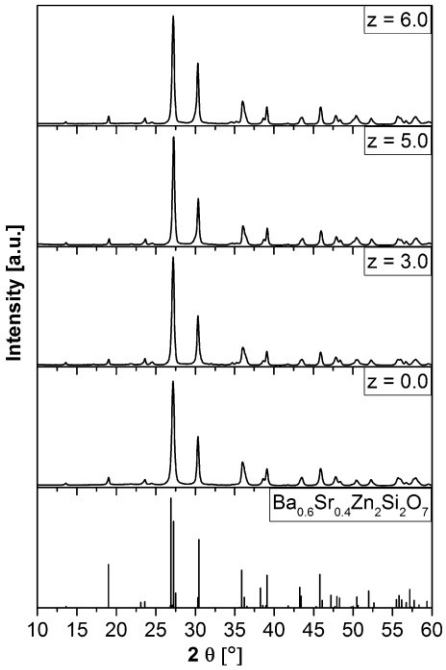

Figure 1 X-ray diffraction patterns of glasses with different ZrO_2 concentrations annealed at 940 °C for 1 h. The theoretical peak positions belong to $Ba_{0.6}Sr_{0.4}Zn_2Si_2O_7$ taken from Ref [11].

of $Ba_{0.6}Sr_{0.4}Zn_2Si_2O_7$ which are also shown at the bottom of Fig. 1 for comparison. This phase has the same structure as the high-temperature phase of $BaZn_2Si_2O_7$, which according to Refs [11, 13] shows a negative thermal expansion at room temperature.

Figure 2a shows DSC profiles of glasses with different ZrO_2 concentrations, recorded at a heating rate of 10 K/min. The glass transition temperature, T_g of the glass without ZrO_2, was 672 °C, while the glasses with ZrO_2 show increasing T_g values with increasing ZrO_2 concentrations. The glass with the highest ZrO_2 concentration exhibits a T_g of 697 °C. Hence, the viscosity increases steadily with increasing ZrO_2 concentration. All four studied glasses show a distinct exothermic peak, which according to the XRD patterns is attributed to the crystallization of the desired phase. The onset of the crystallization peak, T_{on}, is observed in the glass without ZrO_2 at a temperature of 916 °C. If increasing ZrO_2 concentrations are added, T_{on} increases continuously up to a ZrO_2 concentration of 6 mol%, where a T_{on} value of 943 °C

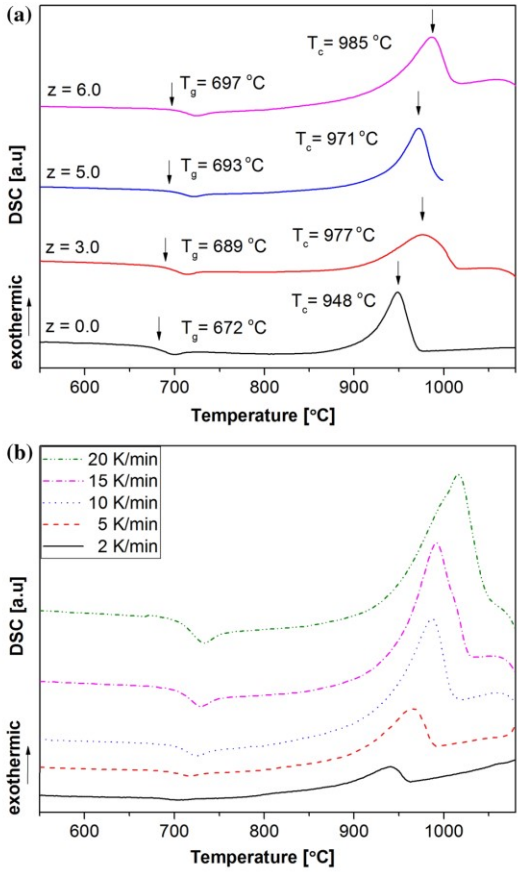

Figure 2 DSC profiles: **a** glasses with different concentrations of ZrO_2 at a heating rate of 10 K/min, **b** DSC profiles for five different heating rates for a glass with 6 mol% ZrO_2.

is reached. The temperature attributed to the crystallization peak, T_p, shows a somewhat different behavior, because the peak observed in the DSC profile of the glass with 3 mol% ZrO_2 is much broader than the peaks observed in the other compositions. Nevertheless, the peak temperature of the sample with the ZrO_2 composition of 6 mol% is as high as 985 °C. The difference between the peak temperature and the glass transition temperature, $T_{on} - T_g$, is 245 K for the glass without ZrO_2, then decreases slightly but significantly for the glass with 3 mol% ZrO_2, and then re-increases to 244 and 247 K for ZrO_2 concentrations of 5 and 6 mol%, respectively. The temperature difference $T_{on} - T_g$ is frequently considered as a measure of the glass stability;

Table 2 Results from the DSC profiles of the samples with different ZrO_2 concentrations recorded at a heating rate of 10 K/min

Name	T_g (°C)	T_{on} (°C)	T_{off} (°C)	T_p (°C)	T_{on}–T_g (K)
$z = 0$	672	916	969	948	245
$z = 3$	689	918	1011	977	232
$z = 5$	693	939	987	971	244
$z = 6$	697	943	1008	985	247

T_g glass transition temperature, T_{on} onset of the crystallization peak, T_{off} offset of the crystallization peak, T_p and $T_{on} - T_g$ temperature of the crystallization peak

the higher the difference, the more stable is the glass against devitrification during heating. These results are summarized in Table 2.

Figure 2b shows DSC profiles of the glass with 6 mol% ZrO_2 recorded at different heating rates ranging from 2 to 20 K/min. While the value of T_g does not change significantly (as expected), the exothermic peak, i.e., the crystallization peak changes notably. For a heating rate of 2 K/min, the peak is observed at a temperature of 940 °C. With increasing heating rates, the peak is shifted to higher temperatures until finally, at a heating rate of 20 K/min, a peak temperature of 1016 °C is observed. The increment of the crystallization temperature can be explained using the equations of Kissinger Eq. (1) and Ozawa Eq. (2) [18–20].

$$\ln\left[\frac{\beta}{T_p^2}\right] = \frac{-E_a}{RT_p} + \text{const} \tag{1}$$

$$\ln[\beta] = \frac{-E_a}{RT_p} + \text{const}, \tag{2}$$

where T_p is the temperature attributed to the crystallization peak, β is the heating rate, E_a is the activation energy, and R is the gas constant.

The simultaneous increase in the area below the peak is due to the increasing heating rate, because the total heat generated during heating is a constant. The same dependency is observed for the other glass compositions [21]. In the case of the Zr-free composition, the crystallization peak appears at 898 °C for the lowest heating rate and increases to 973 °C for the highest one.

Figure 3a, b shows Kissinger plots performed from the DSC profiles recorded using different heating rates for the samples with 0 and 6 mol% ZrO_2, respectively. In these figures, according to Eq. (1), $\ln(\beta/T_p^2)$ is plotted against $1000/T_p$.

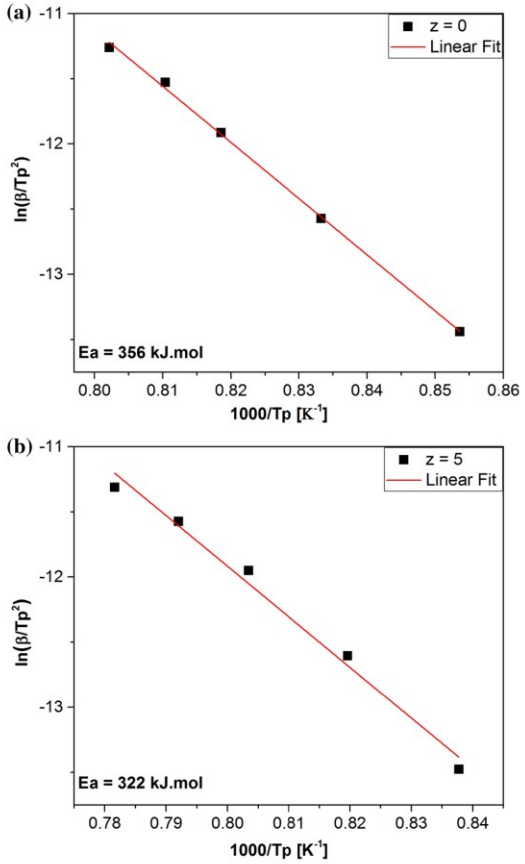

Figure 3 Kissinger plots used to calculate the activation energy of crystallization: **a** for a glass with $z = 0$ mol% ZrO_2, **b** for a glass with $z = 5$ mol% ZrO_2.

For increasing heating rates, T_p increases and hence $1000/T_p$ decreases, while $\ln(\beta/T_p^2)$ increases. From the slope of these graphs, an activation energy, in the following denoted as the Kissinger activation energy, can be calculated [22–24]. The values of Kissinger's activation energies are summarized in Table 3. For the glass without ZrO_2, this activation energy is 356 kJ/mol, while it is 390 kJ/mol for the glass with 6 mol% ZrO_2.

Figure 4a, b shows Ozawa plots for glasses without ZrO_2 and with 5 mol% ZrO_2 at different heating rates ranging from 2 to 20 K/min, respectively. According to Eq. (2), $\ln(\beta)$ is plotted against the reciprocal temperature of the crystallization peak [18, 21, 23]. Respectively, the values of Ozawa's activation energies are summarized in Table 3.

Table 3 Results from the DSC profiles of the samples with different ZrO_2 concentrations recorded at a heating rate of 10 K/min

Name	E_k (kJ mol^{-1})	E_o (kJ mol^{-1})	ρ (g/cm^3)
$z = 0$	356	378	3.832
$z = 3$	341	362	3.955
$z = 5$	322	343	4.029
$z = 6$	390	410	4.069

E_k activation energy determined by the Kissinger plot, E_o activation energy determined by the Ozawa plot, and ρ density of the respective glasses

The data shown in Figs. 3, 4 are fitted by a regression line. The difference in the calculations between the two equations (Eqs. 1, 2) for the respective compositions is less than 6%.

Figure 5a, b shows the Ozawa plots for the determination of Avrami exponents for all studied glasses. The plots are obtained by applying Eq. (3), where $\ln(-\ln(1-x))$ is plotted versus $\ln(\beta)$. The selected temperatures are 920 and 940 °C.

$$-n = \left|\frac{d[\ln(-\ln(1-x))]}{d(\ln\beta)}\right|_T. \quad (3)$$

In Eq. (3), n is the Avrami exponent and $x = At/A$, where A is the total area under the exothermal peak, At is the area under the exothermal peak up to a chosen temperature, and β is the heating rate.

The Avrami parameters, obtained from the slopes as illustrated in Fig. 5a, b, are 1.8, 1.3, 1.5, and 2.1 for 0, 3, 5, and 6 mol% ZrO_2, respectively. The Avrami parameter is largest for a ZrO_2 concentration of 6 mol%. According to a study made by Guedes [21], Avrami parameters equal or close to 1 should be an indicator for surface crystallization. In samples containing 0, 3, and 5 mol% ZrO_2, only surface crystallization is observed. For the sample with 6 mol% of ZrO_2, the Avrami value is equal to 2 which is an indicator for the occurrence of both surface and bulk crystallizations. The plots show also the respective linear regression lines, which are in good agreement with the data points.

Figure 6 presents an optical micrograph of a sample with 6 mol% ZrO_2, which was thermally treated at 720 °C for 48 h, and then in a second step at 840 °C for 1 h. This was done in order to nucleate the glass during the first step at a temperature just 23 K above T_g. The second step was chosen in order to achieve crystal growth and to develop the crystals up to an observable size. The surface of the sample was

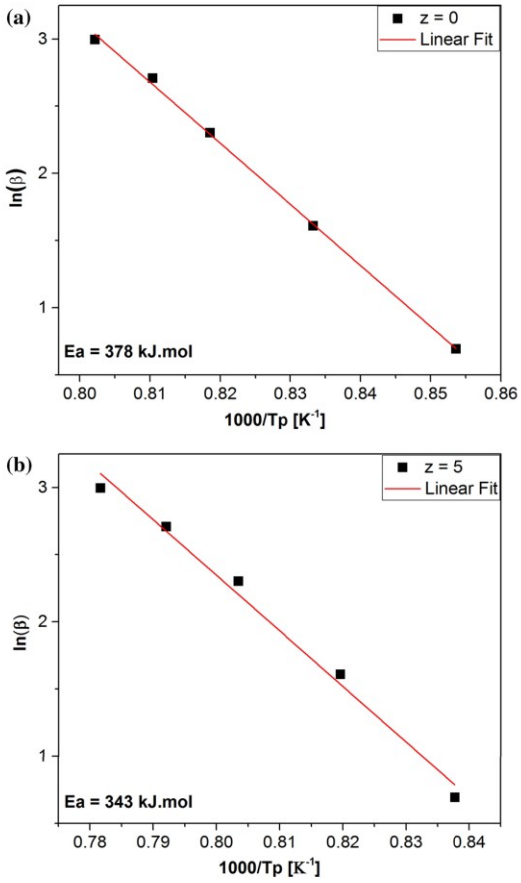

Figure 4 Ozawa plots used to calculate the activation energy of crystallization: **a** for a glass with $z = 0$ mol% ZrO_2, **b** for a glass with $z = 5$ mol% ZrO_2.

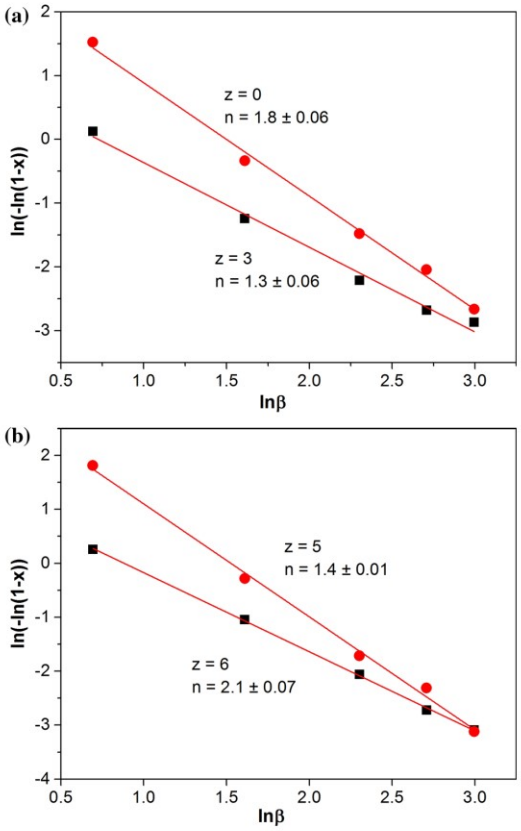

Figure 5 Ozawa plots of $(\ln(\ln(1-x)))$ versus $\ln\beta$ used to calculate the Avrami parameter n.: **a** $z = 0$ and $z = 3$ mol% at 920 °C, **b** $z = 5$ and $z = 6$ mol% at 940 °C.

ground in order to remove a surface-crystallized layer. The Figure shows crystals with a size of approximately 180 μm, which are nucleated in the bulk. The crystals have approximately a spherical shape and all possess approximately the same size.

Figure 7 presents an SEM micrograph of the same sample shown in Fig. 6. The crystallized sample was subsequently cut, ground, and polished. In the center, a large crystal is seen which has a size of approximately 150 μm. The middle of the crystals shows some cracks, and small crystals seem to be grown as spherulites from the middle. However, if differently oriented crystals grow from one and the same location in the crystallographic direction where the crystal growth velocity is maximum, an approximately spherical agglomerate should be the result.

In Fig. 8, an SEM micrograph also of a sample with a ZrO_2 concentration of 6 mol% is shown. In contrast to micrographs shown in Figs. 6, 7, this image was recorded from the surface. Furthermore, the nucleation temperature was only 710 °C, i.e., 10 K less, and the time the crystals were allowed to grow was only 15 min. In this micrograph, the upper edge is the surface from which the crystals start to grow. The crystals grew as bundles with slightly diverging growth directions. The thickness of the surface layer is approximately 10–15 μm, and hence the crystal growth velocity is around 0.8 to 1 μm/min.

The samples with ZrO_2 concentrations of 0, 3, and 5 mol% showed only surface crystallization and did

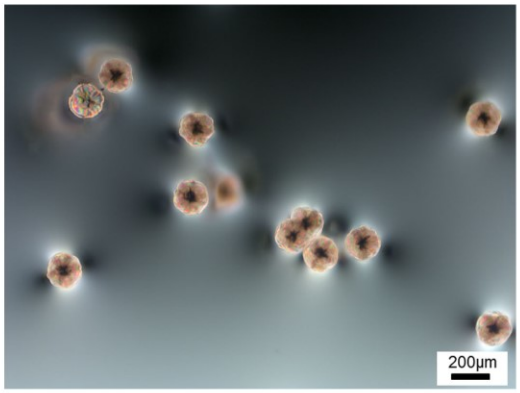

Figure 6 Optical micrograph of a sample with 6 mol% of ZrO_2 nucleated at 720 °C for 48 h and developed at 840 °C for 1 h.

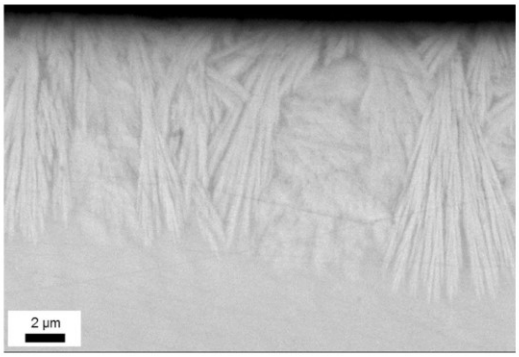

Figure 8 SEM micrograph of a sample with 6 mol% ZrO_2 thermally treated in a first step at 710 °C for 24 h and then at 840 °C for 15 min.

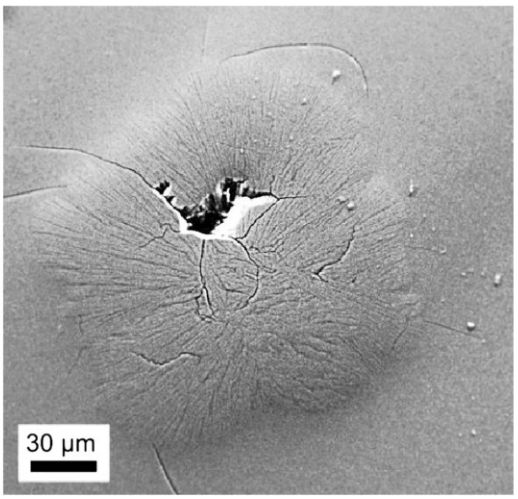

Figure 7 SEM micrograph of a sample with 6 mol% ZrO_2 thermally treated in a first step at 720 °C for 48 h and then at 840 °C for 1 h.

not give any hint at volume crystallization. This corresponds very well with the obtained Avrami parameters and the observed microstructure (not shown).

The surface crystallization of a crystalline phase with very small CTE from a glass with comparatively high CTE and subsequent cooling should result in high compressive stresses at the surface. The thickness of a layer under compressive stresses can be adjusted by the crystallization time; in a first approximation, it should grow linearly with time, if a diffusion barrier is not formed during crystal growth.

Layers with compressive stresses at the surface of glasses can also be achieved by ion exchange processes, e.g., if in a soda aluminosilicate glass Na^+ is exchanged against K^+ at temperatures more than 100 K below T_g. It is known from such techniques that very thin layers lead to maximum compressive stresses and also to maximum mechanical strengths. Unfortunately, layers with a thickness <15 µm are very sensitive to accidental scratching and not long-term reliable. Best results are often achieved with a thickness of a compressive layer ranging from 20 to 30 µm [25, 26].

The thickness of the surface layer formed by $Ba_{0.6}Sr_{0.4}Zn_2Si_2O_7$ crystals can be adjusted by an appropriate crystallization time and temperature. This might be a strategy for the preparation of glass–ceramics with good mechanical properties. In this case, it is advantageous, if bulk nucleation does not take place under the same crystallization conditions.

Otherwise, during sintering a glass powder, the subsequent crystallization is usually governed by the surface crystallization. The thermal expansion of such materials is widely affected by the orientation of the crystals with respect to the former surface of the glass particle [27].

The only glass where a certain extend of volume crystallization was observed is the glass with 6 mol% ZrO_2. It shows that in principle, volume crystallization is possible in the chosen glass system. It should be noted that the formation of ZrO_2 as seed was not

proved, and hence a hint at a heterogeneous crystallization is not obtained.

Conclusions

The effect of up to 5 mol% ZrO_2 on the crystallization of the glass in the BaO/SrO/ZnO/SiO_2 system is not large. The glass transition temperatures as well as the crystallization temperature and the glass stability parameter is scarcely affected. In any case, solely surface crystallization takes place. This is in agreement with detailed analyses of the DSC profiles using Avrami equation. This situation changes if 6 mol% ZrO_2 is added. Then, besides surface crystallization also volume crystallization takes place. The preceding formation of ZrO_2 as seed was not proved, i.e., a hint at heterogeneous nucleation is not given.

Acknowledgements

This work was funded by the German Federal Ministry of Education and Research under the Grant Numbers 03VP01701 and 03VP01702.

References

[1] Zheng XG, Kubozono H, Yamada H et al (2008) Giant negative thermal expansion in magnetic nanocrystals. Nat Nanotechnol 3:724–726

[2] Takenaka K (2012) Negative thermal expansion materials: technological key for control of thermal expansion. Sci Technol Adv Mater 13:013001

[3] Grima JN, Zammit V, Gatt R (2006) Negative thermal expansion. Xjenza 11:17–29

[4] Bach H, Krause D (2005) Low thermal expansion glass ceramics, 2nd edn. Springer, New York

[5] Müller G, Sternitzke M (1993) Computer modelling of structure and thermal expansion of β-quartz and keatite-type aluminosilicates. J Mater Sci Lett 12:278–280

[6] Gillery FH, Bush EA (1959) Thermal contraction of β-eucryptite ($Li_2O{\cdot}Al_2O_3{\cdot}2SiO_2$) by X-ray and dilatometer methods. J Am Ceram Soc 42:175–177

[7] Lind C, Wilkinson AP, Hu Z et al (1998) Synthesis and properties of the negative thermal expansion material cubic $ZrMo_2O_8$. Chem Mater 10:2335–2337

[8] Kerstan M, Rüssel C (2011) Barium silicates as high thermal expansion seals for solid oxide fuel cells studied by high-temperature X-ray diffraction (HT-XRD). J Power Sources 196:7578–7584

[9] Kerstan M, Thieme C, Grosch M et al (2013) $BaZn_2Si_2O_7$ and the solid solution series $BaZn_{2-x}Co_xSi_2O_7$ ($0 < x \leq 2$) as high temperature seals for solid oxide fuel cells studied by high-temperature X-ray diffraction and dilatometry. J Solid State Chem 207:55–60

[10] Kerstan M, Müller M, Rüssel C (2012) Thermal expansion of $Ba_2ZnSi_2O_7$, $BaZnSiO_4$ and the solid solution series $BaZn_{2-x}Mg_xSi_2O_7$ ($0 \leq x \leq 2$) studied by high-temperature X-ray diffraction and dilatometry. J Solid State Chem 188:84–91

[11] Thieme C, Görls H, Rüssel C (2015) $Ba_{1-x}Sr_xZn_2Si_2O_7$—a new family of materials with negative and very high thermal expansion. Sci Rep 5:18040

[12] Thieme C, Waurischk T, Heitmann S, Rüssel C (2016) New family of materials with negative coefficients of thermal expansion: the effect of MgO, CoO, MnO, NiO, or CuO on the phase stability and thermal expansion of solid solution phases derived from $BaZn_2Si_2O_7$. Inorg Chem 55:4476–4484

[13] Thieme C, Rüssel C (2016) Very high or close to zero thermal expansion by the variation of the Sr/Ba ratio in $Ba_{1-x}Sr_{x}Zn_2Si_2O_7$—solid solutions. Dalton Trans 45:4888–4895

[14] Thieme C, Rüssel C (2016) Negative thermal expansion in $Ba_{0.5}Sr_{0.5}Zn_2SiGeO_7$. Materials 9(8):631

[15] Kracker M, Thieme C, Haessler J, Rüssel C (2016) Sol-gel powder synthesis and preparation of ceramics with high- and low-temperature polymorphs of $Ba_xSr_{1-x}Zn_2Si_2O_7$ ($x = 1$ and 0.5): a novel approach to obtain zero thermal expansion. J Eur Ceram Soc 36:2097–2107

[16] Thieme C, Schlesier M, Bocker C et al (2016) Thermal expansion of sintered glass ceramics in the system BaO–SrO–ZnO–SiO_2 and its dependence on particle size. ACS Appl Mater Interfaces 8:20212–20219

[17] Cormier L (2014) Nucleation in glasses—new experimental findings and recent theories. Proc Mater Sci 7:60–71

[18] Donald IW (2004) Crystallization kinetics of a lithium zinc silicate glass studied by DTA and DSC. J Non-Cryst Solids 345:120–126

[19] Kissinger HE (1957) Reaction kinetics in differential thermal analysis. Anal Chem 29:1702–1706

[20] Ozawa T (1976) A modified method for kinetic analysis of thermoanalytical data. J Therm Anal 9:369–373

[21] Arora A, Shaaban ER, Singh K, Pandey OP (2008) Non-isothermal crystallization kinetics of ZnO–BaO–B_2O_3–SiO_2 glass. J Non-Cryst Solids 354:3944–3951

[22] Guedes M, Ferro AC, Ferreira JMF (2001) Nucleation and crystal growth in commercial LAS compositions. J Eur Ceram Soc 21:1187–1194

[23] Ghasemzadeh M, Nemati A, Nozad A et al (2011) Crystallization kinetics of glass-ceramics by differential thermal analysis. Ceram-Silikáty 55:188–194

[24] Wurth R, Pascual MJ, Mather GC et al (2012) Crystallisation mechanism of a multicomponent lithium alumino-silicate glass. Mater Chem Phys 134:1001–1006

[25] Stookey SD, Olcott JS, Olcott JSHM, Rothermel DL (1962) Ultra-high strength glasses by ion exchange and surface crystallization. Advances in Glass Technology, New York, Plenum, pp 397–411

[26] Tashiro M (1985) Crystallization of glasses: science and technology. J Non-Cryst Solids 73:575–584

[27] Tauch D, Rüssel C (2005) Glass-ceramics with zero thermal expansion in the system $BaO/Al_2O_3/B_2O_3$. J Non-Cryst Solids 351:2294–2298

5.2 Heterogeneous nucleation of $Ba_{1-x}Sr_xZn_2Si_2O_7$ from a $BaO/SrO/ZnO/SiO_2$ glass using platinum as nucleation agent

Liliya Vladislavova, Christian Thieme, Tilman Zscheckel, Christian Patzig, Thomas Höche, Christian Rüssel

Journal of the European Ceramic Society 37 (2017) 4801–4808

http://dx.doi.org/10.1016/j.jeurceramsoc.2017.05.020

Authors	Liliya Vladislavova	Christian Thieme	Tilman Zscheckel	Christian Patzig	Thomas Höche	Christian Rüssel
Conception of the research approach	X	X			X	X
Planning of examinations	X	X				X
Data collection	X	X	X	X		
Data analysis and interpretation	X	X	X	X		X
Writing the manuscript	X	X	X	X	X	X
Credits	1.0					

Journal of the European Ceramic Society 37 (2017) 4801–4808

Contents lists available at www.sciencedirect.com

Journal of the European Ceramic Society

journal homepage: www.elsevier.com/locate/jeurceramsoc

Heterogeneous nucleation of $Ba_{1-x}Sr_xZn_2Si_2O_7$ from a $BaO/SrO/ZnO/SiO_2$ glass using platinum as nucleation agent

Liliya Vladislavova[a,*], Christian Thieme[a,b], Tilman Zscheckel[a], Christian Patzig[b], Thomas Höche[b], Christian Rüssel[a]

[a] Otto-Schott-Institut, Jena University, Fraunhoferstr. 6, 07743 Jena, Germany
[b] Fraunhofer Institute for Microstructure of Materials and Systems IMWS, Walter-Hülse-Str. 1, 06120 Halle, Germany

ARTICLE INFO

Article history:
Received 6 February 2017
Received in revised form 8 May 2017
Accepted 13 May 2017
Available online 22 May 2017

Keywords:
Nucleation
Glass-ceramics
Platinum
Activation energy
Avrami parameter

ABSTRACT

Glasses in the system $BaO/SrO/ZnO/SiO_2$ were doped with 0.01% platinum. During thermal treatment, the glasses were crystallized and the phase $Ba_{1-x}Sr_xZn_2Si_2O_7$ was formed. This phase has almost the same structure as the high-temperature phase of $BaZn_2Si_2O_7$, which shows a negative coefficient of thermal expansion. In the obtained glasses, spherical particles of metallic platinum with diameters in the range from 300 nm to 2 μm are present. Detailed analyses of the curves obtained from differential scanning calorimetry enable the determination of the activation energies as well as the Avrami coefficients. The obtained values of the Avrami coefficients were close to 4, which correspond to three-dimensional bulk crystallization. Scanning electron microscopy was used to identify individual $Ba_{1-x}Sr_xZn_2Si_2O_7$ crystals with sizes of approximately 15 μm. Transmission electron microscopy showed that these crystals are nucleated at the surface of spherical platinum particles.

1. Introduction

While solids generally show a positive coefficient of thermal expansion (CTE), i.e. they expand with increasing temperatures [1–3], only a few materials contract during heating. Among these, the most important are alumosilicates, such as beta-quartz, spodumene, keatite or beta-eucryptite [4–6]. These solids are predominantly used to achieve zero thermal expansion, making them useful materials for everyday life products, e.g. as cooktop panels or furnace windows. During temperature changes, they keep their dimensions and shape and therefore, internal stresses are not developed. Such materials are also used as telescope mirror blanks, which must not change their shape under non-isothermal conditions [6].

In the past two decades, further materials which show negative thermal expansion (NTE) have been reported. The system $BaAl_2B_2O_7$ [7–11] was first studied by MacDowell [7] who described a CTE of $2.3 \cdot 10^{-6}\,K^{-1}$ (25–300 °C). Later, Hovhannisyan reported that also zero thermal expansion can be reached [8]. Tauch [9–11] reported glass-ceramic materials with zero thermal expansion based on $BaAl_2B_2O_7$. Unfortunately, the chemical durability of this material is not sufficient for many applications. Another phase with a negative CTE is $ZrMo_2O_8$, in which Zr can also be replaced by Hf [12]. It is a metastable phase with a mean CTE of $-7.2 \cdot 10^{-6}\,K^{-1}$ observed in a wide temperature range from −273 to 777 °C. Since the phase is cubic and hence isotropic, the preparation of useful materials is widely facilitated. A negative thermal expansion is also observed in the systems $Zr_2P_2O_9$ (zirconyl phosphate) and ZrV_2O_7 (zirconium pyrovanadate) [13]. These phases predominantly show surface crystallization, similar to $BaAl_2B_2O_7$ and magnesium alumosilicate based materials.

Alkaline earth silicates, especially barium silicates, have been reported in the literature to possess high coefficients of thermal expansion (CTE), usually in the range from 10 to $16 \cdot 10^{-6}\,K^{-1}$ [14]. The compound $BaZn_2Si_2O_7$ exhibits a high CTE up to around 280 °C, where it shows a phase transition to a high-temperature phase, which runs parallel to a steep increase in volume of around 2% [15]. The low-temperature phase of $BaZn_2Si_2O_7$ has a mean CTE of about $17.6 \cdot 10^{-6}\,K^{-1}$ [15,16] and is monoclinic in the space group C2/c [15]. For the high-temperature phase, which is orthorhombic, two very similar crystal structures with the space groups Cmcm and $Ccm2_1$ are reported [17,18]. This high-temperature polymorph shows a very low and in a certain temperature range negative CTE [15,17]. The partial or total substitution of Zn by Mg [16], Co [15], or Ni [19] stabilizes the low-temperature phase up to temperatures of 950 °C or even higher, which enables the preparation of

* Corresponding author.
E-mail address: liliya.vladislavova@uni-jena.de (L. Vladislavova).

http://dx.doi.org/10.1016/j.jeurceramsoc.2017.05.020
0955-2219/

materials with high CTEs. Substitution of Ba by Sr leads to the opposite effect, i.e., the stabilization of the high-temperature phase. As recently reported, zero or negative thermal expansion of the high-temperature phase can be extended even below room temperature [20,21].

A single crystal with the composition $Ba_{0.6}Sr_{0.4}Zn_2Si_2O_7$ was studied using single crystal X-ray diffraction, which allowed the assignment to the structure of the high-temperature phase [17]. The thermal expansion was determined up to 1000 °C using high-temperature powder diffraction in combination with Rietveld refinement for the respective crystallographic directions. The high-temperature phase, in which a considerable quantity of Ba is substituted against Sr, is also stable at room temperature if Zn is partially substituted by Co, Mg, Ni, Cu, or Mn [22]. Furthermore, the high-temperature phase is still stable at room temperature, if Si is partially substituted by Ge [23]. All compositions with the structure of high-temperature $BaZn_2Si_2O_7$ show low or negative CTE.

The thermal expansion strongly depends on the crystallographic direction, and despite the anisotropy, it enables the preparation of sintered materials with comparably low mean thermal expansion [21]. It was already reported that low thermal expansion materials can also be prepared from sinter active powders using a sol-gel route [24]. Furthermore, glass powders of appropriate compositions can be sintered and subsequently crystallized leading to glass-ceramics with varying CTEs depending on the Ba/Sr ratio [21,25].

By contrast to the other compounds described above, $Ba_{1-x}Sr_xZn_2Si_2O_7$ might be a serious alternative to low thermal expansion materials based on lithium alumosilicates, because their low CTE phase can be crystallized from glasses. This should enable the fabrication of low CTE glass ceramic materials using much lower melting temperatures than necessary for the production of lithium alumosilicate glass ceramics.

Up to now, the phase $Ba_{1-x}Sr_xZn_2Si_2O_7$ was investigated with respect to its structure and the effect of substitution on phase formation and thermal expansion [17,22–24]. Recently, it has been shown that bulk nucleation might be achieved by adding 6 mol% ZrO_2 [26]. It was shown that the addition of ZrO_2 does not lead to a sufficient number of nuclei with homogeneous distribution in the sample bulk. After crystallization, the crystals were too large to obtain a crack-free sample. Hence, in this paper a different approach was chosen. It is well reported in the literature that adding noble metals in controlled quantities leads to bulk nucleation [27]. The formation of the metal nanoparticles in the glass usually occurs during cooling of the glass or during a subsequent heat-treatment. The metallic particles may then act as nuclei for the subsequent crystallization of another phase [28]. Rindone reported on the effect of different platinum concentrations in the $Li_2O{\cdot}4SiO_2$ system. He found that even small amounts of Pt did not only enhance the crystallization process, but also led to a homogeneous distribution of the crystals [29]. This paper describes the effect of platinum as nucleating agent on the crystallization of glasses in the system $BaO/SrO/ZnO/SiO_2$.

2. Materials and methods

The glass batch was prepared from the following raw materials: $BaCO_3$ (Merck, >98.5%), $SrCO_3$ (Ferak Berlin or VEB Laborchemie Apolda, >99%), ZnO (Carl Roth GmbH + Co KG, >99%), SiO_2 (Carl Roth GmbH + Co KG, >99%), ZrO_2 (Tosoh >99%), $PtCl_4$ (Merck, >57.5% Pt). A quantity of 0.01 mol% $PtCl_4$ was dissolved in acetone and then given to the glass batch, thoroughly mixed for 2 h and subsequently dried. The batch (for 400 g glass) was melted at 1300–1350 °C in a platinum crucible using an induction furnace. At first, the glasses were melted at 1300–1350 °C for 1 h afterwards the temperature was risen to 1400–1450 °C for 2 h. During this time, the melt was stirred with 60 min^{-1}. Then the stirrer was removed and the glass was soaked for 10–15 min. The glass was cast on a pre-heated steel mold and transferred to a muffle furnace preheated to 680–700 °C. The furnace was switched off allowing the sample to cool to room temperature with a rate of approximately 3 K/min. The chemical compositions of the respective samples are summarized in Table 1.

Table 1
Chemical compositions of the studied samples (in mol%)

Sample	Chemical composition in mol%					
	BaO	SrO	ZnO	SiO_2	ZrO_2	$PtCl_4$
z = 0	8	8	34	49.99	0	0.01
z = 6	8	8	34	43.99	6	0.01

Differential Scanning Calorimetry (DSC) was carried out using a Linseis DSC Pt 1600. This enabled the determination of characteristic temperatures such as glass transition temperature (T_g), onset of the crystallization peak (T_{on}), offset of the crystallization peak (T_{off}) and the crystallization maximum (T_p). In order to minimize the effect of surface crystallization, bulk samples were used. Therefore, glass powders with a mass of 0.15 g were remelted in a DSC platinum crucible at 1400 °C and quenched in air. The measurements were performed up to a temperature of 1200 °C, using heating rates of 2, 5, 10, 15 and 20 K/min.

X-Ray diffraction (XRD) was performed with a Rigaku MiniFlex 300 diffractometer with Ni-filtered CuKα radiation using samples which were polished, crystallized and in some cases subsequently powdered. The studied 2θ-range was from 10° to 60° with a scan speed of 1 or 0.1°/min. The density was determined with a helium pycnometer Micromeritics AccuPyc 1330.

Transmission electron microscopy (TEM) was performed using an FEI TITAN^3 (80–300 kV) TEM, supplying an acceleration voltage of 80 kV. This comparatively low acceleration voltage was necessary due to the high sensitivity towards deterioration of the samples under the beam. Energy dispersive X-Ray spectroscopy (EDXS) in the TEM was performed with a Super-X EDXS detector that is equipped with four SDD detectors (FEI company). This enabled to display element mappings of different elements, using the commercial software *Esprit* v1.9 (Bruker company). The first steps of the sample preparation were done by a purely mechanical approach (wedge polishing) using a dedicated polishing tool (MultiPrep^{TM}, Allied company). The sample was thinned down to a residual thickness of approximately 20 μm and the further polishing step was done under a low-inclination angle (1.6°). That way, a wedge-shaped sample is formed, with the tip of the wedge being thin enough (some 10 nm only) for electron transparency. Furthermore, the samples underwent a final Ar^+ ion broad-beam milling step (precision ion polishing system PIPS, Gatan company) to remove any polishing residues. As a last step, the samples were carbon coated using a specific coating mask (CoatMaster, 3D-Micromac AG).

Scanning Electron Microscopy was carried out using a (SEM) JEOL 7001 F. The samples were contacted with Ag-paste and covered with carbon at about 10^{-5} Pa in order to avoid surface charging.

3. Results and discussion

3.1. Nucleation and crystallization

The prepared glasses are transparent, however, have a grayish color, which is more pronounced in the case of the sample without ZrO_2. Both glasses are homogeneous and bubble-free.

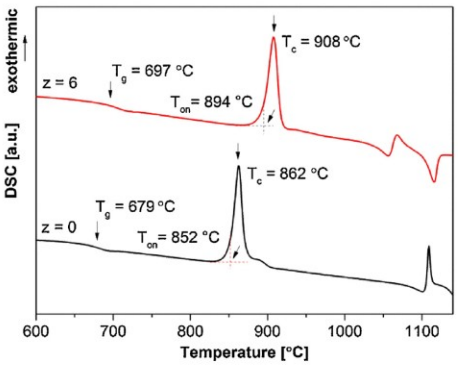

Fig. 1. DSC profiles of glasses without (z = 0) and with (z = 6) ZrO_2 using a heating rate of 10 K/min.

Fig. 1 shows DSC profiles of the glasses with and without ZrO_2. The glass transition temperatures T_g are 679 and 697 °C for the glasses without and with ZrO_2, respectively. Both glasses show exothermic peaks, which are due to crystallization of the respective glasses. The maxima of the crystallization peaks T_p are at 862 and 908 °C for the glasses without and with the addition of ZrO_2, respectively. The differences, frequently considered as the glass stability parameter T_{on}-T_g, are 173 and 197 K for the glasses without and with ZrO_2. That means that the stability against devitrification is better in the ZrO_2 containing glass. The increase in T_g of 18 K while substituting 6 mol% SiO_2 by an equimolar ZrO_2 concentration is not an effect of the platinum addition and was already observed in a previous study on glasses which did not contain platinum [26]. The same tendency was also observed for T_p, however, the shift was 46 K and hence notably larger. The values for T_p for the non-Pt containing glasses were 948 and 985 °C for the glasses without and with ZrO_2, respectively [26]. Fig. 2 shows XRD-patterns of samples without ZrO_2 thermally treated at temperatures of 680, 690, 700, 710 and 720 °C. The patterns recorded at 680 and 690 °C show mostly the glass halo and only two rudiments of peaks, which get obvious using a narrower 2θ-scale (see Fig. 3). At temperatures of 700 °C and more, further low-intensity XRD-peaks are observed. They appear at $2\theta \approx 27$ and 30° and are attributed to the most intense XRD lines of $Ba_{0.6}Sr_{0.4}Zn_2Si_2O_7$ (shown at the bottom of Figs. 2 and 3). The low intensity peak at $2\theta \approx 28.4°$ only appears after crystallization at 700 °C, and is marked with a star in Fig. 2. Most probably, the peak is attributed to the 100% peak of the low temperature phase of $BaZn_2Si_2O_7$. An increase in temperature of thermal treatment leads to a notable decrease of the amount of glassy phase. However, it is still considerably high. Nevertheless, the intensity of the XRD peaks which indicate the presence of crystalline phases increases with increasing temperature. The peaks are clearly attributed to $Ba_{0.6}Sr_{0.4}Zn_2Si_2O_7$. For temperatures of 680, 690, 710 and 720 °C, peaks due to additional crystalline phases are not observed. Fig. 3 shows a narrower 2θ-range from 38 to 48°. The peaks at 2θ = 39.7 and 46.2° are attributed to the high intensity peaks (111) and (200) of metallic platinum (ICSD 64912). The observed intensities obviously match well with the expected relative intensities of 100 and 46%, respectively. With increasing temperature, the intensity ratio of the $Ba_{0.6}Sr_{0.4}Zn_2Si_2O_7$ peaks with respect to the Pt peaks increases strongly, due to the increasing quantity of crystalline $Ba_{0.6}Sr_{0.4}Zn_2Si_2O_7$. An identical study was made for the glass with ZrO_2 thermally treated at temperatures of 700, 710, 720, 730 and 740 °C (not shown here). The XRD patterns of the samples were similar and the Pt peak was detected for all mentioned temperatures.

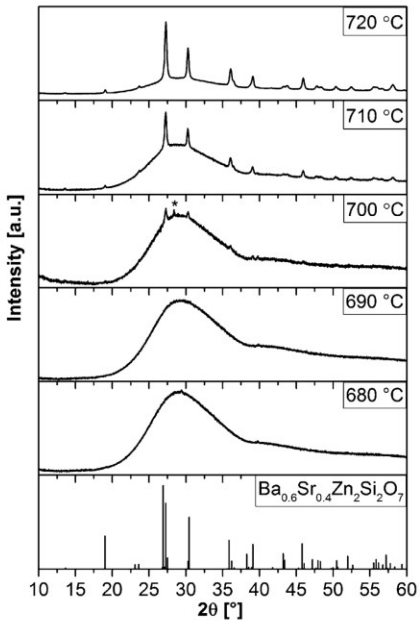

Fig. 2. X-ray diffraction patterns for the glass without ZrO_2. All samples are thermally treated for 48 h at temperatures of 680, 690, 700, 710 and 720 °C. At the bottom, the theoretical peak positions of $Ba_{0.6}Sr_{0.4}Zn_2Si_2O_7$ (ICSD – 429938) phase are shown.

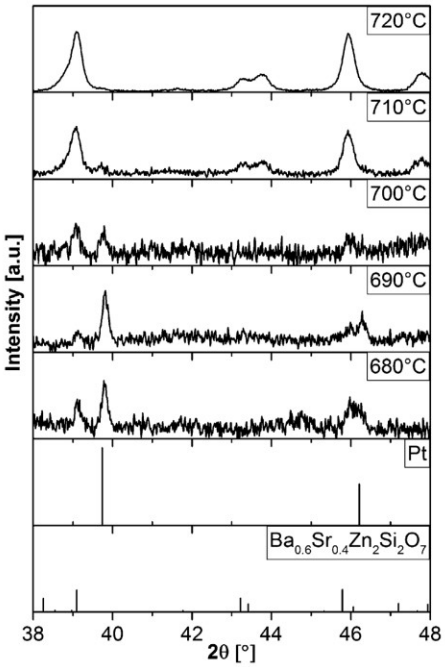

Fig. 3. X-ray diffraction patterns of the ZrO_2-free glass (base line corrected). At the bottom, the theoretical peak positions of metallic platinum (ICSD – 64912) and of $Ba_{0.6}Sr_{0.4}Zn_2Si_2O_7$ (ICSD – 429938) are shown.

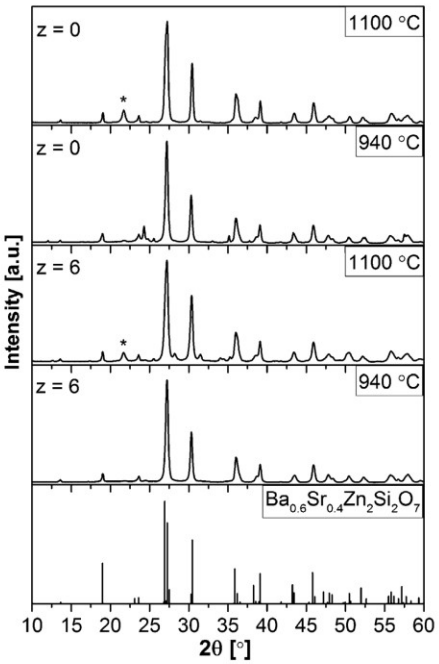

Fig. 4. X-ray diffraction patterns for glasses with (z = 6) and without (z = 0) addition of ZrO_2. The samples are thermally treated at 940 °C and 1100 °C for 1 h. At the bottom, the theoretical peak positions of $Ba_{0.6}Sr_{0.4}Zn_2Si_2O_7$ (ICSD – 429938) phase are shown.

Fig. 4 shows XRD–patterns for both compositions kept for 1 h at temperatures of 940 and 1100 °C, this temperatures were chosen to be above the temperatures of the two exothermic peaks shown in Fig. 1. In all patterns, the amorphous halo is no longer visible and all recorded patterns of the two compositions are fairly similar. In the XRD-patterns of samples thermally treated at a temperature of 1100 °C, an additional peak at 2θ = 21.80° occurs. This peak is attributed to small quantities of crystalline cristobalite and hence might explain the second exothermic peak in the DSC profiles of Fig. 1 at temperatures higher than 1060 °C. In the ZrO_2 containing sample thermally treated at 1100 °C, peaks attributed to Willemite ($Zn_2[SiO_4]$) are detected. They are observed at 2θ = 25.50, 31.49 and 34.03°, and according to the ICSD file (37–148), these peaks are the most intense lines with a relative intensity of 100, and 86% respectively. Other peaks of Willemite are not unambiguously detectable, due to the overlap of the respective peak positions with the main $Ba_{0.6}Sr_{0.4}Zn_2Si_2O_7$ phase. All other peaks that are visible in the XRD spectra are attributed to crystalline $Ba_{0.6}Sr_{0.4}Zn_2Si_2O_7$.

3.2. Kinetics of nucleation and crystal growth

The kinetic crystallization parameters, the Avrami parameter n and the activation energy, E_a were determined from the DSC profiles. Fig. 5 shows DSC profiles of the glasses: a) with 0 mol% of ZrO_2, b) with 6 mol% ZrO_2 recorded using different heating rates in the range from 2 to 20 K/min. While the value of T_g does not change significantly (as expected) for both glasses, the exothermic peak, i.e. the crystallization peak changes notably. In Fig. 5a, the shift of the exothermic peak is illustrated for the glass system without ZrO_2. The crystallization peak is shifted from 799 °C for a heating rate of 2 K/min up to 871 °C for a heating rate of 20 K/min.

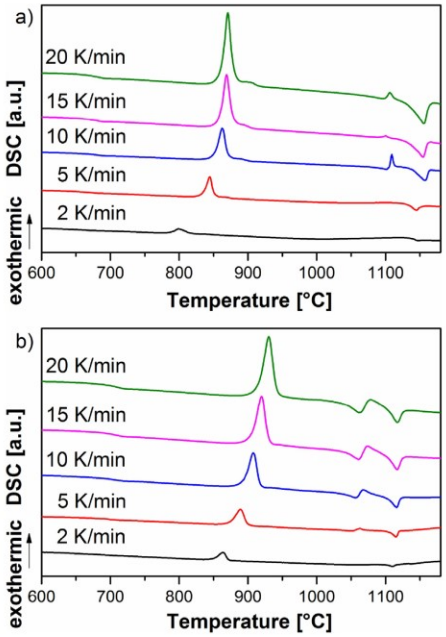

Fig. 5. DSC profile of glasses using 5 different heating rates: a) sample without ZrO_2; b) sample with ZrO_2.

The same tendency is seen in Fig. 5b for the glass system with 6 mol% ZrO_2, where T_p for 2 K/min appears at 864 °C and shifts to 931 °C for 20 K/min. A summary of the characteristic temperatures for all applied heating rates is presented in Table 2.

The Avrami parameter was measured according to the method proposed by Ozawa [30–32] and calculated according to (Eq. (1)):

$$-n = \left|\frac{d\,[\ln(-\ln(1-x))]}{d(\ln\beta)}\right|_T \quad (1)$$

Where: n is the Avrami parameter, x = A_t/A, in this case: A is the total area under the exothermal peak, A_t is the area under the exothermic peak up to a chosen temperature and β is the heating rate. The Ozawa plots present ln(-ln(1-x)) versus ln(β) and – n can be determined from the slope of the linear regression. In both systems, the Avrami parameter possesses values near n = 4, which indicates 3-dimensional volume crystallization.

Fig. 6a and 6b show the Ozawa plots for the samples with and without ZrO_2 at temperatures of 838 and 878 °C, respectively. The linear regressions (red) agree well with the data points, the Avrami parameters are 3.7 and 3.9, respectively. From the shift in the peak temperatures, the activation energy of the crystallization process can be calculated. These values are obtained by using the Kissinger equation (see Eq. (2)) [33–35], the modified Kissinger Equation (see Eq. (3)) [33,35] and the Ozawa equation (see Eq. (4)). In Fig. 7a, according to Eq. (2), $\ln(\beta/T_p^2)$-values are plotted versus $1000/T_p$ for the glass with ZrO_2,

$$\ln\left(\frac{\beta}{T_p^2}\right) = \frac{-E_a}{RT_p} + const \quad (2)$$

$$ln\left(\frac{\beta^n}{T_p^2}\right) = \frac{-mE_a}{RT_p} + const \quad (3)$$

Where: T_p is the temperature attributed to the maximum crystallization peak; β is the heating rate; E_a is the activation energy; and

Table 2
Results from the DSC-profiles of the samples with different ZrO_2 concentrations. Heating rate, β; Glass transition temperature, T_g; onset of the crystallization peak, T_{on}; Offset of the crystallization peak; T_{off}; temperature of the crystallization peak T_p; and T_{on}-T_g.

	β (K/min)	T_g (°C)	T_{on} (°C)	T_{off} (°C)	T_p (°C)	T_{on}-T_g (K)
z = 0	2	–	790	814	799	–
	5	673	835	851	844	162
	10	679	852	871	862	173
	15	680	859	877	869	179
	20	680	861	879	871	181
z = 6	2	–	852	871	864	–
	5	693	873	899	889	180
	10	697	894	917	908	197
	15	700	905	930	920	205
	20	707	915	941	931	208

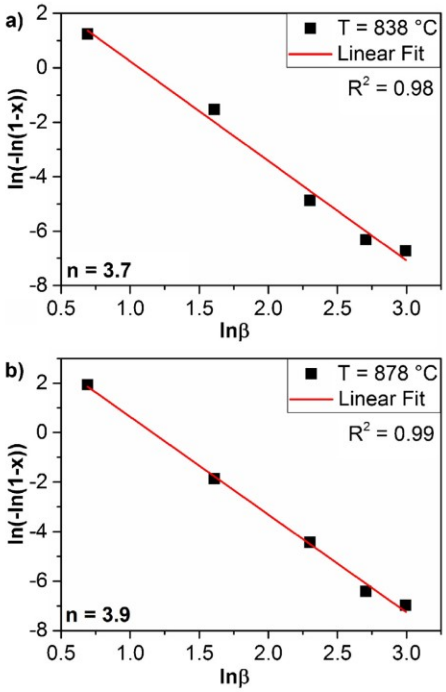

Fig. 6. Ozawa plot of (ln-(ln(1-x))) versus lnβ used to calculate the Avrami parameter n: a) sample without ZrO_2 at 838 °C; b) sample with ZrO_2 at 878 °C.

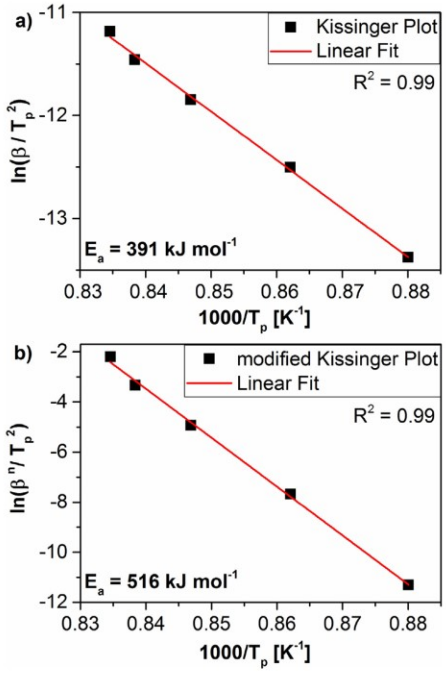

Fig. 7. Graphical presentation of the activation energy for sample with ZrO_2 applying: a) Kissinger plot; b) modified Kissinger plot.

Table 3
E_{ak}: activation energies, determined by the Kissinger plot; E_{ao}: activation energy determined by the Ozawa plot; E_{am}: activation energy, determined by modified Kissinger plot, and density of the respective glasses.

Name	E_{ak} [kJ mol^{-1}]	E_{ao} [kJ mol^{-1}]	E_{am} [kJ mol^{-1}]	ρ [g/cm^3]
z = 0	285	304	399	3.835
z = 6	373	392	516	4.057

R is the gas constant; n (Avrami coefficient) and m (dimensionality of crystal growth) are parameters, depending on the crystallization mechanism.

The calculated activation energies, according to the Kissinger equation (Eq. (2)), are 285 and 373 kJ mol^{-1}, for the glasses without and with ZrO_2, respectively. The activation energies are summarized in Table 3.

Before (Eq. (3)), i.e., the modified Kissinger equation (in some literature denoted as Matusita equation) can be applied, the Avrami parameter n as well as the dimensionality of the crystal growth m must be known [33,35]. As described above, the Avrami parameters are 3.7 and 3.9 for the samples without ZrO_2 and with ZrO_2, respectively. For further calculations, a constant Avrami parameter of n = 4 was assumed for both glasses. The crystal growth constant m is equal to 3 for an Avrami parameter of 4, according to a reference published by Donald [33]. The graphical representation of the modified Kissinger equation for the sample with ZrO_2 is shown in Fig. 7b. In this case, the slope, enabling to determine the activation energy, is calculated from Eq. (3), where $\ln(\beta^n/T_p^2)$ is plotted versus $1000/T_p$. The activation energies calculated from the modified Kissinger equation are 399 and 516 kJ mol^{-1}, for the glass without and with the addition of ZrO_2, respectively.

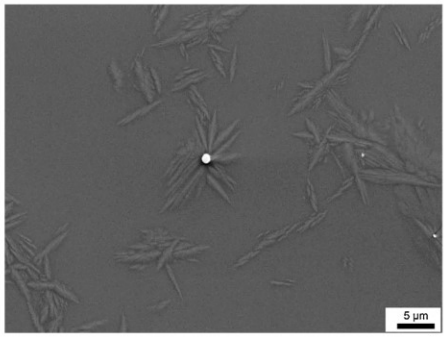

Fig. 8. SEM-micrograph of a sample without ZrO_2 thermally treated at 720 °C for 48 h.

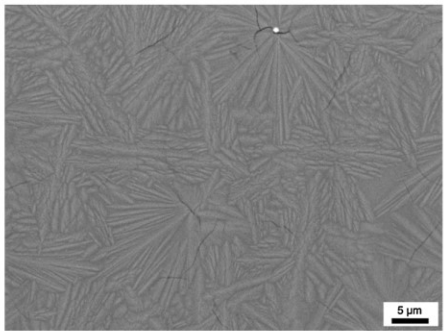

Fig. 9. SEM-micrograph of a sample without ZrO_2 thermally treated at 720 °C for 100 h.

Ozawa equation is given below as Eq. (4) [26,31,33], used for calculation of the activation energy, care has to be taken to distinguish between Ozawa method (see Eq. (1) and Ozawa equation):

$$\ln(\beta) = \frac{-E_a}{RT_p} + const \quad (4)$$

Where: T_p is the temperature attributed to the maximum crystallization peak; β is the heating rate; E_a is the activation energy and R is the gas constant.

The Ozawa equation was also applied for both glass systems where the activation energy for the sample without ZrO_2 is 304 kJ mol^{-1} and with ZrO_2 is 392 kJ mol^{-1}. That means, that the introduction of ZrO_2 into the glass structure leads to a higher activation energy of the overall crystallization process. The data shown in Table 3 were fitted by a linear regression and the results for the sample with ZrO_2 are in an almost perfect alignment with it, scattering is observed for the sample without ZrO_2.

3.3. Microstructure

In order to obtain a fine-grained microstructure, an additional nucleation step was supplied. Generally, this should result in a high density of small crystals and a low quantity of residual glass phase [28]. In order to confirm the results obtained from thermal analysis and the conclusions drawn from the Avrami parameters, the microstructure of the materials was studied by SEM. Figs. 8 and 9 show SEM micrographs from the bulk of the sample without ZrO_2 nucleated at 720 °C, for 48 and 100 h, respectively. In Fig. 8, approximately in the middle of the micrograph, a bright particle is observed, which consists of metallic platinum. From this particle, it can be observed that $Ba_{1-x}Sr_xZn_2Si_2O_7$ crystals (distinguishable by a grayish contrast in the SEM micrograph) start to grow. Additionally, numerous other, $Ba_{1-x}Sr_xZn_2Si_2O_7$ crystals are observed. It is assumed that these crystals also have a platinum particle in their center; however, it is not observed in the micrograph, likely because the platinum particles are not located in the plane of the analyzed sample cross-section surface. The mean size of the formed crystals $Ba_{1-x}Sr_xZn_2Si_2O_7$ is around 15 µm and they are surrounded by an amorphous phase. The majority of crystals does not contact each other and can be clearly distinguished by one another.

Applying a longer crystallization time of 100 h at the same temperature leads to a strong crystallization of the glass, as shown in Fig. 9. The amorphous phase between the $Ba_{1-x}Sr_xZn_2Si_2O_7$ crystals appears to be of very low volume concentration, and the crystals interpenetrate each other, which makes a determination of the mean crystal size unreliable. Due to the anisotropy of the crystal phase, small cracks start to appear.

In Figs. 10 and 11, TEM-micrographs of the glass system without ZrO_2 are shown. In Fig. 10(a), a micrograph of a sample which was not thermally treated is presented. It shows a faceted inclusion with a size of about 600 nm. In order to obtain information on its elemental composition, EDXS analyses were performed using an acceleration voltage of 80 kV. Fig. 10(b), (c) and (d) shows elemental mappings of Pt, Zn and Si, respectively. It is obvious that the faceted particle is metallic platinum. These particles are either already formed at the high temperatures at which the glasses were melted, or they formed during cooling. Platinum particles were observed in both studied glasses without thermal treatment which can easily explain the gray color of these glasses. This interpretation was previously reported by Rindone for platinum doped lithium silicate glasses [29].

In Fig. 11, a TEM micrograph of a sample crystallized for 48 h at 690 °C is shown together with elemental mappings of Pt, Zn and Si. In analogy to Fig. 10, in the middle, a platinum particle is observed. Around this particle, another crystal phase is observed, which, as shown in the EDXS mappings, is enriched in Zn, but slightly depleted in Si with respect to the surrounding glass matrix. These crystals hence are a $Ba_{1-x}Sr_xZn_2Si_2O_7$ solid solution, which is the only occurring crystalline phase detected in the XRD-patterns. Obviously the platinum particle acts as nucleating agent.

The crystallization behavior of the platinum doped samples with and without zirconia is not very different. In a previously published article, the effect of the ZrO_2 [26] on a glass without platinum was investigated. These samples show solely surface crystallization up to a ZrO_2 concentration of 5 mol%.The addition of 6 mol% ZrO_2 leads to minor bulk nucleation, but nevertheless predominantly surface crystallization occurs.

The samples with platinum are somewhat gray also before thermal treatment, which is due to a certain quantity of almost spherical metallic platinum particles, which possess sizes of around 300 nm–2 µm. These particles obviously act as nucleation centers and thus trigger the crystallization of $Ba_{1-x}Sr_xZn_2Si_2O_7$ solid solutions. Hence, the addition of platinum enables the volume crystallization of the desired phase. This is also shown by the Avrami coefficients which are close to n = 4, which implies a three dimensional volume crystallization.

In the literature, the effect of nucleating agents is sometimes described as (i) the precipitation of small particles formed by the nucleating agent and (ii) epitaxial growth of the desired phase on the crystal lattice of the nucleus [28]. In the case of platinum, the particles formed at high temperatures should be single crystalline which is seen from the faceting of the particles. Nevertheless, the $Ba_{1-x}Sr_xZn_2Si_2O_7$ particles are grown in different directions and hence epitaxial growth is unlikely. It should be noted that such an epitaxial growth mechanism is often assumed, but was hardly

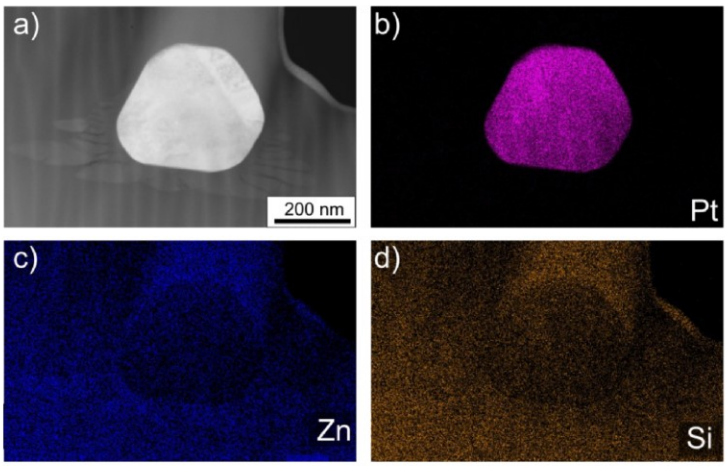

Fig. 10. TEM micrograph of a glass without ZrO_2: a) Pt particle and an adherent crystal phase, b) EDXS mapping for Pt, c) EDXS mapping for Zn, d) EDXS mapping for Si.

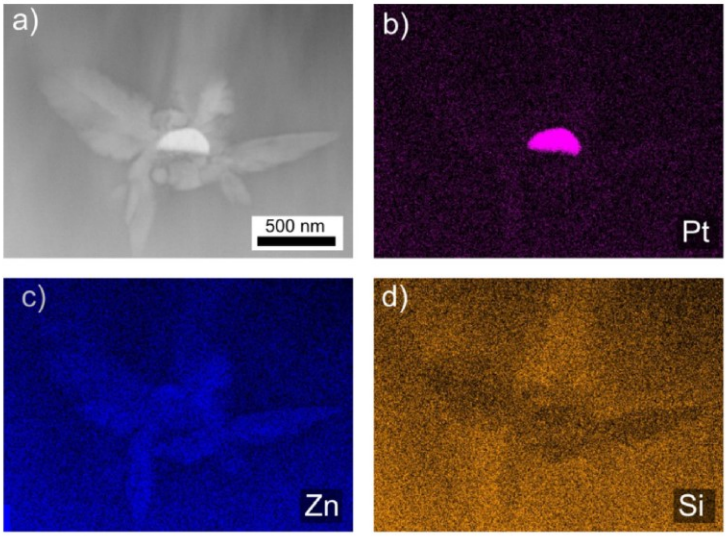

Fig. 11. TEM micrograph of a glass without ZrO_2 nucleated for 48 h at 690 °C: a) Pt particle surrounded by a crystal, b) EDXS mapping for Pt, c) EDXS mapping for Zn, d) EDXS mapping for Si.

proved. In principle, it seems beneficial to further decrease the size of the $Ba_{1-x}Sr_xZn_2Si_2O_7$ crystals by decreasing the size of platinum crystals and hence increasing their number and volume density. However, it has been reported in the past that a certain minimum size of the platinum particles is necessary in order to trigger the crystallization of the second phase [27,36]. Nevertheless, it will be tried in further studies to minimize the size of the $Ba_{1-x}Sr_xZn_2Si_2O_7$.

4. Conclusions

The base glass composition $BaO/SrO/ZnO/SiO_2$ is a suitable candidate for the crystallization of $Ba_{1-x}Sr_xZn_2Si_2O_7$, as proved by X-ray diffraction. Adding Pt to the system leads to bulk nucleation and hence, platinum was proved to be an efficient nucleation agent. However, no evidence was obtained that the addition of ZrO_2 has a significant effect on the crystallization process. The Avrami parameter was calculated to $n \approx 4$, which corresponds to predominant bulk crystallization. The latter was confirmed by the TEM and SEM micrographs of the obtained samples. The analyses of non-heat treated samples show Pt particles with diameters in the range of 300 nm up to 2 μm in the glassy matrix. These particles act as nucleation centers for the formation of $Ba_{1-x}Sr_xZn_2Si_2O_7$ solid solutions. This leads to the desired volume crystallization into the glass matrix and crystals size of around 15 μm. This is a significant decrease in the crystals size in comparison to previously reported sample, where the volume crystals with a size of 180 μm were reported.

Acknowledgment

This work was funded by the German Federal Ministry of Education and Research under the grant numbers 03VP01701 and 03VP01702.

References

[1] J. Petzoldt, Untersuchungen an transparenten, metastabile Quarz-Mischkristalle enthaltenden Glaskeramiken, Glas. Ber. 43 (1970) 127–137.
[2] F.A. Hummel, Thermal expansion properties of some synthetic lithia minerals, J. Am. Ceram. Soc. 34 (1951) 235–239.
[3] M. Sternitzke, G. Müller, Crystal structure and thermal expansion of quartz-type aluminosilicates, J. Mater. Sci. 26 (1991) 3051–3056.
[4] W. Pannhorst, E., Rodek, H. Scheidler, Transparent colored glass ceramic with good thermal stability and variable transmission in the IR region, US Patent 5.212, 122, May 18, 1993.
[5] H. Scheidler, E. Rodek, Li_2O-Al_2O_3-SiO_2 glass-ceramics, Am. Ceram. Soc. Bull. 68 (1989) 1926–1930.
[6] H. Bach, D. Krause, Low Thermal Expansion Glass Ceramics, 2nd edn, Springer, New York, 2005.
[7] J.F. MacDowell, Aluminoborate glass-Ceramics with low thermal expansivity, J. Am. Ceram. Soc. 73 (1990) 2287–2292.
[8] R.M. Hovhannisyan, Rafaelites–new kinds of glass ceramics with low thermal expansion and low melting temperatures on the basis of alkaline earth aluminium borates, Glass Technol. 44 (2003) 96–100.
[9] D. Tauch, C. Rüssel, Glass-ceramics in the system $BaO/TiO_2(ZrO_2)/Al_2O_3/B_2O_3$ and their thermal expansion, J. Non-Cryst. Solids 353 (2007) 2109–2114.
[10] D. Tauch, C. Rüssel, Glass–ceramics with zero thermal expansion in the system $BaO/Al_2O_3/B_2O_3$, J. Non-cryst. Solids 351 (2005) 2294–2298.
[11] D. Tauch, C. Rüssel, Thermal expansion of glass–ceramics in the system $BaO/Al_2O_3/B_2O_3$, J. Non-cryst. Solids 351 (2005) 3483–3489.
[12] C. Lind, A.P. Wilkinson, Z. Hu, S. Short, J.D. Jorgensen, Synthesis and properties of the negative thermal expansion material cubic $ZrMo_2O_8$, Chem. Mater. 10 (1998) 2335–2337.
[13] I. Yamai, T. OOTA, Low-thermal-expansion polycrystalline zirconyl phosphate ceramic, J. Am. Ceram. Soc. 68 (1985) 273–278.
[14] M. Kerstan, C. Rüssel, Barium silicates as high thermal expansion seals for solid oxide fuel cells studied by high-temperature X-ray diffraction (HT-XRD), J. Power Sources. 196 (2011) 7578–7584.
[15] M. Kerstan, C. Thieme, M. Grosch, M. Müller, C. Rüssel, $BaZn_2Si_2O_7$ and the solid solution series $BaZn_{2-x}Co_xSi_2O_7$ ($0< x\leq 2$) as high temperature seals for solid oxide fuel cells studied by high-temperature X-ray diffraction and dilatometry, J. Solid State Chem. 207 (2013) 55–60.
[16] M. Kerstan, M. Müller, C. Rüssel, Thermal expansion of $Ba_2ZnSi_2O_7$, $BaZnSiO_4$ and the solid solution series $BaZn_{2-x}Mg_xSi_2O_7$ ($0\leq x\leq 2$) studied by high-temperature X-ray diffraction and dilatometry, J. Solid State Chem. 188 (2012) 84–91.
[17] C. Thieme, H. Görls, C. Rüssel, $Ba_{1-x}Sr_xZn_2Si_2O_7$-A new family of materials with negative and very high thermal expansion, Sci. Rep. 5 (2015) 18040.
[18] J.H. Lin, G.H. Lu, J. Du, M.Z. Su, C.-K. Loong, J.W. Richardson Jr., Phase transition and crystal structures of $BaZn_2Si_2O_7$, J. Phys. Chem. Solids 60 (1999) 975–983.
[19] C. Thieme, C. Rüssel, High thermal expansion in the solid solution series $BaM_{2-x}Ni_xSi_2O_7$ (M = Zn, Mg Co)-the effect of Ni-concentration on phase transition and expansion, J. Mater. Sci. 50 (2015) 3416–3424.
[20] C. Thieme, C. Rüssel, Very high or close to zero thermal expansion by the variation of the Sr/Ba ratio in $Ba_{1-x}Sr_xZn_2Si_2O_7$ – solid solutions, Dalton Trans. 45 (2016) 4888–4895.
[21] C. Thieme, G.B. Souza, C. Rüssel, Glass–ceramics in the system BaO–SrO–ZnO–SiO_2 with adjustable coefficients of thermal expansion, J. Am. Ceram. Soc. (2016) s1.
[22] C. Thieme, T. Waurischk, S. Heitmann, C. Rüssel, New family of materials with negative coefficients of thermal expansion: the effect of MgO, CoO, MnO, NiO, or CuO on the phase stability and thermal expansion of solid solution phases derived from $BaZn_2Si_2O_7$, Inorg. Chem. 55 (2016) 4476–4484.
[23] C. Rüssel, C. Thieme, Negative thermal expansion in $Ba_{0.5}Sr_{0.5}Zn_2SiGeO_7$, Materials 9 (2016).
[24] M. Kracker, C. Thieme, J. Hässler, C. Rüssel, Sol-gel powder synthesis and preparation of ceramics with high- and low-temperature polymorphs of $Ba_xSr_{1-x}Zn_2Si_2O_7$ (x = 1 and 0.5): A novel approach to obtain zero thermal expansion, J. Eur. Ceram. Soc. 36 (2016) 2097–2107.
[25] C. Thieme, M. Schlesier, C. Bocker, G. Buzatto de Souza, C. Rüssel, Thermal expansion of sintered glass ceramics in the system BaO–SrO–ZnO–SiO_2 and its dependence on particle size, ACS Appl. Mater. Interfaces 8 (2016) 20212–20219.
[26] L. Vladislavova, C. Thieme, C. Rüssel, The effect of ZrO_2 on the crystallization of a glass in the system $BaO/SrO/ZnO/SiO_2$: surface versus bulk crystallization, J. Mater. Sci. 52 (2017) 4052–4060.
[27] K.L. Narayan, K.F. Kelton, C.S. Ray, Effect of Pt doping on nucleation and crystallization in $Li_2O{\cdot}2SiO_2$ glass: experimental measurements and computer modeling, J. Non-Cryst. Solids 195 (1996) 148–157.
[28] P.W. McMillan, Glass-ceramics, 2nd edn, Academic Press, London, 1979.
[29] G. Rindone, Further studies of the crystallization of a lithium silicate glass, J. Am. Ceram. Soc. 45 (1962) 7–12.
[30] A. Arora, E.R. Shaaban, K. Singh, O.P. Pandey, Non-isothermal crystallization kinetics of ZnO–BaO–B_2O_3–SiO_2 glass, J. Non-Cryst. Solids 354 (2008) 3944–3951.
[31] M. Guedes, A.C. Ferro, J.M.F. Ferreira, Nucleation and crystal growth in commercial LAS compositions, J. Eur. Ceram. Soc. 21 (2001) 1187–1194.
[32] M. Ghasemzadeh, A. Nemati, A. Nozad, Z. Hamnabard, S. Baghshahi, Crystallization kinetics of glass-ceramics by differntial thermal analysis, Ceram.-Silikáty 55 (2011) 188–194.
[33] I.W. Donald, Crystallization kinetics of a lithium zinc silicate glass studied by DTA and DSC, J. Non-Cryst. Solids 345 (2004) 120–126.
[34] H.E. Kissinger, Reaction kinetics in differential thermal analysis, Anal. Chem. 29 (1957) 1702–1706.
[35] R. Wurth, M.J. Pascual, G.C. Mather, A. Pablos-Martin, F. Munoz, A. Duran, G.J. Cuello, C. Rüssel, Crystallisation mechanism of a multicomponent lithium alumino-silicate glass, Mater. Chem. Phys. 134 (2012) 1001–1006.
[36] S.D. Stookey, Catalyzed crystallization of glass in theory and practice, Ind. Eng. Chem. 51 (1959) 805–808.

5.3 Surface crystallization of low thermal expansion $Ba_{0.5}Sr_{0.5}Zn_2Si_2O_7$ from an 8 BaO/8 SrO/34 ZnO/50 SiO_2 glass

Michael Kracker, Liliya Vladislavova, Christian Thieme, Tilman Zscheckel,

Katrin Thieme, Thomas Höche and Christian Rüssel

RSC Advances, 2017, 7, 44834-44842

DOI: 10.1039/c7ra08587g

Authors	Michael Kracker	Liliya Vladislavova	Christian Thieme	Tilman Zscheckel	Katrin Thieme	Thomas Höche	Christian Rüssel
Conception of the research approach	X				X	X	X
Planning of examinations	X				X		X
Data collection	X		X	X	X		
Data analysis and interpretation	X		X	X	X		X
Writing the manuscript	X	X	X	X	X	X	X
Credits		0.5					

RSC Advances

PAPER

View Article Online
View Journal | View Issue

Check for updates

Cite this: *RSC Adv.*, 2017, **7**, 44834

Surface crystallization of low thermal expansion $Ba_{0.5}Sr_{0.5}Zn_2Si_2O_7$ from an 8 BaO·8 SrO·34 ZnO·50 SiO_2 glass

Michael Kracker, *[a] Liliya Vladislavova,[a] Christian Thieme,[b] Tilman Zscheckel,[a] Katrin Thieme,[a] Thomas Höche[b] and Christian Rüssel[a]

Received 3rd August 2017
Accepted 5th September 2017

DOI: 10.1039/c7ra08587g

rsc.li/rsc-advances

Thermal treatment of a glass with the composition 8 BaO·8 SrO·34 ZnO·50 SiO_2 has led to the crystallization of a $Ba_{1-x}Sr_xZn_2Si_2O_7$ solid solution. This solid solution has a very low or even negative thermal expansion. The glass system possesses a strong tendency towards surface crystallization, while bulk nucleation is negligible. The surface crystallization behavior was characterized using differential scanning calorimetry, X-ray diffraction, optical microscopy, and scanning electron microscopy including electron backscatter diffraction. The observed morphology strongly depends on the type of surface pretreatment. Two different surface qualities were compared: a polished surface and a surface obtained by cutting. The as-cut surface shows a significantly enhanced nucleation rate, which leads to smaller crystals caused by a growth selection near to the surface. The crystal orientation related to the inward growth starting from the surface was successfully investigated by EBSD, for the first time, using a recently reported crystal structure. The crystals show a preferred orientation of the *c*-axis perpendicular to the surface; this has a significant effect on the crack formation.

Introduction

The most common characteristic of thermal expansion is that materials tend to expand with heating.[1] By contrast, materials possessing zero-thermal expansion (ZTE) or even a negative-thermal expansion (NTE) behavior are scarce.[2] Representatives of this latter type of material, such as beta quartz, spodumene or beta-eucryptite are all non-cubic. Due to crystal symmetry, coefficients of thermal expansion depend on crystallographic direction and typically have positive values along two directions, and only negative values along one specific crystallographic direction. The advantage, however, is that these phases could be crystallized from glasses based on lithium alumosilicate in the former cases. These materials are of great economic importance[3] and consequently also provoke major scientific interest, particularly on considering the intrinsic reasons for unusual thermal expansion processes. There are also cubic phases such as ZrW_2O_8 that show advantageous, isotropic NTE behavior.[4] Unfortunately, from these cubic phases, materials with zero thermal expansion are difficult to prepare, and the usual method of glass crystallization is not suitable since these phases are not glass forming.

Recently, a new oxidic crystal phase corresponding to a solid solution containing Ba, Sr, Zn, and Si was reported.[5] This solid-solution with the composition $Ba_{1-x}Sr_xZn_2Si_2O_7$ (BSZS) also shows negative thermal expansion behavior, although the same phase without Sr is rather well known for very high thermal expansion coefficients.[6] The Sr-free $BaZn_2Si_2O_7$ shows a phase transition to a high temperature phase (HT phase), which already shows negative thermal expansion, at 280 °C.[6] A substitution of more than 10% of Ba by Sr leads to the stabilization of a crystal structure, comparable to the as mentioned HT-phase, down to room temperature;[5] hence, the negative thermal expansion behavior could also be observed at room temperature. Unfortunately, this crystalline phase shows an unfavorable and large anisotropy, thus the CTE in different crystallographic directions varies between around -30×10^{-6} K^{-1} (for the crystallographic *b* axes) and $+20 \times 10^{-6}$ K^{-1} (for the crystallographic *c* axes) in a temperature range from 30 to 600 °C.[7] However, in this case, not only are the thermal properties decisive but also the manufacturing process of the glass-ceramic. A powder with the expected properties could be prepared by a common solid state reaction, but in contrast, the preparation of a ceramic body leads to problems caused by the large anisotropy of the crystal phase.[8] Therefore, in order to avoid mechanical stresses, the crystals should be small.[9,10] It has already been shown that the preparation of single phase BSZS materials is possible using sol–gel derived powders.[8] An alternative synthesis route involves precipitating the expected phase from a glass; however, the respective glasses show a high

[a]Otto-Schott-Institut für Materialforschung, Jena University, Fraunhoferstr. 6, 07745 Jena, Germany. E-mail: kracker.michael@googlemail.com; Fax: +49 3641 948502; Tel: +49 3641 98507

[b]Fraunhofer-Institut für Mikrostruktur von Werkstoffen und Systemen IMWS, Walter-Hülse-Straße 1, 06120 Halle (Saale), Germany

tendency to surface crystallization, which makes the preparation of bulk materials challenging.[11] A detailed characterization and understanding of the mechanisms of phase formation and crystal growth at the surface will help to improve the material properties of BSZS glass-ceramics.

The present glass system containing 8 mol% BaO, 8 mol% SrO, 34 mol% ZnO, and 50 mol% SiO_2 tends, in comparison to many glasses without nucleating agents, toward surface crystallization caused by the preferred formation of nuclei at the surface.[12]

For this purpose, the growth behavior of the negative and strongly anisotropic crystal phase at the surface of a glass has to be examined. Crystal orientation, growth morphology, the effect of the large anisotropy as well as the nucleation behavior will be described, also with respect to future volume crystallization experiments, because the growth behavior is also decisive in this case.

Experimental procedure

The glass was melted from reagent grade raw materials without further purification. The used raw materials were ZnO, $BaCO_3$, $SrCO_3$, ZnO, and SiO_2. The calculated batch with the composition 8 BaO·8 SrO·34 ZnO·50 SiO_2 (mol%) was heated in an induction furnace in a Pt crucible up to 1420 °C and kept for 2 h while stirring. The glass was cast in an Inconel mold coated with a boron nitride film and subsequently heated to 700 °C. The solidified glass was transferred to a muffle furnace also preheated to 700 °C. The furnace was immediately switched off to allow the glass block to cool down slowly.

A proper amount of the cooled glass block was crushed and separated into different particle size fractions to investigate the thermal properties as well as the crystallization behavior. For this purpose, differential scanning calorimetry (DSC) was conducted with a Linseis DSC Pt 1600. Glass powders (60 ± 0.1 mg) with different grain size fractions were placed into Pt crucibles, and heated to 1000 °C at 10 K min^{-1}.

In order to investigate the crystallization behavior, the samples were cut into small discs with a diameter of 10 mm and a thickness of 3 mm. One side of the obtained samples was polished using a cerium oxide containing lapping abrasive with a mean grain size of 1 μm. The other side of the sample remained unpolished. The surface properties were determined with a Zeiss Axio Imager Z1m equipped with a LSM 700 laser-scanning module. The image processing was performed using the Confomap software.

According to the results from the DSC measurements, crystallization was carried out in a muffle furnace at temperatures of 750, 770, and 790 °C for several hours.

To perform microstructure analyses of the volume, the crystallized samples were embedded in a polymer matrix and subsequently cut perpendicular to the former sample surface and then polished. A Jeol JSM 6510 LV equipped with a semiconductor backscattered electron detector was used to study the crystals grown from the surface into the bulk.

In order to investigate the phase composition, an X-ray diffractometer, Rigaku MiniFlex 300, with Ni-filtered CuKα radiation was used. The polished and subsequently heat treated surfaces of bulk samples were measured in Bragg–Brentano-geometry.

Density measurements were performed with a Micromeritics AccuPyc 1330 helium pycnometer. The ultrasound technique was used for the determination of elastic constants, *i.e.*, the Young's Modulus and the Poisson's ratio. The respective samples had a cylindrical shape with a diameter of 15 mm and a length of 30 mm; front faces were made parallel. From the ultrasound velocities of a longitudinal (5 MHz) and a transversal (4 MHz) probe, the elastic constants could be calculated as described in ref. 13.

For the thermal expansion behavior, a Netzsch Dil 402 PC dilatometer equipped with a fused silica sample holder was used by applying a heating rate of 5 K min^{-1}. A glass cylinder with a diameter of 5 mm and a length of 10 mm was used as the sample.

Table 1 Basic properties of the base glass: Young's modulus, density, glass transition temperature, T_g, T_{onset} of surface crystallization, the peak maximum of the exothermic peak, T_{max}, CTE, dilatometric softening temperature

Property	Value	Error	Method
Young's modulus [GPa]	84.0	±1.5	Ultrasonic technique
Density [g cm^{-3}]	3.832	±0.01	He pycnometer
T_g [°C]	677	±5	DSC
	674	±5	Dilatometry
T_{onset} of surface crystallization [°C] for various grain size fractions	801 (< 25 μm)	±5	DSC
	874 (bulk)		
T_{max} of surface crystallization [°C] for various grain size fractions	826 (< 25 μm)	±5	DSC
	939 (bulk)		
CTE [10^{-6} K^{-1}] for different temperature intervals	6.76 (30–600 °C)	±0.1	Dilatometry
	6.69 (100–400 °C)		
	7.54 (400–600 °C)		
Dilatometric softening temperature [°C]	723	±5	Dilatometry
Viscosity	$A = -2.967$ dPa s	±0.070	Beam bending and
	$B = 4074$ °C	±75	rotation viscometer
	$T_0 = 417$ °C	±4.00	

View Article Online
RSC Advances Paper

The viscosities were measured by a beam bending viscometer Bähr VIS 401 ($10^{8.5}$ to $10^{12.5}$ dPa s), supplying a heating rate of 10 K min^{-1} and using glass bars with the dimensions 5 × 5 × 50 and 5 × 4 × 50 mm^3. In order to increase the temperature range in which the beam bending viscosities could be determined, three different loads (10, 50, and 250 g) were used. Moreover, measurements in the low viscosity range $10^{1.2}$ to 10^5 dPa s were performed using a rotation viscometer Bähr VIS 403. For this purpose, different rotation rates (10 and 250 rpm) were used and a cooling rate of 5 K min^{-1} was applied. The determined viscosities were fitted using the Vogel–Fulcher–Tammann equation (VFT-equation).

The crystal morphology was studied on carbon coated samples using a Scanning Electron Microscope (SEM) JEOL 7001 F. The crystal orientation studies were performed by the electron backscatter diffraction (EBSD) technique as a module of the SEM. A Digiview 3 EBSD-camera was used to collect the diffraction patterns, which were interpreted using the software packages TSL OIM Data Collection and Data Analysis 5.31. The patterns were obtained at an acceleration voltage of 20 kV with a working distance of 15 mm. The scan step size was set to 0.25 μm. In order to increase the fraction of reliably indexed data points, Confidence Index (CI) standardization and fit standardization clean-up procedures were applied to the dataset with grain angle tolerance = 5 and minimum CI ≥ 0.1 as parameters. Following this, only points with a CI ≥ 0.1 were used for visualization. The Image Quality (IQ) was used as gray scale in the background, where the gray value increases with crystal perfection from black to white (grain boundaries appear dark, homogeneous monocrystalline regions appear bright). The reference direction of the inverse pole figure (IPF) color code is [001], *i.e.* the normal of the sample surface.

Results

The basic properties of the glass are summarized in Table 1. DSC analyses of glass powders with different grain sizes (see Fig. 1a and b) show the crystallization behavior. The glass transition temperature, which could hardly be seen in Fig. 1, is at 677 °C. The bulk sample shows an exothermal peak at 939 °C (onset at 874 °C); the exothermic peak shifts to lower temperatures and becomes sharper with decreasing grain size. The upper right graph of Fig. 1 shows this behavior in more detail. The bulk values as well as the values for grain sizes below 25 μm are not included in the upper right graph, as the values could not be quantified. For particle sizes below 25 μm, the crystallization peak occurred at 826 °C (onset at 801 °C), which was the lowest observed value. The glass samples were thermally treated at temperatures of 750 °C, 770 °C, and 790 °C, which is somewhat below the lowest crystallization onset of 801 °C. The viscosities determined by beam bending and rotation viscometry were fitted in the entire temperature range using the Vogel–Fulcher–Tammann (VFT)-equation. The rotation viscometry data obtained by the measurement using a rotation rate of 10 rpm were not included in this fit. The results of the beam bending viscometry measurements are shown in Fig. 1 along with the VFT-fit (black solid line). The viscosities were extrapolated for higher temperatures marked by the black dashed line. It is apparent that the choice of the load is decisive for the measurable temperature range. In the inset, the results of the rotation viscometry are displayed. Here, it is obvious that the

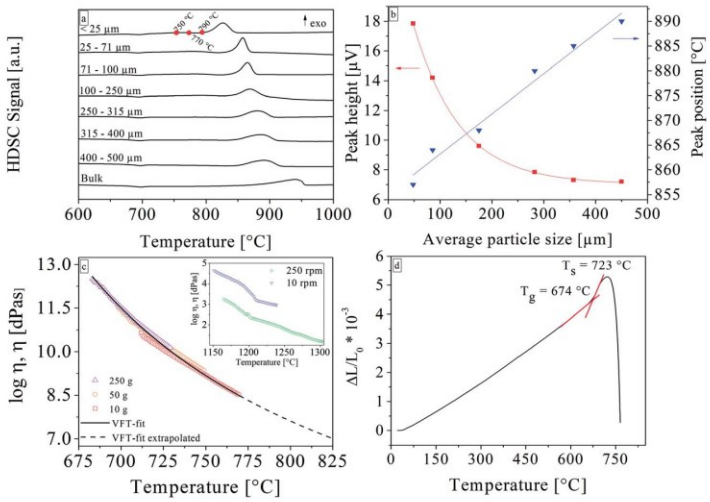

Fig. 1 Results from thermal analyses. (a) DSC profiles of glass samples with different particle sizes and of a compact glass sample. Red dots indicate the selected experimental conditions for the crystallization steps in the present study. (b) Analysis of the DSC curves; peak height (red circles) and peak maximum temperature (blue triangle), both plotted over the particle size. (c) Results from viscometry. The main graph shows the beam bending viscosities dependent on the temperature and fitted with VFT-equation. In the inset, the results from rotation viscometry are also displayed as a function of temperature. (d) Results from dilatometry.

viscosities determined by a measurement using 10 rpm are about 1.5 orders of magnitude higher than those derived from the 250 rpm measurement. Normally, the curves should overlap and solely the measurable temperature range should be different. Moreover, there are several kinks in the viscosity curves. The deviations in the viscosity as well as the kinks were reproduced by repeated measurements using different rates.

The surface morphology of an untreated as-cut surface (directly after the cutting) is presented in Fig. 2. At the top, a reconstructed 3D model calculated from an LSM image stack is shown. After cutting, areas with a high number density of sharp edges and almost smooth shell-like areas are observed. The height scale was established regarding the lowest point in the measured area and is in a range up to 16 μm. The two gray lines (line 1 and line 2 in the upper panel) represent the extracted profiles shown at the lower right side. Additionally, an SEM micrograph of the sample surface is shown at the lower part.

The resulting thickness of the crystal layer was determined using SEM micrographs of cross sections. Fig. 3 shows the resulting thickness of the crystalline layer as an effect of the surface pretreatment, temperature, and treatment time. As expected, the thickness and the growth rate of the crystal layer increase with time and temperature. The thickness of the crystallized layer is also higher for the as-cut surfaces. It must be noted that crystalline layers below approx. 30 μm are not fully closed. At the latter depth, small isolated crystals appear. The largest distance of these crystals perpendicular to the surface is considered as layer thickness. In the case of samples with polished surfaces, subsequently crystallized at 790 and 770 °C, induction times for the crystallization process are observed as indicated by the linear regressions. By contrast, for as-cut surfaces, at an annealing time of 0 h (the heating program is just finished), crystals are present and the layer thickness is above zero.

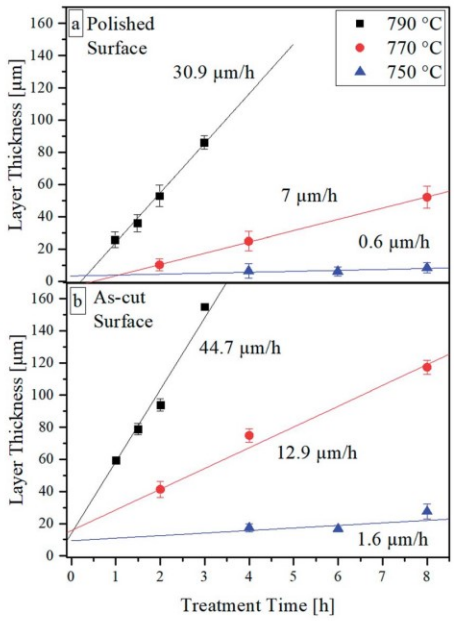

Fig. 3 Crystal growth velocities at different annealing temperatures parallel to (a) a polished surface, (b) a rough surface.

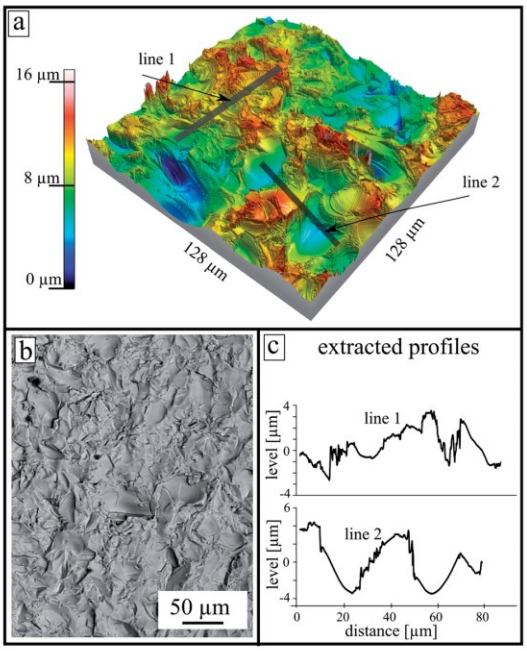

Fig. 2 Surface morphology of a thermally untreated rough surface after cutting, and after use in further experiments. (a) Reconstructed 3D surface model calculated from an LSM image stack. (b) Corresponding SEM micrograph of the same sample. (c) Extracted surface profiles from the indicated gray lines at the upper panel.

The XRD pattern at the bottom of Fig. 4 illustrates the theoretical peak positions and the relative intensities of a crystal with the composition $Ba_{0.6}Sr_{0.4}Zn_2Si_2O_7$. For all bulk samples, the former polished surface was measured by XRD. The untreated and polished surfaces show one broad maximum at a diffraction angle of around 30°. After heat treatment at 750 °C for 4 h, additional peaks according to the theoretical positions are observed, but the broad peak at 30° persists. After treatment at an elevated temperature of 790 °C for 2 h, the relative peak intensities increase, the shape of the pattern becomes sharper, and additional peaks are observed for both the powdered and bulk samples. However, the broad maximum is no longer visible for the bulk sample heat treated at 790 °C for 2 h. All apparent peaks could be attributed to the theoretical peak positions displayed in the lower part of Fig. 4.

The crystallization behavior of the glass was further studied by SEM using a backscatter electron detector. In order to compare the crystallization in different directions, plane-view samples were considered as well as the growth behavior

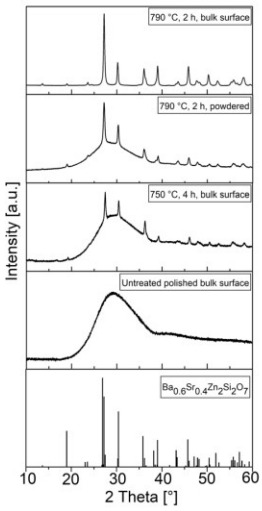

Fig. 4 XRD patterns of surface crystallized bulk and powdered samples at different stages of thermal treatment. The investigated surface was polished before thermal treatment. The lower diffractogram shows the peak positions of a phase with the crystal structure of the HT-phase of $BaZn_2Si_2O_7$ and the exact composition $Ba_{0.6}Sr_{0.4}Zn_2Si_2O_7$ according to ICSD 429938.

perpendicular to the surface by inspection of cross sections. In Fig. 5, a comparison of plane views heat treated at different temperatures and different surface pretreatments are shown. In Fig. 5a, after a heat treatment at 750 °C for 4 h, isolated crystals with sizes of approximately 10 μm are observed. Some of these crystals appear sharp with a clear ray-like morphology and others have a bright rim and generally appear blurred. However, in Fig. 5b, a fully crystallized surface consisting of grains with sizes above 100 μm is observed after heat treatment of 790 °C for 2 h. Also, some cracks at the assumed center of the crystals are seen. Additionally, two different morphologies are present. Sharp, ray-like structures and a blurred area in the upper part of the micrograph were observed. Near the blurred morphology a deepening and/or cavity is located. This impression is enhanced using a superimposed topography mode available in the microscope acquisition software. The lower images Fig. 5c and d are recorded from samples thermally treated at 770 °C for 4 h using different surface roughness. At the initially polished surface, just a few partly isolated crystals with size of around 50 μm were formed. In contrast, more crystals were formed at the as-cut surface. Crystal sizes observed were comparable to those of the polished surface. Some small areas at the surface were not covered with crystals.

As already mentioned above, the crystallization was also studied in samples cut perpendicular to the surface. Fig. 6 compares the surface crystals at an early stage of growth. Both SEM micrographs are presented with the same magnification. The left image shows a plane view of a glass surface after heat treatment at 750 °C for 4 h. Isolated crystals with a morphology comparable to that in Fig. 5 could be identified. In contrast, a cross-section of an equally treated sample is shown on the right panel. Only one crystal could be seen in the whole cross section area. The black area in the upper part of the micrograph belongs to the embedding polymer matrix related to the cross-section preparation method.

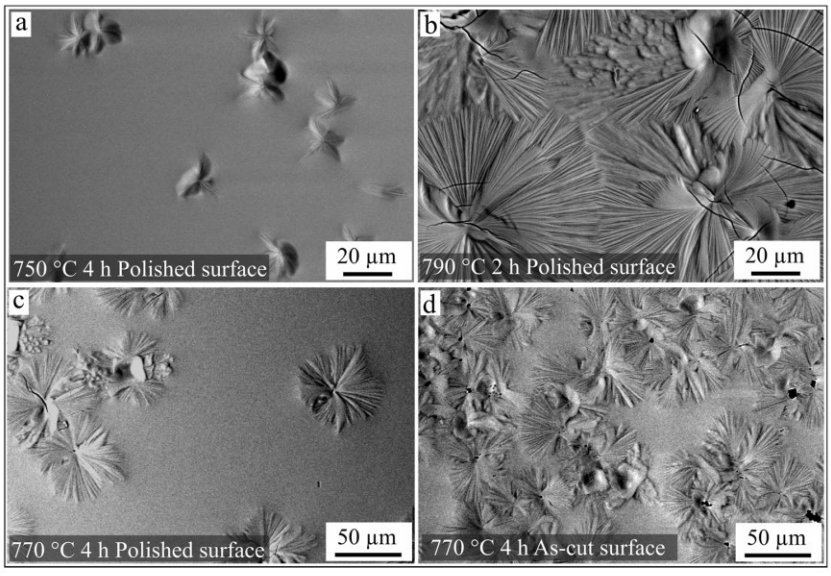

Fig. 5 SEM micrographs of samples heat-treated at different temperatures, and with surfaces having different pretreatments. (a) Polished surface heat treated at 750 °C for 4 h; (b) polished surface heat treated at 790 °C for 2 h; (c) polished surface heat treated at 770 °C for 4 h; (d) as-cut surface (compare with Fig. 2) heat treated at 770 °C for 4 h.

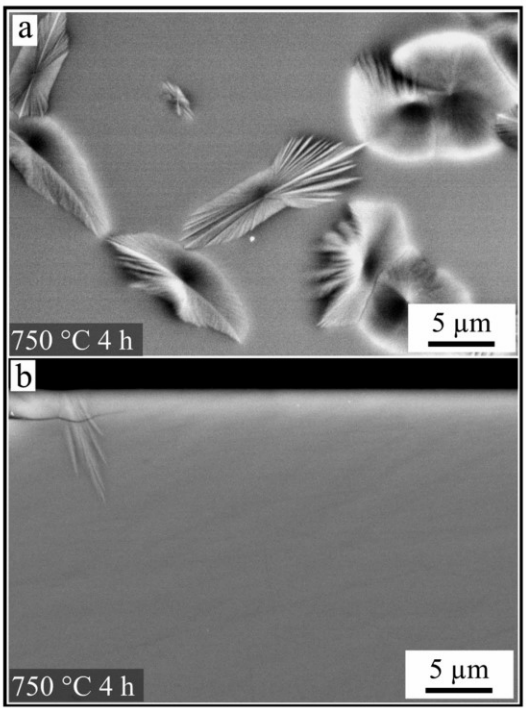

Fig. 6 Microstructures of a polished surface after a heat treatment at 750 °C for 4 h. Comparison of crystals observed in plane view (a) and corresponding cross section (b) at the same magnification.

Fig. 7 provides an overview of the crystal morphologies of cross sections dependent on the heat treatment and the initial surface conditions. Fig. 7a shows the cross section of a polished sample surface, annealed at 750 °C for 6 h. Some isolated crystals with sizes between 2 and 6 µm are shown. In Fig. 7b, an SEM micrograph of the same sample but with an as-cut surface is depicted. A closed crystalline layer with an average thickness of 15 µm has formed. The resulting morphologies after thermal treatment at higher temperatures (790 °C for 1.5 h) are illustrated in Fig. 7c and d for a polished and an as-cut surface, respectively. The crystals grow from a former polished surface (c) to form a closed layer; however, the thickness varies between 20 and 40 µm. In the case of the as-cut surface (see Fig. 7d), many more crystals were formed at the surface and the crystals were longer and thinner. In contrast to Fig. 7b and c, the overall thickness of the crystalline layer varied by only a few microns.

In order to investigate how crystals formed at the surface were oriented, and to what extent the cracks correlated with crystal orientation, combined EBSD-EDXS measurements were performed at the cross section on a sample crystallized from a polished surface at 790 °C for 1.5 h. Fig. 8 shows an SEM micrograph superimposed with a combined IQ and IPF-map, as well as the elemental analysis, containing the signals of Ba, Si and Zn. The collected EBSD-patterns and EDX-Spectra originate from positions within the black frame. The patterns of this sample were indexed using the ICSD data file no. 429939 of $Ba_{0.6}Sr_{0.4}Zn_2Si_2O_7$. The colors of the IPF map represent the crystal direction normal to the plane of image. Within the three large ray-like domains, the orientation is similar and changes only gradually. The color changes indicate stresses in the crystals. Due to the small structures in combination with the stresses, the general IQ-value is quite low and not all patterns from the crystalline regions could be indexed reliably. Orientations of some single structures were visualized by white unit cells, where the orientations of the *c*-axes are highlighted by labeled white arrows. Red dots in the center of the unit cells mark the corresponding data points. In the three ray-like

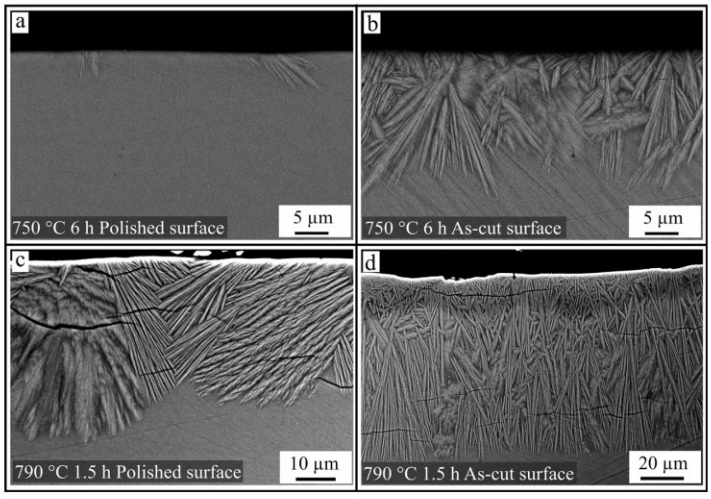

Fig. 7 SEM micrographs of cross sections of glass samples heat treated at different temperatures, times and surface pretreatments. (a) Polished surface, 750 °C for 6 h; (b) as-cut surface, 750 °C for 6 h; (c) polished surface, 790 °C for 1.5 h; (d) as-cut surface, 790 °C for 1.5 h.

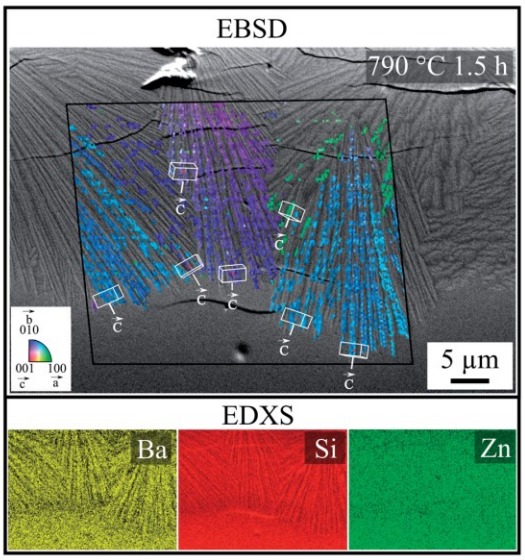

Fig. 8 SEM micrograph and combined EBSD-EDXS measurement of a cross section after crystallization for 1.5 h at 790 °C, stemming from an as-cut surface. The combined IQ and IPF map of the EBSD scan are superimposed onto the SEM micrograph to illustrate orientations relative to the image plane. Crystal orientation and *c*-axes are additionally marked. The black frame represents the scanned area. Lower part: simultaneously measured elemental analysis of the combined EBSD-EDXS scan.

domains, the *c*-axis is oriented parallel to the length axis of the thin sub crystals and perpendicular to the cracks at the same time. The elemental analysis shows only small differences in the chemical composition of the glass and the crystal. The contrast and brightness of the elemental distribution map was adapted for a suitable recognizability. The ray-like structure was also reflected in the distribution maps of Ba and Si and it seems that the needles were enriched with Ba, whereas Si was enriched beyond the needles, and the distribution of Zn is homogenous.

Discussion

The crystallization behavior was studied first by thermal analysis (DSC). A change in the surface to volume ratio of the glass powder by using smaller grain sizes while keeping the mass constant, leads to a shift in the crystallization peak and the crystallization onset temperature towards lower temperatures.[14–16] Furthermore, smaller particle sizes also lead to a higher and sharper exothermic peak. With decreasing grain size, the crystallization starts at lower temperatures because the ratio surface to volume increases. A higher surface area leads to more nucleation processes and thus to a more pronounced exothermic reaction. These results prove that this glass system crystallizes from the surface.

The DSC results from the powder fraction smaller than 25 µm and the bulk sample are not included in Fig. 1b because the mean particle size could not be quantified. Nevertheless, it should be noted that the onset for the grains smaller than 25 µm reveals a strong additional shift towards lower temperatures. These are the lowest crystallization temperatures found in all DSC profiles. The temperature attributed to the onset of the exothermic peak is 801 °C and therefore temperatures slightly below this value were chosen for the static crystallization experiments. This was done in order to study the initial stages of crystallization, to get a better insight into the underlying processes and also to describe an easy to handle procedure with respect to a further technical application.

The results from the viscosity measurements are also shown in Fig. 1. The fact that a higher rotation rate leads to viscosities drastically lower than those of the measurements using the lower speed indicates the non-Newtonian behavior of the glass melt. Strictly speaking, the viscosity does not follow the VFT-equation and therefore the viscosities were only extrapolated up to 820 °C. The kinks in the rotation viscometry curves could be related to crystallization during cooling of the melt. This behavior was previously reported for glass ceramic melts of lithium disilicate[17] and fluoroapatite.[18,19]

Two different surface pretreatments were used to describe the effect of surface roughness. The samples were cut by a diamond saw and subsequently polished. In order to compare the crystallization behavior, one side of the sample retained the typical rough structure of an as-cut surface. Fig. 2 shows such a surface morphology measured by LSM. The surface shows areas with a high number of edges, and almost smooth areas. This is a typical structure of a brittle fracture due to the glass cutting step because if the formed stresses in the glass matrix are too high during the cutting process, cracks are formed that propagate into the material. These cracks create new surfaces that are then very smooth and reveal a shell-like structure, called a conchoidal fracture.[20] The cutting step creates two different types of surfaces, one with a high number density of edges, tips and striae caused by the diamond saw, as well as the described smooth clamshell marked fractures. Both types have a different effect on the crystallization properties[21] as discussed below.

Most glass systems described in literature tend to nucleate and crystallize at their surfaces. In many systems, the formation of nuclei is strongly preferred at the surface. The reason for this behavior is frequently considered to be due to the smaller energy required for elastic deformations.[21] In this sense, it is not surprising that an as-cut surface leads to a higher crystal number density than a polished surface. Such behavior has been discussed in detail in glasses such as stoichiometric cordierite.[21,22] At a rough surface, more sites exist where the required energy for material displacement is further reduced, *i.e.*, at an edge or at a tip (compare with Fig. 2). Furthermore, Fig. 3 exactly represents this behavior. Therefore, nucleation and crystal growth start earlier and the total number of crystals is higher than at a polished surface (see also Fig. 7). Also, the possibility of a smaller interfacial energy being required if the interfacial energy crystal/glass is replaced by the interfacial energy crystal/gas atmospheres should not be disregarded.

A higher number density of nuclei leads to a higher number of growing crystals and consequently, the crystals should

preferably grow with their fastest growing axis perpendicular to the surface because otherwise, the crystals, which have another orientation hinder each other during growth. Thus, at the same growth velocity, a somewhat thicker crystal layer should be formed.

Finally, since crystal growth is usually controlled by diffusion, higher temperatures should result in higher crystal growth velocities.

The theoretical peak positions of the desired crystal phase, which possess a negative thermal expansion, are shown in the pattern at the bottom of Fig. 4. Before thermal treatment, the sample shows just a broad halo at around 30°, which corresponds to the glass structure. Discrete peaks at other 2θ values are not observed and there are therefore no indications of residual raw materials or spontaneous crystallization during cooling of the glass melt. A heat treatment at 750 °C for 4 h results in numerous sharp diffraction peaks, which all are attributable to the desired BSZS crystal phase. Nevertheless, the halo at 30° is still visible. The crystalline layer is therefore just not thick enough to fully absorb the diffracted signals for the underlying glass. In contrast, the amorphous background signal completely disappears after heat treatment at 790 °C for 2 h. This agrees with the observation that the glassy structure could also be seen again if the same sample is powdered and examined. This is due to the fact that the crystals grown at the surface are mixed with the residual glass between the layers.

Since the structures in the powdered samples are comparable to those recorded from the sample surface, it could be concluded that the crystal phase growing into the glass matrix is the same as that grown at the glass surface.

Furthermore, additional peaks that could be attributed to other phases than the BSZS solid solutions are not observed.

The growth morphology at the top of the surface is shown in Fig. 5. After crystallization at a temperature of 750 °C maintained for 4 h, small isolated crystals were grown. In contrast, after crystallization at 790 °C, a few huge crystals were observed and a residual glassy phase in between the crystals could no longer be observed; the different numbers of the crystals at different treatment temperatures is striking. Obviously, at a crystallization temperature of 750 °C, the nuclei have more time to form, whereas at 790 °C, the crystal growth velocity is much higher and the complete surface is crystallized before numerous new nuclei may have formed. Supposedly, the nucleation rate does not increase with temperature in the same manner as the crystal growth velocity increases. Thus, the number of formed crystals is much higher after thermal treatment at 750 °C. This behavior was expected, following the nucleation and crystallization theory of glasses, where the temperature attributed to the maximum nucleation rate is lower than the temperature where a maximum crystal growth velocity is observed.[23,24] The effect of the increased nucleation rate at a rough surface is shown in Fig. 5c and d. The numbers of the formed crystals are much higher for a surface that was rough. Caused by the cutting procedure, surface areas with high densities of edges, tips and fine glass grains are formed. These sites are known to result in a high nucleation rate because of the high number density of energetically favorable places.[21,25] In contrast, a cutting morphology also reveals areas where crack propagation into the bulk occurs. These places are very smooth and lead to a very low nucleation rate. This could be a possible explanation for the inhomogeneous surface coverage shown in Fig. 5d.

A further special aspect of the crystallization is presented in Fig. 6. While a micrograph of the surface shows a fairly large number of crystals, in the cross section only one crystal is observed. This might be explained as follows: after a nucleus is formed, it grows along the surface with a depth of only a few nanometers. These crystals could not therefore be observed in the micrograph of a cross section, since the immediate surface layer could hardly be characterized by SEM, due to the superimposed edge effect. Hence, it could be assumed that the first formed crystals are aligned with their fastest growing axes parallel to the surface.

Fig. 7 shows the resulting morphology as an effect of the surface treatment for two different temperatures. The polished surface of the sample crystallized at 750 °C shows some isolated crystals. In comparison, at the as-cut surface, the number of grown crystals is much higher and consequently, due to the lack of space, the crystals are smaller. The surface roughness initiates nucleation caused by numerous, energetically more favorable positions at the edges and tips of the glass/atmosphere interface.[17] However, the roughly cut surface also has very smooth areas caused by the conchoidal fracture of the glass. These areas do not contribute to the increased nucleation rate. Hence, the enhanced nucleating behavior does not result in a homogeneous distribution of the crystals at the surface (see Fig. 2).

The effect of as-cut and polished surfaces at a higher temperature (790 °C) is shown in Fig. 7c and d. If the crystallization temperature is increased to 790 °C, crystals grown from a polished surface become very large and reveal a ray-like morphology. Because of the large size of these structures, the formed crystal layer is uneven in thickness and the crystallized regions show a high number of cracks. In the case of the as-cut surface, the fine granular growth continues as already shown in Fig. 7b. However, the crystal size of the whole structure increases during growth into the bulk. It follows that in the regions near the surface, a growth selection takes place due to the large number of crystals; thus, at some distance from the surface, only a few crystals remain. Nevertheless, the resulting morphology is still narrower than that grown from the polished surface.

It has already been mentioned that the formed crystal phase has a large anisotropy concerning the thermal expansion along individual crystallographic axes. The thermal expansion is very large in the direction of the crystallographic *c*-axis, while it is strongly negative in the direction of the *b*-axis.

According to the EDXS map, the difference in chemical composition is low; hence, the grown crystals have a similar chemical composition. For this reason and in agreement with the XRD-patterns (see Fig. 4), ICSD file no. 429939 ($Ba_{0.6}Sr_{0.4}Zn_2Si_2O_7$) is used for the EBSD indexing process. Furthermore, only this ICSD file results in the reliable indexing of the EBSD-patterns. As shown by EBSD, the orientation of the crystals is

not statistical, but oriented. During growth of the crystals into the bulk, they become more and more oriented with their *c*-axes perpendicular to the surface, which is a strong hint at growth selection.

During the formation of crystals at the surface at temperatures well above the glass transition temperature of the glass, the glass-ceramic material should be free of stress because the glassy matrix is able to relax stress. During cooling, the contraction of the crystals is largest perpendicular to the surface, which is caused by the highest CTE in the direction of the crystallographic *c*-axis. It is therefore not surprising that the direction of the cracks is correlated to the strongly contracting crystallographic axis; hence, the crack is oriented according to the ray-like growing morphology, as seen in Fig. 7c. For this purpose, an EBSD analysis was carried out to determine the orientation of the grown crystals. Fig. 8 shows a superimposed SEM micrograph containing the information on the crystal orientation. Confirming this approach, the ray-like domains show the discrete correlation between *c*-axis and morphology.

Conclusions

The surface crystallization behavior in a system with the composition 8 BaO·8 SrO·34 ZnO·50 SiO_2 has been studied using DSC, XRD, SEM, and LSM. Two different surface conditions where compared. On the one hand, a well-polished surface and on the other hand a surface as obtained after cutting. The influence of the surface pretreatment is correlated to size, morphology, frequency, and crystal growth rate. It has been found that not only does the number density of nuclei increase, but also the growth morphology is decisively changed if the surface remains unpolished. The growth rate is apparently higher, but this could be attributed to growth selection and the resulting more homogeneous layer thickness within the first microns. Also at the as-cut surfaces, differences in the number density of nucleation sites were found and explained by the presence of conchoidal fracture morphologies. In contrast to the polished surface, the crystals become larger and spread out simultaneously. Thus, a non-uniform layer thickness and surface coverage was obtained.

A special growth mechanism was found where in the early stages of growth, crystals were spread parallel to the surface and afterwards they started growing into the volume of the glass; hence, the growth along the surface might initially be preferred.

Due to the strong anisotropy of the thermal expansion of the crystallized phase, the obtained glass ceramic is interspersed with cracks. The present study is the first where EBSD is successfully applied on glass ceramics with the crystal structure of $Ba_{0.6}Sr_{0.4}Zn_2Si_2O_7$. It has been shown that the propagation direction of the cracks is correlated to the grown *c*-axes and their thermal expansion. Hence, the cracks are perpendicular to the *c*-axis, which is the crystallographic direction with the highest coefficient of thermal expansion. As oriented surface crystallization is found along the *c* axis of BSZS, cracks are mainly aligned parallel to the surface.

Conflicts of Interest

There are no conflicts of interest to declare.

Acknowledgements

This study was funded by the German Federal Ministry of Education and Research under the grant numbers 03VP01701 and 03VP01702.

References

1 M. A. H. Gepreel, *Key Eng. Mater.*, 2011, **495**, 62–66.
2 J. R. Salvador, F. Guo, T. Hogan and M. G. Kanatzidis, *Nature*, 2003, **425**, 702–705.
3 K. Bauch, *Low Thermal Expansion Glass Ceramics*, Springer-Verlag Berlin Heidelberg, Berlin, Heidelberg, 2005.
4 T. A. Mary, J. S. O. Evans, T. Vogt and A. W. Sleight, *Science*, 1996, **272**, 90–92.
5 C. Thieme, H. Görls and C. Rüssel, *Sci. Rep.*, 2015, **5**, 18040.
6 J. Lin, G. Lu, J. Du, M. Su, C.-K. Loong and J. Richardson, *J. Phys. Chem. Solids*, 1999, **60**, 975–983.
7 C. Thieme and C. Rüssel, *Dalton Trans.*, 2016, **45**, 4888–4895.
8 M. Kracker, C. Thieme, J. Häßler and C. Rüssel, *J. Eur. Ceram. Soc.*, 2016, **36**, 2097–2107.
9 Y. Ohya, Z.-e. Nakagawa and K. Hamano, *J. Am. Ceram. Soc.*, 1987, **70**, C-184–C-186.
10 S. Sakka, Applications of Sol-Gel Technology, *Handbook of Sol-Gel Science and Technology. Processing, characterization and applications*, Kluwer, Boston [u.a.], 2005, vol. 3.
11 L. Vladislavova, C. Thieme and C. Rüssel, *J. Mater. Sci.*, 2017, **52**, 4052–4060.
12 M. O. Prado, M. L. F. Nascimento and E. D. Zanotto, *J. Non-Cryst. Solids*, 2008, **354**, 4589–4597.
13 U. Veit and C. Rüssel, *Ceram. Int.*, 2016, **42**, 5810–5822.
14 V. Reynoso, K. Yukimitu, T. Nagami, C. Carvalho, J. Moraes and E. Araújo, *J. Phys. Chem. Solids*, 2003, **64**, 27–30.
15 M. J. Pascual, C. Lara and A. Durán, *Phys. Chem. Glasses: Eur. J. Glass Sci. Technol., Part B*, 2006, **47**, 572–581.
16 C. S. Ray and D. E. Day, *Thermochim. Acta*, 1996, **280–281**, 163–174.
17 J. Deubener and R. Brückner, *J. Non-Cryst. Solids*, 1997, **209**, 96–111.
18 Y. Z. Yue, G. Carl and C. Rüssel, *Glass: Sci. Technol.*, 1999, **72**, 67–75.
19 Y. Yue, C. Moisescu, G. Carl and C. Rüssel, *Phys. Chem. Glasses*, 1999, **40**, 243–247.
20 D. R. Askeland and W. Fahland, *Materialwissenschaften*, Spektrum Akad. Verl., Heidelberg, 1996.
21 J. Schmelzer, J. Möller, I. Gutzow, R. Pascova, R. Müller and W. Pannhorst, *J. Non-Cryst. Solids*, 1995, **183**, 215–233.
22 V. M. Fokin, N. S. Yuritsin, V. N. Filipovich and A. M. Kalinina, *J. Non-Cryst. Solids*, 1997, **219**, 37–41.
23 K. Thieme and C. Rüssel, *J. Eur. Ceram. Soc.*, 2014, **34**, 3969–3979.
24 W. Vogel, *Glaschemie*, Springer, Berlin, 3rd edn, 1992.
25 R. Müller, E. D. Zanotto and V. M. Fokin, *J. Non-Cryst. Solids*, 2000, **274**, 208–231.

5.4 $BaO/SrO/ZnO/SiO_2$ Glass System: Influence of Different Nucleation Agents:Bulk Versus Surface Crystallisation

Liliya Vladislavova, Christian Thieme, TilmanZscheckel, Christian Patzig, ThomasHöche, and Christian Rüssel

Springer Nature

NATO Science for Peace and Security Series - B: Physics and Biology, Volume Advanced Nanotechnologies for Detection and Defense against CBRN Agents Springer-Verlag, (2018) chapter 35, 361-366

Authors	Liliya Vladislavova	Christian Thieme	Tilman Zscheckel	Christian Patzig	Thomas Höche	Christian Rüssel
Conception of the research approach	X				X	X
Planning of examinations	X					X
Data collection	X		X			
Data analysis and interpretation	X		X			X
Writing the manuscript	X	X	X	X	X	X
Credits	1.0					

Chapter 35
$BaO/SrO/ZnO/SiO_2$ Glass System: Influence of Different Nucleation Agents: Bulk Versus Surface Crystallisation

Liliya Vladislavova, Christian Thieme, Tilman Zscheckel, Christian Patzig, Thomas Höche, and Christian Rüssel

Abstract In the present study, detailed investigations on the crystallisation behaviour for the recently discovered $Ba_{1-x}Sr_xZn_2Si_2O_7$ phase were performed. This solid solution may possess zero to negative thermal expansion. In contrast to many other phases with negative thermal expansion, this phase can be crystallised from glasses and hence should be suitable for the preparation of cooking panels, telescope mirrors, and other mass production materials, where the thermal expansion properties have to be tailored exactly. Due to the high anisotropy of the phase, inducing volume crystallisation and reducing the crystal size is of main interest. The influence of ZrO_2 and Pt as nucleating agents in the glass system $BaO/SrO/ZnO/SiO_2$ was studied by calculating the Avrami parameter (n). The microstructure was investigated with scanning electron microscopy.

Keywords Nucleation · Glass-ceramics · Platinum-ZrO_2 · Activation energy · Avrami parameter

35.1 Introduction

The $Ba_{1-x}Sr_xZn_2Si_2O_7$ phase is a new and challenging solid solution which has a similar structure as the high-temperature (HT) modification of $BaZn_2Si_2O_7$. The new solid solution possesses negative or close to zero thermal coefficients which make it suitable for fabrication of materials such as cooking panels, telescope mirrors and

L. Vladislavova (✉) · T. Zscheckel · C. Rüssel
Otto Schott Institute, Chair of Glass Chemistry I, Jena University, Jena, Germany
e-mail: liliya.vladislavova@uni-jena.de

C. Thieme
Otto Schott Institute, Chair of Glass Chemistry I, Jena University, Jena, Germany

Fraunhofer Institute for Microstructure of Materials and Systems IMWS, Halle, Germany

C. Patzig · T. Höche
Fraunhofer Institute for Microstructure of Materials and Systems IMWS, Halle, Germany

P. Petkov et al. (eds.), *Advanced Nanotechnologies for Detection and Defence against CBRN Agents*, NATO Science for Peace and Security Series B: Physics and Biophysics, https://doi.org/10.1007/978-94-024-1298-7_35

others [1, 2]. Using single-crystal X-ray diffraction (XRD), the thermal expansion was determined as a function of temperature and crystallographic directions, combined with a Rietveld refinement [3]. The thermal expansion varies significantly in the different crystallographic directions which causes a high anisotropy in the system and may lead to crack formation in the obtained materials. Reducing the crystal size and provoking volume crystallisation is one of the most commonly applied methods to overcome crack formation [1]. Both ZrO_2 and Pt are well-known nucleation agents used in the past e.g. for the $Li_2O{\cdot}2SiO_2$ system [1, 4]. This paper describes the effect of Pt and ZrO_2 as nucleating agents in glasses from the system BaO/SrO/ZnO/SiO_2/ZrO_2.

35.2 Experimental

35.2.1 Preparation of the Glasses

The glass batch was prepared from the following chemically pure raw materials: $BaCO_3$, $SrCO_3$, ZnO, SiO_2, ZrO_2, and $PtCl_4$. For the platinum containing glass, 0.01 mol% $PtCl_4$ was dissolved in acetone and then given to the glass batch, thoroughly mixed for 2 h and subsequently dried. The batch (for 400 g glass) was melted at 1300–1350 °C for 1 h in a platinum crucible using an induction furnace. Then, the temperature was increased to 1450 °C for 2 h. During this time, the melt was stirred with 60 min^{-1}. Then, the stirrer was removed and the glass was soaked for 10–15 min. The glass was cast in a preheated steel mould and transferred to a muffle furnace preheated to 700 °C. The furnace was switched off allowing the sample to cool to room temperature. The base chemical compositions of the glasses is 8BaO/8SrO/34ZnO/44SiO_2/6ZrO_2.

35.2.2 Characterization Methods

Differential Scanning Calorimetry (DSC) was carried out using a Linseis DSC Pt 1600. Characteristic temperatures such as the glass transition temperature (T_g), the onset of the crystallisation peak (T_{on}), the offset of the crystallisation peak (T_{off}) and the crystallisation maximum (T_p) were determined. Bulk samples were used in order to minimise the effect of surface crystallisation; samples with a mass of 0.15 g were remelted in a DSC platinum crucible at 1450 °C and then quenched in air. The measurements were performed up to a temperature of 1200 °C, using heating rates of 2, 5, 10, 15 and 20 K/min.

Scanning Electron Microscopy was carried out using an (SEM) JEOL 7001 F. The samples were mounted using Ag paste; a carbon coating was applied at about 10^{-5} Pa in order to avoid surface charging.

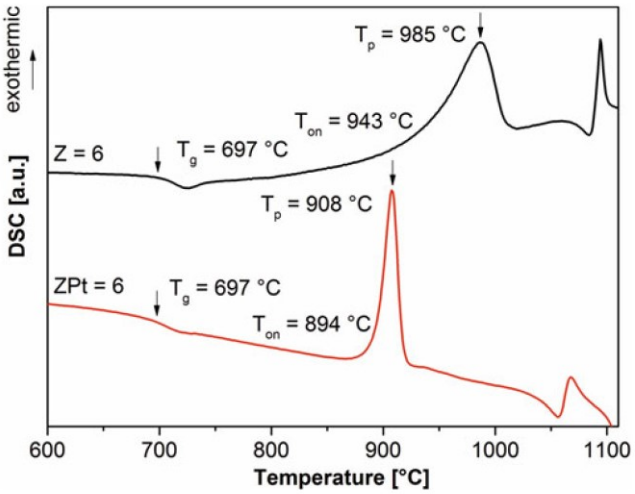

Fig. 35.1 DSC profiles: glasses with 6 mol% ZrO_2 with and without platinum, using a heating rate of 10 K/min

35.3 Results and Discussion

The produced glasses appear to be without bubbles, crystals, and striae. The sample which contained only ZrO_2 is transparent. However, adding platinum to the system led to the formation of small platinum particles with a mean size of 1 μm in the non–thermally treated glass which causes a greyish colouration [5].

Figure 35.1 shows the DSC profiles of the glasses prepared with (Z6Pt) and without (Z6) addition of platinum recorded with a heating rate of 10 K/min. The platinum addition does not affect T_g which for both systems is equal to 697 °C. The onset and peak temperatures of the Pt-containing and the Pt-free glass vary significantly. The Pt-containing glass has an onset at 894 and a peak temperature at 908 °C, whereas the Pt-free glass shows these characteristics at 943 and 985 °C, respectively. Also, a significant change in the shape of the crystallisation peaks can also be seen. The platinum-containing glass has a sharp and narrow peak whose intensity is much higher compared to that of the ZrO_2 containing glass, where the intensity is significantly lower and the peak is broader. As already reported in the literature, this is a significant indication for a change in the crystallisation mechanism [5–7].

Figure 35.2 presents Ozawa plots for the determination of the Avrami parameter for the studied glasses. The plots are obtained according to Eq. (35.1) where (ln(-ln (1-x))) is plotted versus ln (β) and the parameter value is determined from the slope using a linear regression [8, 9]. To obtain statistically significant data, the measurements were performed using five different heating rates.

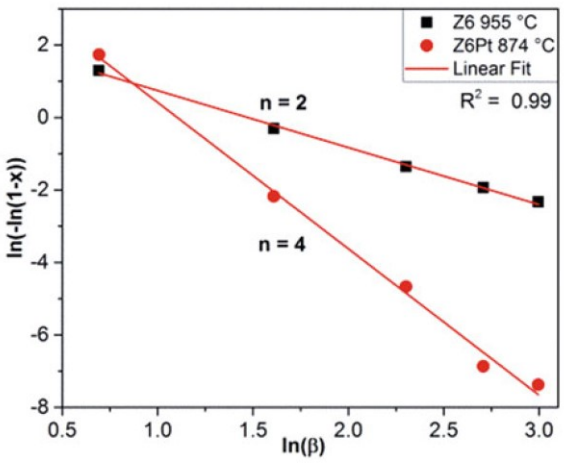

Fig. 35.2 Ozawa plot of (ln-(ln(1-x))) versus ln (β) used to calculate the Avrami parameter for Z6: 955 °C and Z6Pt: 874 °C

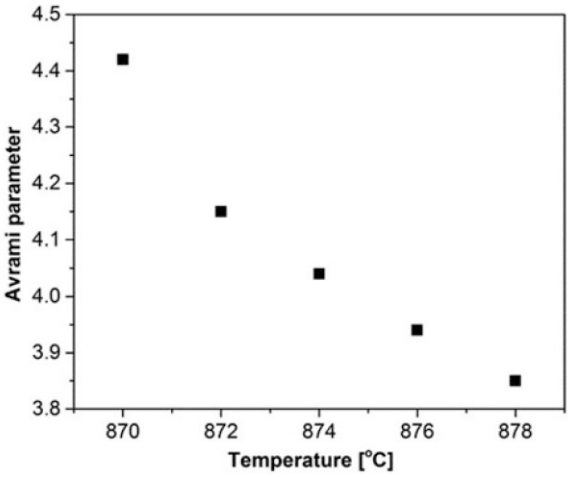

Fig. 35.3 Avrami parameter versus temperature for Z6Pt

$$-n = \left|\frac{\mathrm{d}[\ln(-\ln(1-x))]}{\mathrm{d}(\ln\beta)}\right|_{\mathrm{T}} \tag{35.1}$$

In this equation, n is the Avrami parameter and $x = A_t/A$ where A is the total area under the exothermic peak, A_t is the area under the exothermic peak up to a chosen temperature, and β is the heating rate.

The calculated Avrami parameter for the glass with 6 mol% ZrO_2(Z6) for 955 °C is approximately equal to 2 which is an indication of a mix between surface and volume crystallisation [8]. The glass composition with platinum (Z6Pt) has an Avrami parameter equal to 4 at 874 °C. This is an indication of 3D bulk crystallisation [8, 9]. As can be seen from Fig. 35.3, the Avrami parameter versus the temperature can vary slightly depending on the chosen temperature. In order to

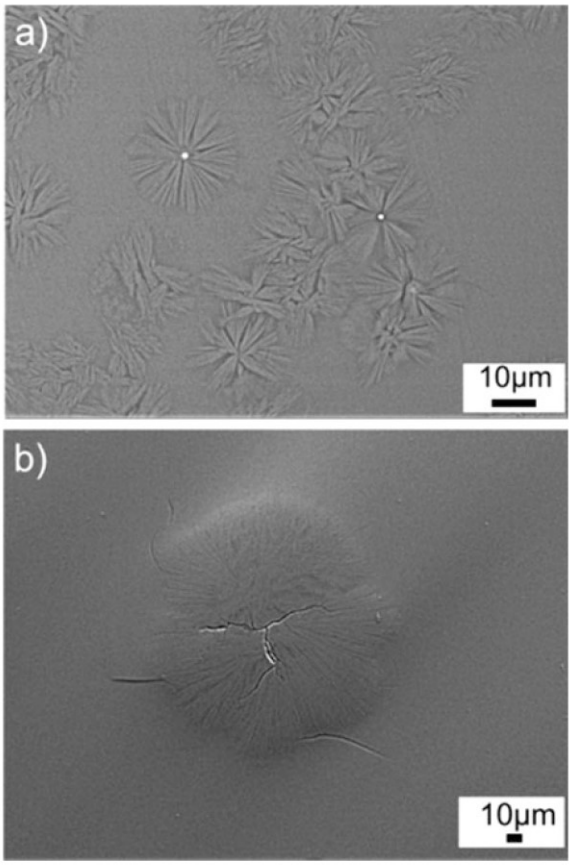

Fig. 35.4 SEM-micrographs of different samples: (**a**) Z6Pt thermally treated in the first step at 720 °C for 48 h and then at 780 °C for 5 h; (**b**) Z6 thermally treated in a first step at 720 °C for 48 h and then at 840 °C for 1 h

obtain more accurate Avrami parameters, the following should be taken into account: The heating rates should be chosen in a way that the area under the peak is the range from $0.2 \leq \times \leq 0.8$. As seen from Fig. 35.3, the Avrami parameter for the platinum containing glass varied between 4.42 and 3.85 which is close to 4. Despite the fact that the Ozawa method is quite accurate in the prediction for the crystallisation mechanism regarding the $Ba_{1-x}Sr_xZn_2Si_2O_7$ phase, additional microstructural studies are necessary for a complete overview of the crystallisation processes.

Figure 35.4 shows SEM micrographs of the studied glass ceramics. Figure 35.4a presents the platinum containing sample nucleated at 720 °C for 48 h and then thermally treated at 780 °C for 5 h. A significant amount of volume crystals is observed in the micrographs. From statistical analyses made on the samples, the mean particle size of the volume crystals was determined to be around 11 µm. The bright spheres in the middle of the crystals are platinum particles with a mean size of 1 µm which are formed during cooling of the glass [5]. All volume crystals should have a platinum particle in their centres which, however, in many cases are not

visible in the SEM micrographs, due to the different cut planes and the limited information depth of SEM. This is a good example of a heterogeneous nucleation where the metal particles act as a precursor of the crystal phase. Figure 35.4b shows the ZrO_2 containing sample nucleated at 720 °C for 48 h and then thermally treated at 840 °C for 1 h. In this case, the mean size of the volume crystals is 180 µm and the number of the crystals is significantly reduced. Also, crack formation is visible from the centre of the crystal which in combination with the surface crystallisation leads to a brittle material [7]. From this observation it can be concluded that ZrO_2 alone is not a sufficient nucleation agent.

35.4 Conclusions

Using DSC and applying the Ozawa method in order to determine the Avrami parameters proved to be suitable to predict the crystallisation behaviour and also the microstructure. The addition of 6 mol% ZrO_2 induces predominantly surface and besides, a small amount of volume crystallisation. The mean crystallite size is 180 µm which is too large for overcoming the crack formation in the samples. Adding small quantities of Pt significantly increases the volume crystallisation and reduces the mean crystallite size to 11 µm. Nevertheless, some cracks still occur inside the samples, but they are localised and do not lead to a destruction of the material.

References

1. McMillan PW (1979) Glass-ceramics, 2nd edn. Academic, London
2. Bach H, Krause D (2005) Low thermal expansion glass ceramics, 2nd edn. Springer, New York
3. Thieme C, Görls H, Rüssel C (2015) $Ba_{1-x}Sr_xZn_2Si_2O_7$-A new family of materials with negative and very high thermal expansion. Sci Rep 5:18040
4. Rindone G (1962) Further studies of the crystallization of a lithium silicate glass. J Amer Ceram Soc 45:7–12
5. Vladislavova L, Thieme C, Zscheckel T, Patzig C, Höche T, Rüssel C (2017) Heterogeneous nucleation of $Ba_{1-x}Sr_xZn_2Si_2O_7$ from a BaO/SrO/ZnO/SiO_2 glass using platinum as nucleation agent. J Eur Ceram Soc 37:4801–4808
6. Massera J, Fagerlund S, Hupa L, Hupa M (2012) Crystallization mechanism of the bioactive glasses, 45S5 and S53P4. J Am Ceram Soc 95:607–613
7. Vladislavova L, Thieme C, Rüssel C (2017) The effect of ZrO_2 on the crystallization of a glass in the system BaO/SrO/ZnO/SiO_2: surface versus bulk crystallization. J Mater Sci 52:4052–4060
8. Guedes M, Ferro AC, Ferreira JMF (2001) Nucleation and crystal growth in commercial LAS compositions. J Eur Ceram Soc 21:1187–1194
9. Donald IW (2004) Crystallization kinetics of a lithium zinc silicate glass studied by DTA and DSC. J Non-Cryst Solids 345:120–126

5.5 Crystallisation of $Ba_{1-x}Sr_xZn_2Si_2O_7$ from BaO/SrO/ZnO/SiO_2 glass with different ZrO_2 and TiO_2 concentrations

Liliya Vladislavova, Michael Kracker, TilmanZscheckel, Christian Thieme, Christian Rüssel

Solid State Sciences 78 (2018) 107-115

https://doi.org/10.1016/j.solidstatesciences.2018.02.011

Authors	Liliya Vladislavova	Michael Kracker	Tilman Zscheckel	Christian Thieme	Christian Rüssel
Conception of the research approach	X	X			X
Planning of examinations	X				X
Data collection	X		X	X	
Data analysis and interpretation	X		X	X	X
Writing the manuscript	X	X	X	X	X
Credits	1.0				

Solid State Sciences 78 (2018) 107–115

Contents lists available at ScienceDirect

Solid State Sciences

journal homepage: www.elsevier.com/locate/ssscie

Crystallisation of $Ba_{1-x}Sr_xZn_2Si_2O_7$ from BaO/SrO/ZnO/SiO_2 glass with different ZrO_2 and TiO_2 concentrations

Liliya Vladislavova [a, *], Michael Kracker [a], Tilman Zscheckel [a], Christian Thieme [a, b], Christian Rüssel [a]

[a] Otto-Schott-Institut, Jena University, Fraunhoferstr. 6, 07743 Jena, Germany
[b] Fraunhofer Institute for Microstructure of Materials and Systems IMWS, Walter-Hülse-Str. 1, 06120 Halle, Germany

ARTICLE INFO

Article history:
Received 31 July 2017
Received in revised form
5 January 2018
Accepted 19 February 2018
Available online 21 February 2018

Keywords:
Nucleation
Crystallisation
Low thermal expansion
Avrami parameter
Barium strontium zinc silicate

ABSTRACT

The effect of different nucleation agents such as ZrO_2 and TiO_2 was investigated for a first time with respect to their crystallisation behaviour in the glass system BaO-SrO-ZnO-SiO_2. In all studied glasses, a $Ba_{1-x}Sr_xZn_2Si_2O_7$ ($0.1 \leq x \leq 0.9$) solid solution crystallized. This phase was first described in 2015 to possess a similar structure as the high temperature phase of $BaZn_2Si_2O_7$ and a thermal expansion close to zero or even negative. It may find applications e.g. as cook panels, telescope mirrors, and furnace windows. Kinetic parameters of the crystallisation process were determined by supplying different heating rates in a differential scanning calorimeter (DSC). The results were evaluated using the equations of Ozawa and Kissinger with respect to the activation energies. Furthermore, the Ozawa method was used for the determination of Avrami parameters, which provides further information on the nucleation and crystallisation processes. Scanning electron microscopy including electron backscatter diffraction (EBSD) was used to characterise the microstructure, to determine the crystallite size and the crystal orientation. For the characterisation of the occurring crystalline phases, X-ray diffraction was used.

1. Introduction

Glass-ceramics are versatile materials because their properties can be tailored with respect to the intended applications. They are used in various fields such as chemistry, medicine, optics and mass production industry due to their valuable properties such as high strength, biocompatibility, transparency and low coefficient of thermal expansion [1,2]. These properties can be adjusted in a relatively wide range by the chemical composition of the parent glass, the subsequent heat treatment and in the case of surface crystallisation also the surface pre-treatment. Tailoring these properties is enabled by the crystal size and morphology, the composition of the crystal and the residual glass phase as well as their volume concentrations [2]. A further effect is achieved by the addition of minor components denoted as nucleation agents or nucleation inhibitors which consequently may lead to enhanced nucleation or, however, may decelerate the nucleation process [1,3]. Depending on the glass composition, the mechanism and the supplied temperature/time schedule, a small concentration of a precursor phase enriched in the nucleation agent can be precipitated and subsequently trigger the crystallisation of the major phase. Here, often an epitaxial growth is assumed, however, has been confirmed only in few cases [1,4]. Another possible mechanism is that the nucleation agent leads to a liquid/liquid phase separation which may subsequently lead to crystallisation, e.g. by the enrichment of certain components in a droplet phase [1].

Depending on the crystalline phase, materials may exhibit very different thermal behaviour. Most of the common materials exhibit a positive coefficient of thermal expansion (CTE) and expand during heating [5,6], while only a few materials show a CTE which is zero or even negative, i.e. they do not change their dimensions or contract during heating [2,7,8]. In order to obtain a glass-ceramic with a CTE of zero, a crystalline phase with negative CTE is required, because the residual glass phase has a positive CTE [2,9] in any case. The most common applications of such materials are cooktop panels, telescope mirrors and gyroscopes. The most frequently used materials with zero thermal expansion are based on the system Li_2O-Al_2O_3-SiO_2 [3,10]. Other materials such as ZrW_2O_8, $ZrMo_2O_8$

* Corresponding author.
E-mail addresses: liliya.vladislavova@uni-jena.de (L. Vladislavova), Kracker.Michael@googlemail.com (M. Kracker), tilman.zscheckel@uni-jena.de (T. Zscheckel), christian.thieme@imws.fraunhofer.de (C. Thieme), ccr@uni-jena.de (C. Rüssel).

https://doi.org/10.1016/j.solidstatesciences.2018.02.011
1293-2558/

and related compounds are frequently investigated nowadays but do not offer the possibility to be crystallized from glasses [11,12].

By contrast, alkaline earth silicates and especially barium silicates typically exhibit a high positive CTE [13]. The compound $BaZn_2Si_2O_7$ occurs as two polymorphs. At a temperature lower than 280 °C, the structure is monoclinic with the space group *C*2/*c* and the CTE is around $17.6 \cdot 10^{-6} K^{-1}$ [14]. Above that temperature, a phase transition occurs and the structure becomes orthorhombic with the space group $Ccm2_1$ and the CTE is negative in a broad temperature range [5,15].

It was recently reported that if a certain amount of Ba is replaced by Sr, a new crystalline structure occurs, which has a similar structure as the high-temperature phase of $BaZn_2Si_2O_7$ but is also stable at room temperature [9,16]. In order to characterise the structure of the $Ba_{1-x}Sr_xZn_2Si_2O_7$ phase, single-crystal X-ray diffraction (XRD) was performed [17]. The thermal expansion was determined as a function of the temperature and the crystallographic directions; using high-temperature powder diffraction in combination with Rietveld refinement. The thermal expansion of the phase is strongly dependent on the crystallographic direction and varied between −32.1 (for the crystallographic b axes) and $+23.1 \cdot 10^{-6} K^{-1}$ (for the crystallographic c-axes) in a temperature range from 30 to 600 °C. This leads to a variation in the CTE from −4.3 to $-14.8 \cdot 10^{-6} K^{-1}$ [17] in the temperature range from 100 to 800 °C, the variation in the CTE also depends on the preparation technique used to obtain the materials (such as sintering or sol-gel routes) [18].

In previous papers, it was reported that partial substitution of Zn^{2+} or Si^{4+} in the orthorhombic high-temperature phase is possible. If Zn^{2+} in the low temperature phase $BaZn_2Si_2O_7$ is substituted by divalent cations with similar atomic radii, such as Cu^{2+}, Mn^{2+}, Co^{2+}, Mg^{2+} or Ni^{2+}, the monoclinic low-temperature phase is found stable even up to 1000 °C [8,19,20], i.e. the temperature, at which the phase transition to the high temperature phase takes place, increases. In analogy, also Si can be substituted against Ge which also favours the low-temperature phase [21]. If these above mentioned ions substitute Zn^{2+} in $Ba_{1-x}Sr_xZn_2Si_2O_7$, up to certain concentration thresholds, these solid solutions possess similar structure as the orthorhombic high-temperature phase of $BaZn_2Si_2O_7$ and exhibit a low or negative CTE. Nevertheless, the incorporation of the above mentioned divalent ions in Zn^{2+} sites as well as the substitution of Si^{4+} by Ge^{4+} leads to higher phase transition temperature. If the respective concentrations exceed a certain threshold, the high temperature phase is no longer stable at room temperature, despite the incorporation of Sr^{2+} in Ba^{2+} sites.

One of the benefits of the $Ba_{1-x}Sr_xZn_2Si_2O_7$ solid solutions is that they can easily be crystallized from silicate glasses. It was previously shown that the base glass system tends to surface crystallisation, which might lead to mechanically less stable materials due to the microcracking of the crystalline samples caused by the high anisotropy in the thermal expansion [22]. To overcome this problem, the addition of nucleation agents is an obvious solution in this case, which should provoke volume crystallisation and smaller crystals size. Adding oxides as nucleation agents such as ZrO_2, TiO_2 and other are already well reported for others systems in the literature [1,2,10].

The present paper is dedicated to the $Ba_{1-x}Sr_xZn_2Si_2O_7$ phase which has an exceptionally low coefficient of thermal expansion. It was previously reported that 6 mol% of ZrO_2 act as nucleation agent and trigger volume crystallisation [22]. Unfortunately, the quantity of crystals is not sufficient and their size is too large to obtain crack free materials. This paper describes the effect of TiO_2 and the combination of ZrO_2 and TiO_2 as nucleating agents in the glass system $BaO/SrO/ZnO/SiO_2$.

2. Experimental procedure

The glasses in the base system $BaO/SrO/ZnO/SiO_2$ and different concentrations of ZrO_2 and TiO_2 were melted in a platinum crucible in an inductively heated furnace. The chemical compositions of the prepared glasses are summarised in Table 1. For the preparation of the batches, the following raw materials were used: $BaCO_3$ (Merck, > 98.5%), $SrCO_3$ (VEB Laborchemie Apolda, > 99%), ZnO (Carl Roth GmbH + Co KG, > 99%), SiO_2 (Carl Roth GmbH + Co KG, > 99%), ZrO_2 (Tosoh, > 99%), and TiO_2 (VEB Laborchemie Apolda, > 99%). For every composition, a glass batch with a total mass of 400 g was melted at a temperature in the range from 1300 to 1400 °C for 1 h. Then, the melting temperature was increased to 1400 or 1450 °C depending on the ZrO_2/TiO_2 concentration and kept for 2 h while the melt was stirred with 60 min^{-1} for better homogenisation of the glass batch. Later, the Pt-stirrer was removed and the glass was soaked for 10 min, subsequently cast in a preheated mould and placed in a furnace preheated to temperatures in the range from 670 to 700 °C. The furnace was switched off and the sample was allowed to cool using a rate of approximately 3 K/min. The masses of the respective glasses were measured after melting and found to be in agreement with those expected from the batch compositions. Hence any hint at the evaporation of components was not obtained.

In order to characterise the obtained glasses and crystallized materials, X-Ray Diffraction (XRD) was implemented using powdered samples and a Rigaku Miniflex 300 diffractometer with Ni-filtered Cu Kα radiation. The scanned 2θ-range was from 10° to 60° with a scan speed of 1°/min.

Differential Scanning Calorimetry (DSC) was done with a Linseis DSC Pt 1600. From the obtained profile, the glass transition temperature (T_g), the onset of crystallisation (T_{on}), the offset of crystallisation (T_{off}) and the crystallisation maximum (T_p) were obtained. In order to minimise the effect of surface crystallisation, glass cylinders with a diameter of 5 mm, a height of 3 mm and mass of 0.21 g were used. The glass samples were given into a small Pt crucible; the profiles were recorded using different heating rates (2, 5, 10, 15 and 20 K/min).

The crystal morphology was studied from cross sections of volume samples, ground and polished using Scanning Electron Microscopes (SEM) JEOL 7001 F and JEOL 6510 LV at a pressure of about 10^{-5} Pa. The samples were carbon coated at 10^{-3} Pa and contacted with Ag paste to prevent charging. The contrast was always maximised for back scattered electrons that provide the material contrast. For samples studied with electron backscatter diffraction (EBSD), colloidal silica was used in an additional final polishing step. A Digiview 3 EBSD-camera was used to collect the diffraction patterns, which were interpreted using the software packages EDAX TSL OIM Data Collection 5.31 and EDAX TSL OIM Analysis 5.31. In order to show reliable data, grain Confidence Index standardisation and grain Fit standardisation clean up procedures were applied to the dataset. Following this, a partition filter was activated using: Grain size 10, Grain tolerance angle 3, CI $\geq$ 0.2. The reference direction of the inverse pole figure (IPF) colour code is [001], i.e. the normal of the sample surface. Due to simultaneously

Table 1
Chemical compositions of the studied samples in mol %.

Name	Chemical composition in mol%					
	BaO	SrO	ZnO	SiO_2	ZrO_2	TiO_2
T5	7.5	7.5	34.0	46.0	0.0	5.0
Z5T5	7.5	7.5	34.0	41.0	5.0	5.0
Z5T3	7.5	7.5	34.0	43.0	5.0	3.0
Z6T2	7.5	7.5	34.0	43.0	6.0	2.0
Z7T1	7.5	7.5	34.0	43.0	7.0	1.0

collecting of EDXS and EBSD signals, a compromise was made between better spatial resolution and good EBSD pattern quality at low acceleration voltage on the one hand and on the other the chemical information of Sr K_α (14.163 keV) or Zr K_α (15.776 keV) lines and thermal damage of the sample at high acceleration voltage of 30 kV. In this material system, good EBSD patterns can be acquired with a step size of 280 nm at 20 kV, where information of Zn K_α, Si K_α, Ba L_α and Zr L_α are simultaneously available. While the Sr L_α line (1.806 keV) is very close to the Si K_α line (1.740 keV) and is therefore mainly superimposed, the Si concentration is multiples higher than the Sr concentration, which allows using the Si K_α line to show Si enrichments. The Zr L_α line (2.042 keV) is clearly distinguishable from all other lines expected from the samples and was included into the interpretation.

The densities were determined using a helium pycnometer Micromeritics AccuPyc 1330.

3. Results

The produced glasses appear to be transparent without bubbles, crystals or striae. The colouration of the glasses changed in dependency of the TiO_2 concentration, from colourless to light ochre. The chemical composition shown in Table 1 was confirmed by weight for all glass compositions. There was no hint at the evaporation of certain components of the batch. Fig. 1 represents DSC profiles of glasses with different ZrO_2/TiO_2 concentrations, applying a heating rate of 10 K/min. Adding different ZrO_2 concentrations led to systematic shifts in T_g. The lowest glass transition temperature (667 °C) was detected for the sample with 5 mol% of TiO_2 (T5); in the sample with the same concentration of TiO_2 and additionally 5 mol % ZrO_2 (Z5T5), T_g increased to 682 °C. By comparison, for the sample with 5 mol % ZrO_2 and 3 mol% TiO_2 (Z3T5), T_g was 687 °C. For the samples with increasing concentration of ZrO_2 and decreasing TiO_2, the T_g values were 689 and 694 °C for samples Z6T2 and Z7T1 respectively. The DSC profiles of all glasses show an intense crystallisation peak, followed by a second peak at around 1060 °C. Just for the composition Z7T1 (containing 7 mol% ZrO_2 and 1 mol% TiO_2), no additional crystallisation peak is observed. The first exothermic peak is related to the crystallisation of $Ba_{1-x}Sr_xZn_2Si_2O_7$ while the second was attributed to the crystallisation of cristobalite. For the ZrO_2-free glass, the lowest crystallisation peak temperature is observed (925 °C). This temperature increases to 946 °C for the glass composition with 5 mol% TiO_2 and

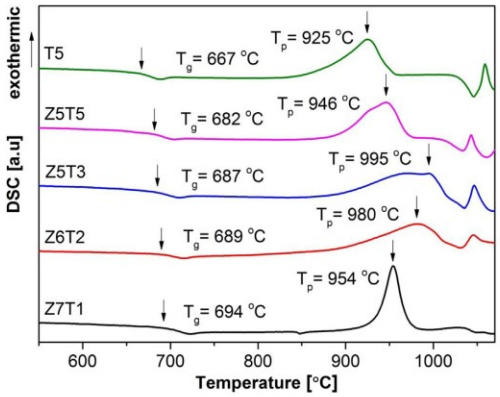

Fig. 1. DSC profiles: glasses with different concentration of ZrO_2 and TiO_2 using a heating rate of 10 K/min.

Table 2
Results from the DSC-profiles of the samples with different ZrO_2/TiO_2 concentrations recorded with a heating rate of 10 K/min. Glass transition temperature, (T_g); onset of the crystallisation peak, (T_{on}); offset of the crystallisation peak, (T_{off}); temperature of the crystallisation peak (T_p); and T_{on}-T_g.

Name	T_g (°C)	T_{on} (°C)	T_{off} (°C)	T_p (°C)	T_{on}-T_g (K)
T5	667	880	949	925	213
Z5T5	682	896	971	946	214
Z5T3	687	891	1021	995	204
Z6T2	689	913	1018	980	224
Z7T1	694	936	969	954	242

5 mol% ZrO_2. The crystallisation peaks for the other three samples occur at temperatures up to 995 °C. All characteristic temperatures from the DSC profiles are summarised in Table 2.

In Fig. 2, XRD patterns of samples thermally treated at 940 °C for 1 h are shown for different ZrO_2/TiO_2 - concentrations. This temperature near the crystallisation maxima of all investigated samples was chosen in order to achieve a high volume concentration of crystals. The patterns of the respective glass compositions are fairly similar and do not exhibit noticeable differences. The sample containing 7 mol% ZrO_2 and 1 mol% TiO_2 shows additional peaks with low intensity at $2\theta = 31.52$ and 33.98°, which are attributed to two intense peaks of Willemite (Zn_2SiO_4) according to the ICSD file 2425. The other patterns do not show lines due to additional crystalline phases, such as ZrO_2, TiO_2 or $ZrTiO_4$. All of the registered peaks are consistent with the ICSD pattern 429938 of

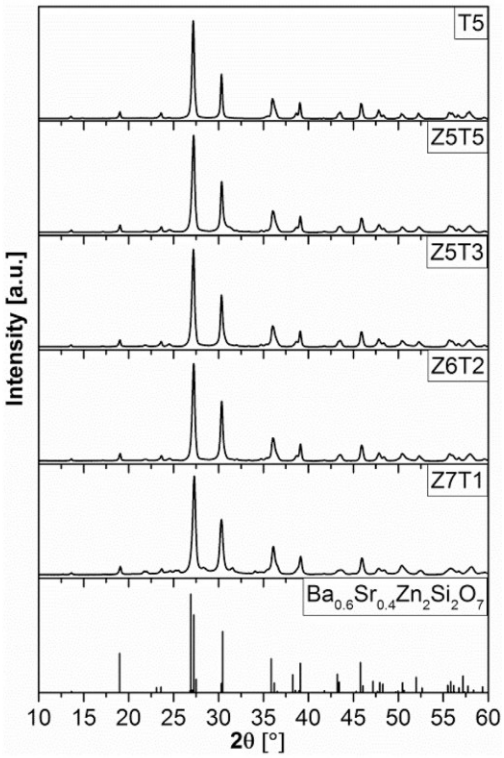

Fig. 2. X-ray diffraction patterns of glasses with different ZrO_2 and TiO_2 concentrations annealed at 940 °C for 1 h. The theoretical peak positions belong to $Ba_{0.6}Sr_{0.4}Zn_2Si_2O_7$ (ICSD 429938).

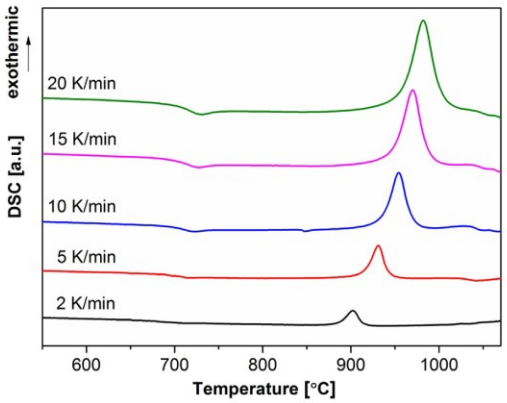

Fig. 3. DSC profiles of glasses using 5 different heating rates for the glass Z7T1.

$Ba_{0.6}Sr_{0.4}Zn_2Si_2O_7$ which is shown at the bottom of Fig. 2 for comparison.

Fig. 3 shows DSC profiles of the glass with 7 mol% ZrO_2 and 1 mol % TiO_2 recorded using different heating rates in the range from 2 to 20 K/min. While the value of T_g does not change significantly (as expected), the exothermic peak, i.e. the crystallisation peak changed notably. For a heating rate of 2 K/min, the peak is observed at a temperature of 902 °C. With increasing heating rates, the peaks are shifting to higher temperatures up to 982 °C for a heating rate of 20 K/min. The onsets and offsets of the crystallisation peaks are systematically shifted to higher temperatures as well. Using the same condition for all glass compositions and applying the following equations, kinetic parameters are obtained.

The determination of the activation energy can be obtained by different methods and equations [23–25]. In this paper were compare the activation energies using Kissinger (Eq. (1)) [23,26] and Ozawa (Eq. (2)) [23,27] Equations.

$$\ln\left[\frac{\beta}{T_p^2}\right] = \frac{-E_a}{RT_p} + const \tag{1}$$

$$\ln[\beta] = \frac{-E_a}{RT_p} + const \tag{2}$$

Where: T_p is the temperature attributed to the crystallisation peak; β is the heating rate; E_a is the respective activation energy and R is the gas constant.

The graphical representation of the activation energies is shown in Figs. 4 and 5 for the glass compositions with 5 mol% TiO_2 as well as for the composition with 7 mol% ZrO_2 and 1 mol% TiO_2, respectively.

Figs. 4 a and b shows Kissinger plots: according to Eq. (1), ln (β/T_p^2) is plotted against 1000/T_p. For increasing heating rates, T_p increases and hence 1000/T_p decreases, while ln (β/T_p^2) increases. From the slopes of these regression lines, the activation energy, in the following denoted as the Kissinger activation energy, was calculated. For the ZrO_2-free (T5) glass, this activation energy is 367

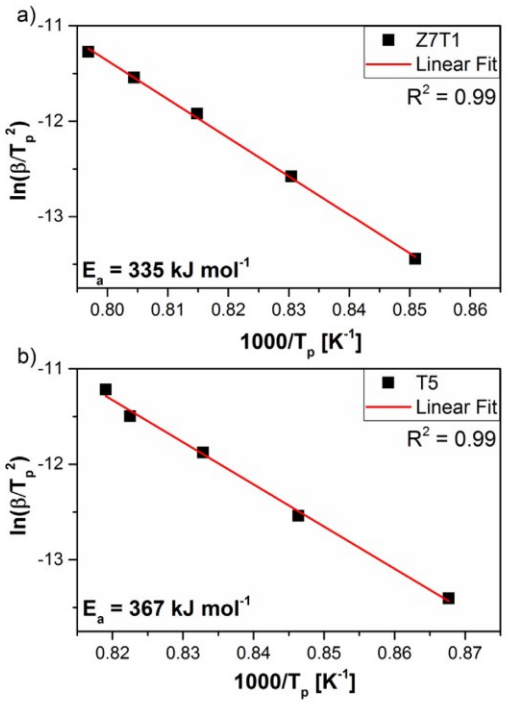

Fig. 4. Kissinger plots used to calculate the activation energy of crystallisation: a) for glass Z7T1; b) for glass T5.

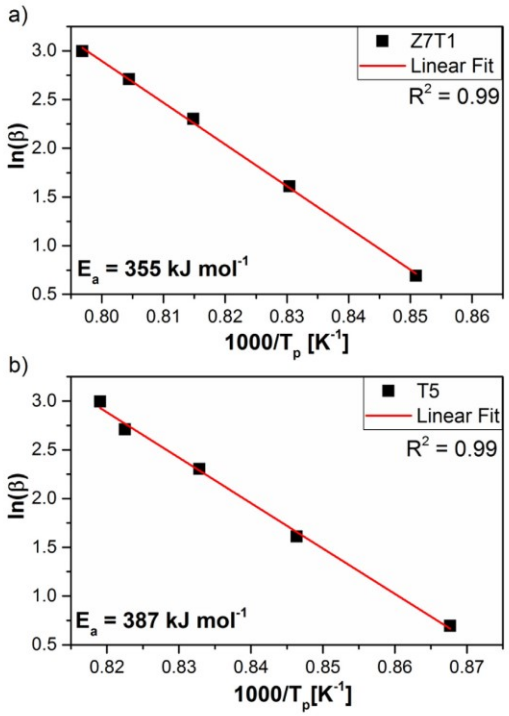

Fig. 5. Ozawa plots used to calculate the activation energy of crystallisation: a) for glass Z7T1; b) for glass T5.

Table 3
Activation energy, determined by the Kissinger plot, E_k; activation energy determined by the Ozawa plot, E_o and density of the respective glasses, ρ.

Name	E_k [kJ·mol^{-1}]	E_o [kJ·mol^{-1}]	ρ [g/cm^3]	Avrami parameter
T5	367	387	3.943	1.3
Z5T5	370	390	4.089	1.5
Z5T3	319	339	4.044	1.2
Z6T2	311	331	4.069	1.3
Z7T1	335	355	4.080	2.2

kJ/mol^{-1}, while it is 335 kJ/mol^{-1} for the glass with 7 mol% ZrO_2 and 1 mol% TiO_2. The values of Kissinger activation energies are summarised in Table 3.

Figs. 5 a and b presents the activation energies using the Ozawa equation. This method has some similarities to that of Kissinger's equation, the main difference is that the slope of the graph is calculated from a plot of ln(β) versus 1000/T_p. The obtained activation energies are slightly different from the Kissinger activation energies. They are little affected by the glass composition and are equal within a limit of 6% for all investigated systems. In Fig. 5 a the activation energy is 355 kJ·mol^{-1} for the sample Z7T1 and 387 kJ·mol^{-1} for the sample T5 (see Fig. 5 b).

Another important parameter is the Avrami parameter, which is attributed to the crystallisation mechanism of the obtained glass ceramics [23,24,28].

$$-n = \left| \frac{d[\ln(-\ln(1-x))]}{d(\ln \beta)} \right|_T \quad (3)$$

Where: n is the Avrami parameter, $x = A_t/A$, where A is the total area under the exothermal peak, A_t is the area under the exothermic peak up to a chosen temperature (the values of x should be in the range from $0.2 \leq x \leq 0.8$) and β is the heating rate.

The graphical presentation of the Avrami parameter is shown a Fig. 6, where (ln (-ln (1-x))) is plotted against ln(β), the Avrami parameter is then obtained by a linear fit. The Avrami parameters of all glass compositions are summarised in Table 3. In Fig. 6 a, the Avrami parameter n is equal to 1.5 calculated for the glass system with 5 mol% ZrO_2 and TiO_2 at a temperature of 896 °C. A similar result is obtained for the glass with 5 mol% TiO_2 (T5) where n is equal to 1.3 at 890 °C. It is important to mention that for the chosen temperatures and for all supplied heating rates, the parameter x (see Eq. (3)) is in between 0.2 and 0.8. The Avrami parameter is a dimensionless constant which might predict the crystallisation behaviour of the samples.

SEM studies were performed in order to compare calculation and actual microstructure. Fig. 7 a shows an SEM micrograph of a sample containing 6 mol% ZrO_2 and 2 mol% TiO_2 (Z6T2), nucleated at 710 °C for 48 h and then crystallized at 840 °C for 45 min. The sample exhibits surface crystallisation with a layer thickness of 76 μm. No evidence of volume crystallisation was found in this sample. The glass composition with 7 mol% of ZrO_2 and 1 mol% of TiO_2 (Z7T1) exhibits volume crystallisation, as seen in Fig. 7 b. The volume crystals have a mean size of 87 μm and an approximately spherical shape. All crystals have a core in the middle from which radial growth of the crystalline phase starts. The crystals seem to have a high aspect ratio and most probably grow with the morphology of thin sheets. The sample was nucleated at 750 °C

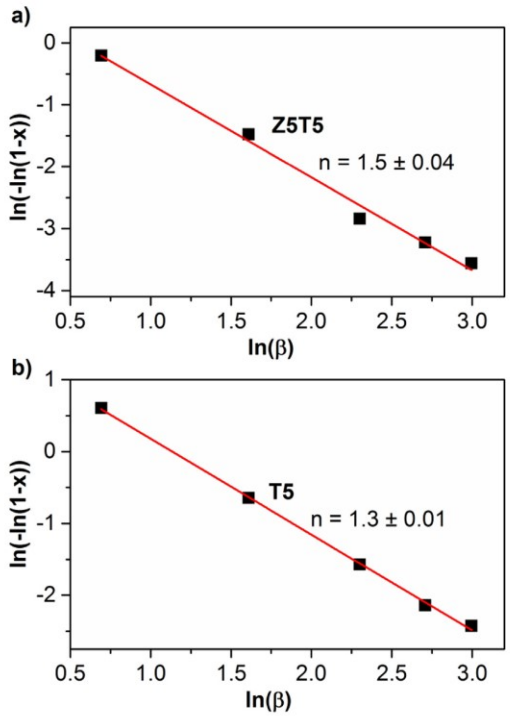

Fig. 6. Ozawa plot of (ln-(ln (1-x))) versus lnβ used to calculate the Avrami parameter: a) for glass Z5T5 at 869 °C; b) for glass T5 at 890 °C.

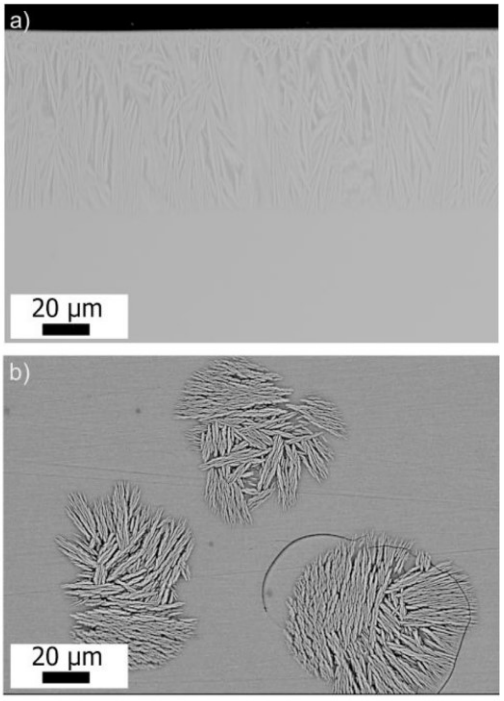

Fig. 7. SEM-micrographs of different samples: a) Z6T2 thermally treated in a first step at 710 °C for 48 h and then at 840 °C for 45 min, b) Z7T1 thermally treated in a first step at 750 °C for 48 h and then at 840 °C for 45 min.

near the softening point of the glass for 48 h and subsequently treated at 840 °C for 45 min.

The relation between microstructure and crystal orientation was studied by EBSD. Fig. 8 a shows a micrograph of a cut perpendicular to the surface of sample Z6T2 (the same as studied in Fig. 7 a. In analogy to Fig. 7 a, the crystallized layer shows a homogenous thickness and contains thin and elongated crystals. With increasing distance to the surface, they become more parallel to each other and more perpendicular to the surface, while few cracks obviously run perpendicular to the length axis of the crystals. The corresponding crystal orientations are shown by white unit cells in Fig. 8 b). Red arrows highlight the direction of the c-axis, which points parallel to the length axis of the crystals.

Fig. 9 a shows the micrograph of a cut through volume crystal of sample Z7T1 (the same as studied in Fig. 7 b). The structure is almost circular and shows cracks which run concentric to the middle of the structure. The circular structure shows substructures which are predominantly long and thin and they exhibit a length axis from the centre of the main structure to the border. The cracks run almost perpendicular to the longest axis of the crystals. The related crystal orientations are shown in Fig. 9 b) that shows a combined Image Quality (IQ) and inverse pole figure (IPF)-map. The Image Quality is illustrated by the grey value and gives an impression of the grain structure and morphology. The greyscale reaches from black to white (bright), i.e. from amorphous regions, over strongly stressed crystals and grain boundaries up to almost perfect monocrystalline regions. The IQ-map is used to show the IPF-map more gently for the eyes. All patterns of the scan that showed diffraction lines could be attributed to the orthorhombic structure of the $Ba_{0.6}Sr_{0.4}Zn_2Si_2O_7$; the colour code of the inverse pole figure describes the crystal direction perpendicular to the sample surface. Around the crystal in Fig. 9 b) structured EBSD patterns were not obtained. These regions consist of residual glass, and therefore are illustrated in black. The patterns from the centre, that should be crystalline (compare with Fig. 9 a) could not be reliably indexed and are also illustrated in black. The IPF-colour shows systematic gradual changes of the orientation from the centre of the structure to the fringe. The white unit cells and the corresponding $\vec{c}$-axis directions help to read the map. Typically, the dimensions of these cells are a = 12.98, b = 7.71, and c = 6.59 Å [17]. The $\vec{c}$-axes [001] develop from more or less perpendicular to the cut plane in the centre to almost parallel to the cut plan and also parallel to the length axis of the substructures with increasing distance from the centre. Thereby, the green coloured structures are attributed to the $\vec{a}$-axis [100] perpendicular to the cut plane, while the blue coloured parts show the $\vec{b}$-axis [010] perpendicular to the cut plane. The courses of the cracks are highlighted with blue lines and are perpendicular to the $\vec{c}$-axes of the broken crystals.

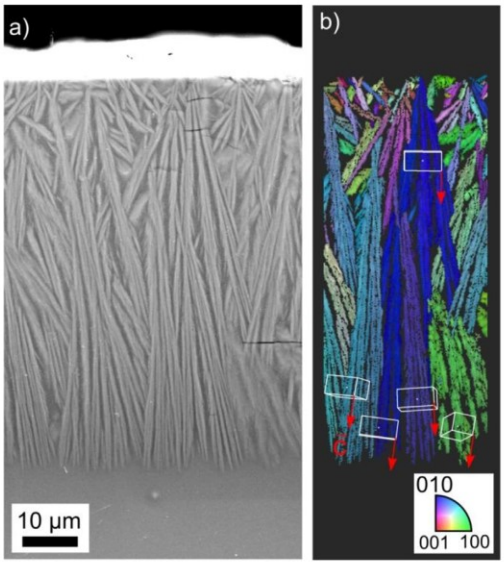

Fig. 8. Sample Z6T2, thermally treated in a first step at 710 °C for 48 h and then at 840 °C for 45 min: a) micrograph of a cut perpendicular to the surface, b) combined Image Quality (IQ) + inverse pole figure (IPF)-map with white lined unit cells. The direction of the c-axis is indicated by red arrows at certain crystal positions. (For interpretation of the references to colour in this figure legend, the reader is referred to the Web version of this article.)

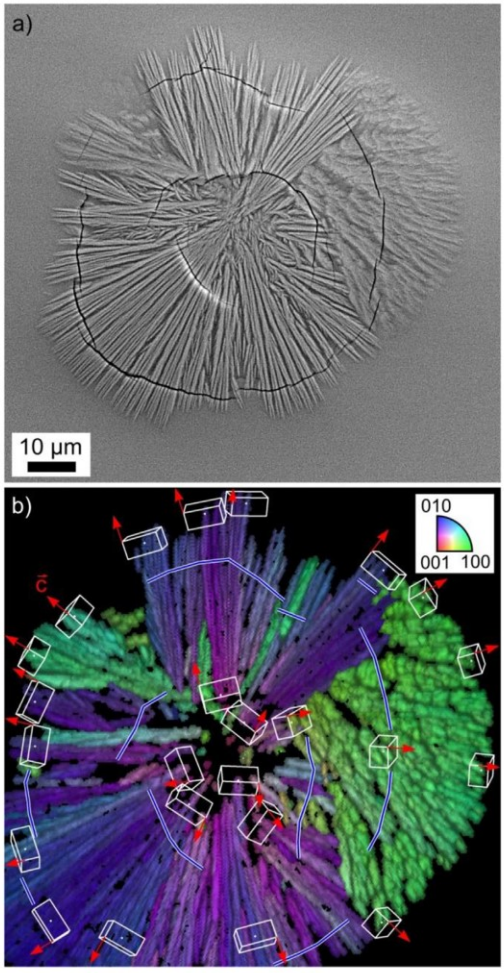

Fig. 9. Sample Z7T1, thermally treated in a first step at 750 °C for 48 h and then at 840 °C for 45 min: a) representative micrograph of a volume crystal containing concentric cracks around its centre; b) combined IQ + IPF-map. White lined unit cells with c-axis direction (red lined) at certain crystal positions and blue lined courses of cracks are highlighted. (For interpretation of the references to colour in this figure legend, the reader is referred to the Web version of this article.)

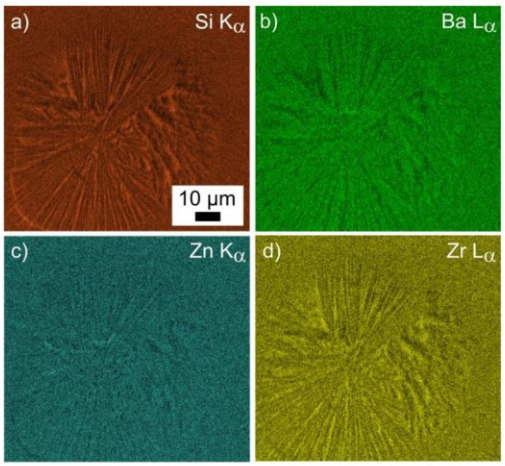

Fig. 10. Elemental mapping of sample Z7T1, thermally treated in a first step at 750 °C for 48 h and then at 840 °C for 45 min. Bright points show high net counts: a) Si K_α, net count scale 912–1333; b) Ba L_α, net count scale 150–281; c) Zn K_α, net count scale 207–362 and d) Zr L_α, net count scale 208–361.

Fig. 10 shows an elemental mapping of the same volume crystal of the sample Z7T1 as presented in Fig. 9. Figs. 10 a, b, c and d show elemental mappings of Si K_α, Ba L_α, Zn K_α and Zr L_α, respectively. The scale contrast reaches from the lowest to the highest net count in the map for each element. Bright points represent high net counts, i.e. enrichment of the element in comparison to dark points. Therefore, absolute concentrations cannot be taken from the mappings. The illuminated volume emitting X-ray quants of each measured point has a diameter in the range of few micrometres while the scan step size is only 280 nm, i.e. the chemical information of neighboured points overlaps. Although this prevents a quantification of chemical data, tendencies of elemental enrichment or depletions can be obtained from the mappings. As seen from the image, Si and Zr are shoved away from the crystal structure, while the mapping for Ba and Zn runs exactly in the opposite direction and an enrichment of these elements is observed in the crystal. Due to the topography and corresponding signal errors at cracks (see SEM of Fig. 9 a), the apparent enrichments of Si at these regions are artefacts.

4. Discussion

The sample with the lowest TiO_2 concentration (1 mol%) and 7 mol% ZrO_2 is transparent and colourless. The different ZrO_2 concentrations do not affect the transparency or the colour of the obtained glasses. By contrast, increasing the TiO_2 concentration has a notable effect; the glasses stay transparent but show a yellow to brown colouration, and the colour intensity increases with increasing TiO_2 concentration. The sample with 5 mol% TiO_2 possesses yellow to light brown colouration. Similar results are observed for other silicate glasses containing TiO_2 [29,30]. This colouration is due to the presence of Ti^{4+} which forms a charge transfer complex with Fe^{3+}. This charge transfer complex (Fe^{3+}-O-Ti^{4+}) is frequently denoted as ilmenite colouration and occurs in any titanium containing silicate glass. The Fe impurities are introduced in small concentrations from the raw materials and contribute to the absorption in the UV and visible range, which lead to the above described absorption in the near UV and visible range [30].

The DSC profiles were used for successful calculation of kinetic parameters. Heating rates of 2, 5, 10, 15 and 20 K/min were applied because they give statistically significant data. Another important factor for choosing these specific heating rates is that the shift of the crystallisation peak is less pronounced which facilitates to determine the area under the peak which for all heating rates should be in the range from $0.2 \leq x \leq 0.8$. Fig. 3 shows DSC profiles for all supplied heating rates for sample Z7T1 and illustrate the mentioned systematic shift of the peaks to higher temperatures. This is well pronounced for T_p: supplying heating rates of 2 and 20 K/min leads to a shift from 902 to 982 °C. The onsets and offsets of the exothermic peaks are 889 and 912 °C for 2 K/min, and 956 and 1004 °C for 20 K/min. Similar results are obtained for all studied glass compositions (see Table 1). This systematic shift of the temperatures is explained by Ozawa and Kissinger equations [23–25] which enables the calculations of the activation energies (see Table 3).

The addition of higher ZrO_2 concentrations to the base glass leads to systematic shifts of T_p, to higher temperatures which is not surprising because it has already been reported for this and other glass systems [22,31]. Previously was reported that the maximum concentration of ZrO_2 in this glass system is 6 mol% [22], however, combining ZrO_2 and TiO_2 obviously improves the solubility of ZrO_2 by 1 mol%. Furthermore, the addition of TiO_2 to the glasses significantly affects the crystallisation peak and very slightly the T_g of the glasses. This is visible in Fig. 1 for the glass systems Z5T3 and Z5T5, where T_g values of 687 and 682 °C were respectively obtained. However, the change in T_p is more significant (995–946 °C). There is also a noticeable change in the shape and height of the peaks which is consistent through all heating rates. Numerous studies published in the past proved that the change in the shape, the width and the intensity of the crystallisation peak are usually an indication of a change in the crystallisation mechanism [32–34]. This can be observed for sample Z7T1 where a significant change in the width and the intensity of the exothermic peak compared to the other glasses was observed. This is due to a change from surface crystallisation to a mixture of surface and volume crystallisation.

Another possibility to conclude on the crystallisation behaviour is the determination of the Avrami parameter. One of the most accurate and most frequently used approaches is the Ozawa method (Eq. (3)), where depending on the value of the obtained parameter conclusions on the crystallisation mechanism are possible. The Avrami parameter (n) is a dimensionless constant where 1 is an indication of sole surface crystallisation, 2 is an indication of a combination of both surface and volume crystallisation, but still dominated by surface crystallisation, and a parameter equal to 3 is attributed to volume crystallisation [23–25,28]. As shown in Table 3 and Fig. 6, all studied compositions except the glass Z7T1 have an Avrami parameter equal to 1 which is consistent with surface crystallisation. Microstructural studies performed by SEM were carried out with samples after suitable thermal treatments. In sample Z7T1 with the $n \approx 2$, a significant contribution of volume and surface crystallisation was found (Fig. 7 b). For all other glasses, n was around 1 and surface crystallisation was predominant. However, a very low number of volume crystals were also found in samples Z5T5 and T5. It cannot be excluded that this small amount of volume crystals is caused by the formation of bubbles or impurities from the raw materials, which do not affect the overall kinetics of the crystallisation processes and cannot be predicted by the Avrami parameter.

The activation energies for all glass compositions were determined by applying Kissinger equation (Eq. (1)) and Ozawa equation (Eq. (2)); all values are summarised in Table 3. The analysis assumes the maximum rate of a reaction to occur at the peak temperature,

this means that the method is not suitable for used systems where the peak of crystallisation cannot be determined unambiguously [23]. The results obtained by Ozawa equation are fairly similar. By comparing the results from Table 3, it can be concluded that the addition of ZrO_2 to the glass systems leads to a decrease in the activation energies, while the addition of TiO_2 leads to an increase. This tendency does not depend on the method used for the determination of the activation energies.

In order to study the phase formation and the microstructure of the samples via XRD, a crystallisation temperature of 940 °C was chosen. As shown in the DSC profiles (Fig. 1), this temperature is above the temperature of the crystallisation peak of all glasses. A crystallisation time of 1 h ensures the full crystallisation of the samples. As seen in Fig. 2, the predominant crystalline phase in all samples is a $Ba_{1-x}Sr_xZn_2Si_2O_7$ solid solution [8,17,22]. This shows that adding different nucleation agents does not provoke the formation of other phases. XRD patterns recorded from samples nucleated at different temperatures above T_g (not shown here), do not show peaks which are attributed to ZrO_2, or $ZrTiO_4$ as reported from other systems, e.g. from $Li_2O/Al_2O_3/SiO_2$ [3] or $MgO/Al_2O_3/SiO_2$ [35]. Additional peaks are detected in the glass composition Z7T1 which are contributed to willemite, however, this is not very surprising; due to the excess of ZnO and SiO_2 in the glass composition and the fact that willemite is the only binary compound in the ZnO-SiO_2 phase diagram. Similar results were reported previously independent of the used nucleation agent [22,36].

The $\vec{c}$-axis perpendicular to the courses of cracks is caused by the anisotropy of the CTE. This has also been recently reported a glass ceramic obtained from the $Ba_{1-x}Sr_xZn_2Si_2O_7$ base glass without the nucleation additives. The $\vec{c}$-axis shows the highest positive value and, hence, contracts strongest during cooling, while $\vec{b}$-axis expands and the $\vec{a}$-axis contracts slightly. Therefore, cracks perpendicular to the $\vec{c}$-axis seems to be a logical consequence, because the crystals get under tensile stresses during cooling.

5. Conclusions

The addition of TiO_2 in different concentrations leads to a decreasing T_g and a decreasing activation energy, compared to the solely ZrO_2 containing glasses, where the opposite behaviour is observed. In nearly all studied systems except the sample with the highest ZrO_2 concentration of 7 mol%, predominantly surface crystallisation was observed. From the obtained results, we can conclude that using TiO_2 and ZrO_2 proves to be not an efficient nucleation agent. Although in one glass (Z7T1) volume crystallisation occurs, the sizes of the crystals are too large and cracks appear in the volume. The EBSD analysis shows that all cracks run perpendicular to the $\vec{c}$-axis and are most probably caused by the anisotropy of the CTE.

Acknowledgment

This work was funded by the German Federal Ministry of Education and Research under the grant number 03VP01701 and 03VP01702.

References

[1] P.W. McMillan, Glass-ceramics, second ed., Academic Press, London, 1979.
[2] H. Bach, D. Krause, Low Thermal Expansion Glass Ceramics, second ed., Springer, New York, 2005.
[3] K. Thieme, C. Rüssel, Nucleation inhibitors - the effect of small concentrations of Al_2O_3, La_2O_3 or TiO_2 on nucleation and crystallization of lithium disilicate, J. Eur. Ceram. Soc. 34 (2014) 3969–3979.
[4] G. Rindone, Further studies of the crystallization of a lithium silicate glass, J. Amer. Ceram. Soc. 45 (1962) 7–12.
[5] M. Kerstan, C. Rüssel, Barium silicates as high thermal expansion seals for solid oxide fuel cells studied by high-temperature X-ray diffraction (HT-XRD), J. Power Sources 196 (2011) 7578–7584.
[6] F.A. Hummel, Thermal expansion properties of some synthetic lithia minerals, J. Am. Ceram. Soc. 34 (1951) 235–239.
[7] J.S.O. Evans, T.A. Mary, A.W. Sleight, Negative thermal expansion materials, Phys. B Condens. Matter 241 (1997) 311–316.
[8] C. Thieme, T. Waurischk, S. Heitmann, C. Rüssel, New family of materials with negative coefficients of thermal expansion: the effect of MgO, CoO, MnO, NiO, or CuO on the phase stability and thermal expansion of solid solution phases derived from $BaZn_2Si_2O_7$, Inorg. Chem. 55 (44) (2016) 76–4484.
[9] C. Thieme, C. Rüssel, Very high or close to zero thermal expansion by the variation of the Sr/Ba ratio in $Ba_{1-x}Sr_xZn_2Si_2O_7$ - solid solutions, Dalton Trans. 45 (2016) 4888–4895.
[10] H. Scheidler, E. Rodek, Li_2O-Al_2O_3-SiO_2 glass-ceramics, Am. Ceram. Soc. Bull. 68 (1989) 1926–1930.
[11] I. Yamai, T. Oota, Low-thermal-expansion polycrystalline zirconyl phosphate ceramic, J. Am. Ceram. Soc. 68 (1985) 273–278.
[12] C. Lind, A.P. Wilkinson, Z. Hu, et al., Synthesis and properties of the negative thermal expansion material cubic $ZrMo_2O_8$, Chem. Mater. 10 (1998) 2335–2337.
[13] M. Kerstan, M. Müller, C. Rüssel, Binary ternary and quaternary silicates of CaO, BaO and ZnO in high thermal expansion seals of solid oxide fuel cells studied by high-temperature X-ray diffraction (HT-XRD), Mater. Res. Bull. 46 (2011) 2456–2463.
[14] M. Kerstan, M. Müller, C. Rüssel, Thermal expansion of Ba_2ZnSiO_7, $BaZnSiO_4$ and the solid solution series $BaZn_{2-x}Mg_xSiO_2$ ($0 \leq x \leq 2$) studied by high temperature X-ray diffraction and dilatometry, J. Solid State Chem. 188 (2012) 84–91.
[15] J.H. Lin, G.X. Lu, J. Du, M.Z. Su, C.K. Loong, J.W. Richardson Jr., Phase transition and crystal structures of $BaZn_2Si_2O_7$, J. Phys. Chem. Solids 60 (1999) 975–983.
[16] C. Thieme, G.B. Souza, C. Rüssel, Glass-ceramics in the system BaO–SrO–ZnO–SiO_2 with adjustable coefficients of thermal expansion, J. Am. Ceram. Soc. 99 (9) (2016) 3097–3103.
[17] C. Thieme, H. Görls, C. Rüssel, $Ba_{1-x}Sr_xZn_2Si_2O_7$-A new family of materials with negative and very high thermal expansion, Sci. Rep. 5 (2015), 18040.
[18] M. Kracker, C. Thieme, J. Hässler, C. Rüssel, Sol-gel powder synthesis and preparation of ceramics with high- and low-temperature polymorphs of $Ba_xSr_{1-x}Zn_2Si_2O_7$ (x =1 and 0.5): a novel approach to obtain zero thermal expansion, J. Eur. Ceram. Soc. 36 (2016) 2097–2107.
[19] M. Kerstan, C. Thieme, M. Grosch, M. Müller, C. Rüssel, $BaZn_2Si_2O_7$ and the solid solution series $BaZn_{2-x}Co_xSi_2O_7$ ($0< x\leq 2$) as high temperature seals for solid oxide fuel cells studied by high-temperature X-ray diffraction and dilatometry, J. Solid State Chem. 207 (2013) 55–60.
[20] C. Thieme, C. Rüssel, High thermal expansion in the solid solution series $BaM_{2-x}Ni_x Si_2O_7$ (M = Zn, Mg, Co)-the effect of Ni-concentration on phase transition and expansion, J. Mater. Sci. 50 (2015) 3416–3424.
[21] C. Thieme, C. Rüssel, Negative thermal expansion in $Ba_{0.5}Sr_{0.5}Zn_2SiGeO_7$, Materials 9 (2016) 631–636.
[22] L. Vladislavova, C. Thieme, C. Rüssel, The effect of ZrO_2 on the crystallization of a glass in the system BaO/SrO/ZnO/SiO_2: surface versus bulk crystallization, J. Mater. Sci. 52 (2017) 4052–4060.
[23] I.W. Donald, Crystallization kinetics of a lithium zinc silicate glass studied by DTA and DSC, J. Non-Cryst. Solids 345 (2004) 120–126.
[24] M. Guedes, A.C. Ferro, J.M.F. Ferreira, Nucleation and crystal growth in commercial LAS compositions, J. Eur. Ceram. Soc. 21 (2001) 1187–1194.
[25] A. Arora, E.R. Shaaban, K. Singh, O.P. Pandey, Non-isothermal crystallization kinetics of ZnO–BaO–B_2O_3–SiO_2 glass, J. Non-Cryst. Solids 354 (2008) 3944–3951.
[26] H.E. Kissinger, Reaction kinetics in differential thermal analysis, Anal. Chem. 29 (1957) 1702–1706.
[27] T.A. Ozawa, Modified method for kinetic analysis of thermoanalytical data, J. Therm. Anal. 9 (1976) 69–373.
[28] R. Wurth, H.J. Pascual, G.C. Mather, et al., Crystallisation mechanism of a multicomponent lithium alumino-silicate glass, Mater. Chem. Phys. 134 (2012) 1001–1006.
[29] M. Schneider, W. Richter, R. Keding, C. Rüssel, XPS investigations on coordination and valency of Ti in fresnoite glasses and glass ceramics, J. Non-Cryst. Solids 226 (1998) 273–280.
[30] M. Chavoutier, D. Caurant, O. Majérus, R. Boulesteix, P. Loiseau, C. Jousseaume, E. Brunet, E. Lecomte, Effect of TiO_2 content on the crystallization and the color of (ZrO_2, TiO_2)-doped Li_2O–Al_2O_3–SiO_2 glasses, J. Non-Cryst. Solids 384 (2014) 15–24.
[31] K. Thieme, C. Rüssel, Nucleation and growth kinetics and phase analysis in zirconia-containing lithium disilicate glass, J. Mater. Sci. 50 (2015) 1488–1499.
[32] J. Augis, J. Bennett, Calculation of the Avrami parameters for heterogeneous solid state reactions using a modification of the Kissinger method, J. Therm. Anal. Calorim. 13 (1978) 283–292.
[33] C.S. Ray, W. Huang, D.E. Day, Crystallization kinetics of a lithia–silica glass:

effect of sample characteristics and thermal analysis measurement techniques, J. Am. Ceram. Soc. 74 (1991) 60–66.
[34] J. Massera, S. Fagerlund, L. Hupa, M. Hupa, Crystallization mechanism of the bioactive glasses, 45S5 and S53P4, J. Am. Ceram. Soc. 95 (2012) 607–613.
[35] O. Dargaud, G. Calas, L. Cormier, L. Galoisy, C. Jousseaume, G. Querel, M. Newville, In situ study of nucleation of zirconia in an $MgO–Al_2O_3–SiO_2$ glass, J. Am. Ceram. Soc. 93 (2010) 342–344.
[36] L. Vladislavova, C. Thieme, T. Zscheckel, C. Patzig, T. Höche, C. Rüssel, Heterogeneous nucleation of $Ba_{1-x}Sr_xZn_2Si_2O_7$ from a $BaO/SrO/ZnO/SiO_2$ glass using platinum as nucleation agent, J. Eur. Ceram. Soc. 37 (2017) 4801–4808.

5.6 The effect of different platinum concentrations as nucleation agent in the $BaO/SrO/ZnO/SiO_2$ glass system

Liliya Vladislavova, Michael Kracker, Tilman Zscheckel, Christian Thieme,

Journal of Materials Science **53** (2018) 11204–11215.

https://doi.org/10.1007/s10853-018-2399-9

Authors	Liliya Vladislavova	Michael Kracker	Tilman Zscheckel	Christian Thieme	Christian Rüssel
Conception of the research approach	X	X			X
Planning of examinations	X	X			X
Data collection	X	X	X		
Data analysis and interpretation	X	X	X		X
Writing the manuscript	X	X	X	X	X
Credits	1.0				

J Mater Sci (2018) 53:11204–11215

Ceramics

The effect of different platinum concentrations as nucleation agent in the BaO/SrO/ZnO/SiO_2 glass system

Liliya Vladislavova[1,*], Michael Kracker[1], Tilman Zscheckel[1], Christian Thieme[1,2], and Christian Rüssel[1]

[1] Otto-Schott-Institut, Chair of Glass Chemistry I, Jena University, Fraunhoferstr. 6, 07743 Jena, Germany
[2] Fraunhofer Institute for Microstructure of Materials and Systems IMWS, Walter-Hülse-Str. 1, 06120 Halle, Germany

Received: 2 February 2018
Accepted: 2 May 2018
Published online: 14 May 2018

ABSTRACT

The recently reported solid solution of $Ba_{1-x}Sr_xZn_2Si_2O_7$ has a similar structure to the high-temperature phase of $BaZn_2Si_2O_7$ and possesses a coefficient of thermal expansion close to zero or even negative. Without nucleating agents, glasses in this system show solely surface crystallization. In order to stimulate volume crystallization, different quantities of platinum were added to the glass. The characteristic temperatures of the glasses were obtained by differential scanning calorimetry. In order to achieve volume crystallization, a two-step thermal treatment (nucleation and crystal growth) above the glass transition temperature was carried out. The phase identification was performed by X-ray diffraction, and the microstructure was studied by scanning electron microscopy including energy-dispersive X-ray spectroscopy and electron backscatter diffraction.

Introduction

In the past decade, materials with negative coefficients of thermal expansion (NTE) or close to zero thermal expansion (ZTE) are attracting considerable interest [1–3]. Although most materials expand during heating, crystalline phases which exhibit NTE exist. One of the most important class of materials with NTE behavior is based on glass ceramics containing lithium alumosilicates, such as β-quartz, eucryptite, spodumene or keatite [1]. These phases are crystallized from glass and hence enable to tailor the thermal expansion by optimizing the temperature–time schedule used for the crystallization process. Besides, other materials, such as $BaAl_2B_2O_7$, ZrW_2O_8, $ZrMo_2O_8$ [2–4], are also reported in the literature. The latter, however, are not industrially produced as compact material, because the chemical durability is not sufficient for many applications. ZrW_2O_8 and $ZrMo_2O_8$ cannot be crystallized from glasses in concentrations where zero thermal expansion can be achieved [4–7].

Materials which possess zero thermal expansion have found wide applications, e.g., as cooktop panels and as telescope mirror blanks, due to their high thermal shock resistance and because they keep their

Address correspondence to E-mail: liliya.vladislavova@uni-jena.de

https://doi.org/10.1007/s10853-018-2399-9

shape with high accuracy also under non-isothermal conditions [1, 8]. Another field which is still of interest where new materials with these characteristics are highly desired are the space programs funded by NASA, SpaceX and others [3, 9].

Another crystalline phase recently reported to possess negative thermal expansion is $Ba_{0.5}Sr_{0.5}Zn_2Si_2O_7$. This compound is now intensely studied because of its complex behavior. The pure phase $BaZn_2Si_2O_7$ occurs as a low-temperature (LT) phase or as a high-temperature (HT) phase [10]. The LT phase is stable up to 280 °C and is monoclinic with the space group $C2/c$; the mean coefficient of thermal expansion (CTE) for the temperature range (100–300 °C) is about 17.6×10^{-6} K^{-1} [11]. The low-temperature phase can be stabilized to temperatures up to 800–950 °C by the partial or total substitution of Zn by Co, Cu, Mn, Mg or Ni [11–13]. In analogy, also Si can be substituted against Ge which also stabilizes the low-temperature phase [14]. The $BaZn_2Si_2O_7$ compound shows a phase transition which occurs above a temperature of 280 °C and is accompanied by a high volume expansion of around 2% caused by a change in the structure from monoclinic below the phase transition to orthorhombic above the phase transition. In the case where the orthorhombic lattice is observed, the CTE is low and partially negative [12]. Recently, it was reported that a substitution of more than 10% of Ba by Sr leads to the formation of a new phase which has a structure similar to the high-temperature phase of $BaZn_2Si_2O_7$ which, however, is stable at room temperature [15, 16].

For the characterization of this phase, a single crystal with the composition $Ba_{0.6}Sr_{0.4}Zn_2Si_2O_7$ was studied by single-crystal X-ray diffraction and the thermal expansion was determined as a function of the temperature and the crystallographic direction using high-temperature powder diffraction in combination with Rietveld refinement [16]. Unfortunately, this phase exhibits some drawbacks also observed for other low thermal expansion materials, such as highly anisotropic CTEs, which in the different crystallographic directions of the $Ba_{1-x}Sr_xZn_2Si_2O_7$ can vary between -30×10^{-6} K^{-1} (for b-axis) and $+20 \times 10^{-6}$ K^{-1} (for c-axis) in a temperature range from 30 to 600 °C [1, 16]. This effect often leads to crack formation and may result in a failure of the material. Nevertheless, it has been shown that crack-free sintered materials with low thermal expansion, based on $Ba_{1-x}Sr_xZn_2Si_2O_7$, can be prepared using a sol–gel method and subsequent hot pressing [17]. It has also been shown that sintering of a glass and subsequent crystallization lead to glass–ceramics with very different CTEs depending on the ratio of Ba/Sr and the used particle size [15, 17].

The main advantage of the $Ba_{1-x}Sr_xZn_2Si_2O_7$ solid solutions is that they can easily be crystallized from silicate glasses in high volume concentrations [18, 19]. For this purpose, the degree of crystallinity, the crystallite size and its distribution must be optimized by tailoring the glass composition and the temperature–time schedule during crystallization. From previous investigations on $Ba_{1-x}Sr_xZn_2Si_2O_7$, it is known that the surface crystallization is predominant and that the crystal growth of the surface layer depends on the surface pre-treatment of the samples [20]. This is a good indication that controlling the crystal size is possible. In a previous study, the effect of different nucleation agents to the base glass was shown and how they change the crystallization behavior. Adding one of the most commonly used nucleating agents, such as ZrO_2 [18], did not result in sufficient volume crystallization. The number of the crystals was too low and the Avrami parameter showed a combination between surface and volume crystallization which is disadvantageous in order to obtain a fine-grained microstructure.

Up to now, only the addition of platinum as a nucleation agent shows promising results and predominant volume crystallization [19]. This paper describes the effect of different concentrations of platinum, which acts as a nucleating agent in the system $BaO/SrO/ZnO/SiO_2$.

Materials and methods

Glass preparation

The glass batch was prepared from the following raw materials: $BaCO_3$ (Merck > 98.5%), $SrCO_3$ (Ferak Berlin or VEB Laborchemie Apolda > 99%), ZnO (Carl Roth GmbH + Co KG > 99%), SiO_2 (Carl Roth GmbH + Co KG > 99%) and $PtCl_4$ (Merck > 57.5% Pt). A quantity of 0.01% $PtCl_4$ was dissolved in acetone and then given to the glass batch, thoroughly mixed for 2 h and subsequently dried. The batch (for 400 g glass) was melted in a platinum crucible using an induction furnace. For 1 h, a temperature in the range from 1300 to 1350 °C was applied and

subsequently increased to 1400 °C and kept for additional 2 h. During this time, the melt was stirred using a platinum stirrer with 60 min^{-1}. Then the stirrer was removed and the glass was soaked for another 10 min. The glass was cast on a preheated steel mold and transferred to a muffle furnace preheated to a temperature of 680 °C. Then the furnace was switched off, and the sample was allowed to cool with a rate of approximately 3 K/min. The batch compositions of the respective samples are summarized in Table 1.

Optical measurements

The optical transmission spectra were recorded using a Shimadzu UV-3102 PC UV–Vis–NIR scanning spectrophotometer in a wavelength range from 300 to 700 nm at polished samples with a thickness of 11 mm. All measurements were generally taken in a two-beam mode using a polished reference sample with a thickness of 1 mm made from the same glass. Hence, the effective sample thickness is 10 mm. Generally, two different optical setups were used. First, a direct transmission setup where sample and reference were placed in the light beams and the transmitted light was captured by the detector. A slit wide of 2 nm and an increment of 0.5 nm were used for the direct transmission setup. Second, a transmission setup where sample and reference were placed in the front of an integrated sphere attachment (Shimadzu ISR-3100) in order to capture an additional amount of scattered light. For this setup, a slit wide of 20 nm and an increment of 1 nm was used. For a reliable coloration representation of the glasses, a flatbed scanner (Canon CanoScan 8800F) with different illumination modes was used [21]. A black background was applied in order to show the backscattered light, and a backlight module was used to record the transmitted light.

Table 1 Batch compositions of the studied samples

Sample (ppm)	Chemical composition in mol%				
	BaO	SrO	ZnO	SiO_2	$PtCl_4$
100*	8	8	34	49.99	0.01
50	8	8	34	50	0.005
30	8	8	34	50	0.003
10	8	8	34	50	0.001
0*	8	8	34	50	–

*The value for the glasses is taken from Refs. [18, 19]

Differential thermal analysis

Differential scanning calorimetry (DSC) was carried out using a Linseis DSC Pt 1600. This enabled the determination of characteristic temperatures such as glass transition temperature (T_g), onset of crystallization (T_{on}), offset of crystallization (T_{off}) and the crystallization maximum (T_p). In order to minimize the effect of surface crystallization, glass powder with a mass of 0.15 g was given to a DSC platinum crucible, heated to the liquidus temperature for 5 min in a muffle furnace and then cooled in air. The measurements were taken in the DSC device using different heating rates (2, 5, 10, 15 and 20 K/min).

DSC measurements are a useful tool for collecting kinetic data including the activation energies and the order of reaction (n) known as Avrami parameter. The order of crystallization was calculated by the method proposed by Ozawa for the determination of the Avrami parameter using Eq. (1) [22–24].

$$-n = \left|\frac{d[\ln(-\ln(1-x))]}{d(\ln\beta)}\right|_T \quad (1)$$

Here, n is the Avrami parameter, x describes the crystallization degree defined as the ratio A_t/A (A—the total area under the exothermic peak, A_t—area under the exothermic peak up to a chosen temperature) and β is the heating rate in units of (K/min).

The area under the crystallization peak for a chosen temperature was calculated for all supplied heating rates. The temperature varied depending on the glass composition and is usually determined by the rule that the A_t/A has to be in the range from $0.2 \leq x \leq 0.8$, which improves the accuracy of the method.

Furthermore, the activation energy was calculated by the Kissinger equation, Eq. (2) [22, 25, 26]:

$$\ln\left[\frac{\beta}{T_p^2}\right] = \frac{-E_a}{RT_p} + \text{const} \quad (2)$$

as well as by Ozawa equation (for calculating the activation energy), Eq. (3) [22, 27]:

$$\ln[\beta] = \frac{-E_a}{RT_p} + \text{const} \quad (3)$$

The modified Kissinger equation [Matusita and Sakka method, see Eq. (4)] [22, 24, 25] gives a better approximation for the activation energy if volume crystallization takes place. This is related to the nucleation and growth of the crystallites in the amorphous matrix.

$$\ln\left[\frac{\beta^n}{T_p^2}\right] = \frac{-mE_a}{RT_p} + \text{const} \quad (4)$$

In these equations, T_p is the temperature attributed to the maximum of the crystallization peak, β is the heating rate, E_a is the activation energy, R is the gas constant, and n (Avrami coefficient, calculated from Eq. 1) and m are the dimensionality of crystal growth. The values of m depend on the crystallization mechanism and can be found in Ref. [22].

Additionally, 60 mg of powders with different particle sizes (25–500 µm) was given in platinum crucibles and heated up with a rate of 10 K/min to 1000 °C.

Microstructural analyses

The crystal morphology was studied on polished and carbon-coated samples using the scanning electron microscopes (SEM) JEOL 7001 F and JEOL 6510LV.

For samples studied with electron backscatter diffraction (EBSD), colloidal silica was used in an additional final polishing step. The carbon coat was applied under vacuum at 10^{-3} Pa in order to avoid surface charging. A DigiView 3 EBSD camera was used to collect the diffraction patterns at an acceleration voltage of 20 kV, a working distance of 15 mm and a step size = 280 nm between neighbored points of the scan. The patterns were saved and interpreted using the software packages TSL OIM Data Collection and Data Analysis 5.31. Grain Confidence Index Standardization procedure with a grain size = 6 and the grain tolerance angle = 5° CI $\geq$ 0.1. The reference direction of the inverse pole figure (IPF) color code is [001], i.e., the normal of the sample surface. Energy-dispersive X-ray spectroscopy (EDXS) was carried out using an acceleration voltage of 10 kV with a working distance of 15 mm. The element distribution maps show net counts for the regions of interest (ROI); quantitative analyses were not performed.

The densities were determined using a helium pycnometer Micromeritics AccuPyc 1330.

Results

The obtained glasses are transparent without bubbles, crystals and striae; however, a greyish coloration starts to appear after adding 30 ppm of platinum and the intensity increases with the platinum concentration. Figure 1a shows transmission spectra of glasses with different platinum concentrations using different measurement setups. The solid lines are recorded by a simultaneous direct two-beam transmission measurement of samples with a thickness of 11 mm and a reference which had a thickness of 1 mm and was made of the same glass. Thus, the effective thickness is 10 mm. The transmission is decreased with increasing platinum content from 99.6% for 0 ppm platinum to 28.2% for 100 ppm platinum. The dashed lines represent a different transmission measurement setup using an integrated sphere attachment. The transmission is also decreased with increasing the platinum content from 98.6% for 0 ppm platinum to 47.3% for 100 ppm platinum.

In Fig. 1c, the solid black line represents the transmission values at 500 nm measured by the direct transmission. The black dashed line, however, shows the transmission values at 500 nm using the integrated sphere attachment. The difference between the direct transmission and integrated transmission is shown by the solid red line. With increasing platinum content, the difference between these two measurements also increases.

The optical appearance of the glasses is shown in Fig. 1b. A flatbed scanner was used to capture the images. The black background is used to show the scattering behavior. The white background (backlight setup) allows the presentation of the realistic coloration of the samples and corresponds to the direct transmission setup in Fig. 1a. With increasing platinum concentration, the samples become more greyish and at the same time, the samples show also a stronger white coloration using the black background.

Figure 2 presents DSC profiles of glasses with different platinum concentrations in comparison with the base glass without platinum, supplying a heating rate of 10 K/min. Adding different concentrations of platinum does not significantly change the glass transition temperature T_g. The lowest T_g of 672 °C is observed in the base glass, while the highest value 680 °C was obtained from the glass with 30 ppm platinum. The other characteristic temperatures are strongly affected by the addition of platinum. For the base glass, the onset and the crystallization peak temperature are 916 and 948 °C, respectively. An addition of 10 ppm platinum already leads to a shift of the onset and the crystallization peak to 837 and

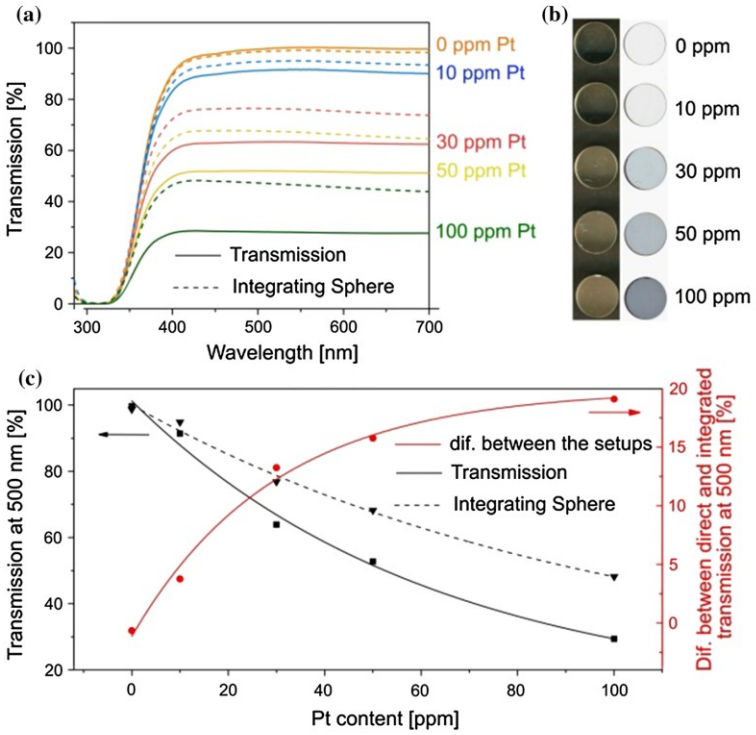

Figure 1 Recorded UV–Vis spectra in order to see and explain the darkening and scattering of the samples with different Pt concentrations. **a** Optical transmission spectra using a direct two-beam transmission setup (solid lines) and using an additional integrated sphere attachment behind the samples (scattered lines). **b** Images obtained with a flatbed scanner using a black background (left) and a backlight illumination (right). **c** Measured direct transmission at a wavelength of 500 nm (black solid line), measured integrated transmission at a wavelength of 500 nm (black dashed line), difference in transmission between the direct two-beam setup and the used integrated sphere attachment at a wavelength of 500 nm (red line).

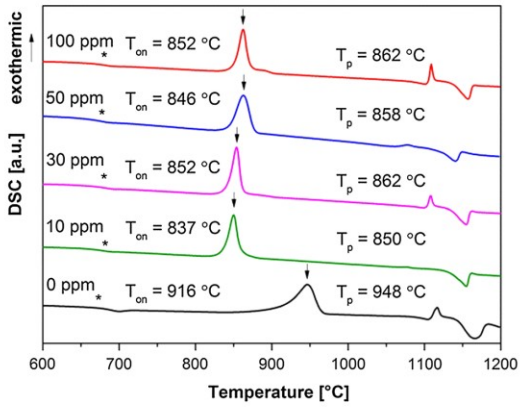

Figure 2 DSC profiles of glasses with different platinum concentrations using a heating rate of 10 K/min. The arrows and stars mark the maxima of the exothermic peaks and the glass transition temperatures, respectively.

850 °C, respectively. Regardless the initial shift to lower temperatures, a further increase in the platinum concentration does not lead to significant changes in the onset and the crystallization peak temperatures. For 30 and 50 ppm platinum, the onset temperatures are 852 and 846 °C, respectively. The crystallization peak temperatures show a similar change and are 862 °C for 30 ppm and 858 °C for 50 ppm platinum. The sample doped with 100 ppm has the same characteristic temperature as that with 30 ppm. All characteristic temperatures are summarized in Table 2.

In Fig. 3, the effect of different platinum concentrations on the exothermic crystallization peak observed in the DSC curves is shown. Maximum peak temperatures T_p (Fig. 3a), full widths at half maximum (FWHM, Fig. 3b), and peak heights (Fig. 3c) are shown as a function of the platinum concentration using two different heating rates (5 and 20 K/min). As demonstrated in Fig. 3a, T_p decreases strongly if platinum is added to the glass. The peak temperature is, within the limits of the method, almost not affected by a further increase in the platinum concentration. Figure 3b shows a decrease in the FWHM with the increase in the platinum concentration up to 50 ppm; a further increase in the

Table 2 Results from the DSC profiles of the samples with different platinum concentrations

Name (ppm)	T_g (°C)	T_{on} (°C)	T_{off} (°C)	T_p (°C)	T_m (°C)	T_{on}–T_g (K)
100*	679	852	871	862	1153	173
50	677	846	864	858	1155	173
30	680	852	868	862	1156	166
10	679	837	859	850	1154	170
0*	672	916	969	948	1165	245

T_g glass transition temperature, T_{on} onset of the crystallization peak, T_{off} offset of the crystallization peak, T_p temperature of the crystallization peak, T_m temperature of melting

*The values for these glasses are taken from Refs. [18, 19]

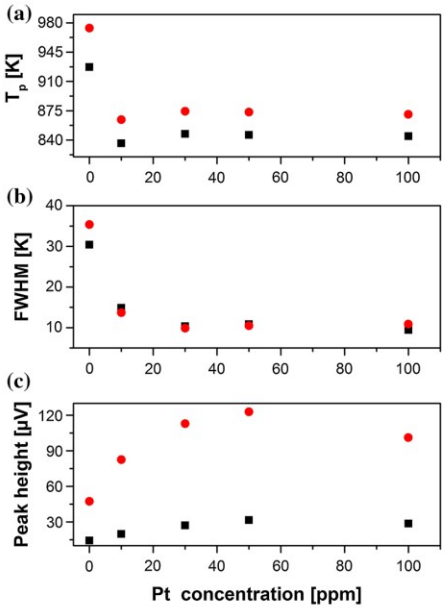

Figure 3 Evaluation of the exothermic effects observed in the DSC measurements. Peak temperature, T_p, full width at the half maximum, FWHM and peak height are given as a function of the platinum concentration using heating rates of 5 K/min (filled square) and 20 K/min (filled circle).

platinum concentration, however, did not result in a further decrease in the FWHM. By contrast, in Fig. 3c, an increase in the peak height is observed up to 50 ppm of platinum, while for a higher platinum concentration of 100 ppm, the peak height is slightly decreased. The two heating rates (5 and 20 K/min) show that the results are independent of the heating rate and change with the platinum concentration.

Figure 4 presents the crystallization behavior of the sample doped with 100 ppm platinum; the peak heights and the peak positions are plotted versus the average particle size. Up to a size of around 200 µm, the peak heights increase and the peak temperatures are shifted to higher values. Further increasing particle sizes do not result in further changes and both, the peak temperature and the peak height remain constant within the limits of error.

In Fig. 5, SEM micrographs of the studied glass compositions with different platinum concentrations nucleated at 720 °C for 100 h are presented. After the heat treatment, the samples were cut in the middle to ensure observation of the sample volume. It can be seen that an increase in the platinum concentration also leads to an increase in the number of crystals and hence the amount of residual glass phase decreases. The platinum particles can clearly be seen as white spots due to the much higher atomic mass of metallic platinum in comparison with the surrounding oxide material. In some cases, but not for all observed crystals, a platinum particle can be found in the center of the oxide crystals. Small cracks appear near the center of some of the crystals. Nevertheless, a small amount of glass can still be found between the

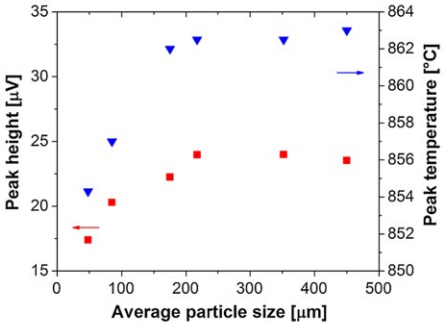

Figure 4 Analysis of the DSC curves of the glass with 100 ppm Pt; height (filled down triangle) and temperature of the crystallization peak (filled square) as a function of the particle size.

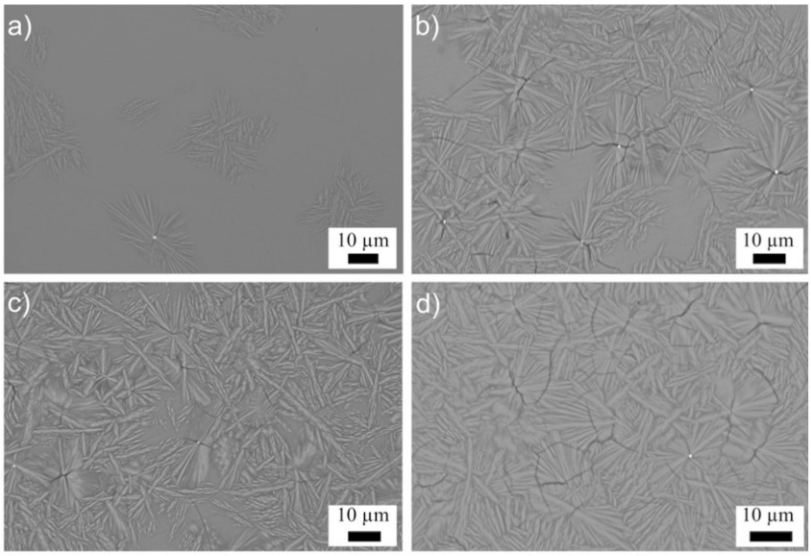

Figure 5 SEM micrographs of glasses with different platinum concentrations heat treated at 720 °C for 100 h: **a** 10 ppm; **b** 30 ppm; **c** 50 ppm; **d** 100 ppm.

crystal lamellae. In Fig. 6, the results from an EDXS measurement performed within the white frame in Fig. 6a are illustrated. The sample with a platinum concentration of 50 ppm was thermally treated at 710 °C for 48 h followed by 30 min at 780 °C. Figure 6b–e shows elemental mappings of Pt, Si, Ba and Zn, respectively. Ba and Zn are enriched in the crystals, while Si is depleted. The bright spot in the middle of Fig. 6a is metallic platinum and the starting point of the crystal.

Electron backscatter diffraction was used for the identification of the crystal phases and the

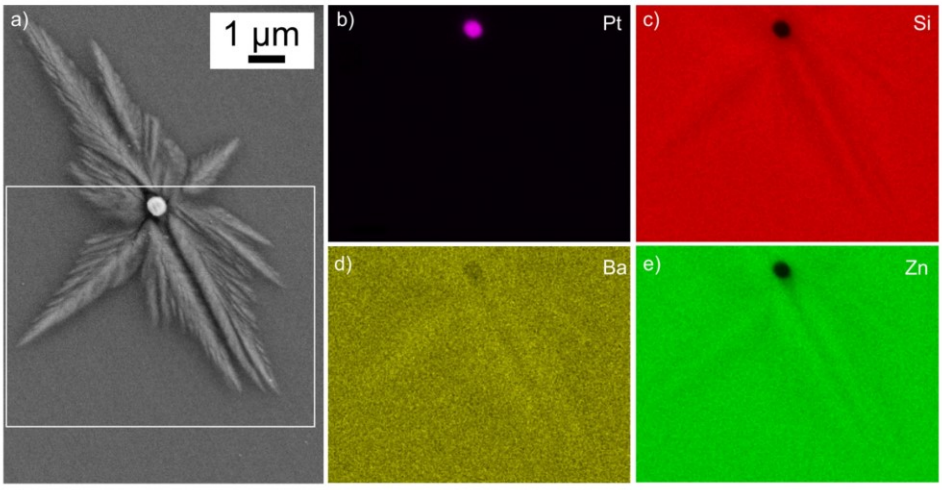

Figure 6 EDXS mapping of the sample with 50 ppm platinum thermally treated in a first step at 710 °C for 48 h and then at 780 °C for 30 min: **a** SEM micrograph with a Pt particle in the middle, EDXS mappings obtained at an acceleration voltage of 10 kV for **b** Pt M_α (2.048 keV), **c** Si K_α (1.740 keV), **d** Ba L_α (4.465 keV) and **e** Zn L_α (at 1.012 keV).

orientations of the respective crystals. Figure 7 shows an SEM micrograph and a combined image quality (IQ) + inverse pole figure map (IPF) of a sample with 50 ppm platinum thermally treated at 710 °C for 48 h followed by 30 min at 780 °C. In this figure, a representative crystal structure with a platinum particle in the center is shown. All patterns of the scan that fulfill the criteria of reliability were attributable to the orthorhombic structure of the $Ba_{0.6}Sr_{0.4}Zn_2Si_2O_7$ (ICSD no. 429938). The color code of the inverse pole figure describes the crystal direction perpendicular to the sample surface. The white unit cells and the corresponding *c*-axis directions help to read the map. The *c*-axes [001] are oriented parallel to the long axis of the crystal. Furthermore, the most parts of the crystal show different absolute orientations, but the *a*-axes [100] are almost perpendicular to the sample surface (green dots). Diffraction patterns from the platinum particle were of very low IQ and did not fulfill the criteria of reliable indexing, and hence there were not included to the results.

Discussion

Optical analysis

With increasing platinum concentration, the optical transmission is reduced from 99.6% to 28.2% for 0 and 100 ppm platinum, respectively. In contrast to the direct measurement, the samples are placed in front of an integrated sphere (comparable to an Ulbricht sphere). Hence, forward scattered portions of the transmitted light are additionally collected and integrated into the sphere. The dashed lines in Fig. 1a represent the spectra measured by the integrating sphere attachment. The transmission is much higher in the case of the integrated sphere. For a platinum content of 100 ppm, the difference at a wavelength of 500 nm is 19.1%. This indicates that the influence of scattered light increases with increasing platinum concentration.

By contrast, the sample with 0 ppm platinum shows almost no difference between the measurement setups. Hence, the described effect is not an artifact of the measurement setup. The detected differences at 0 ppm platinum are solely caused by the error of measurement.

The scattering intensity rises with increasing platinum concentrations. This is also indicated by the increasing white, greyish coloration using a black background behind the samples during the image capturing inside a flatbed scanner (Fig. 1c). Most of the light transmitted through the sample is absorbed by the black background. Only the backscattered light can be measured. Due to the different positions of light source and detector inside the optical system, the specular reflection of the sample surface is not imaged, as seen for the fully transparent sample without platinum. The white background is achieved by backlight illumination and represents a realistic coloration of the glass samples. Besides, this method represents the direct transmission setup shown in Fig. 1a, b. This method has been applied successfully

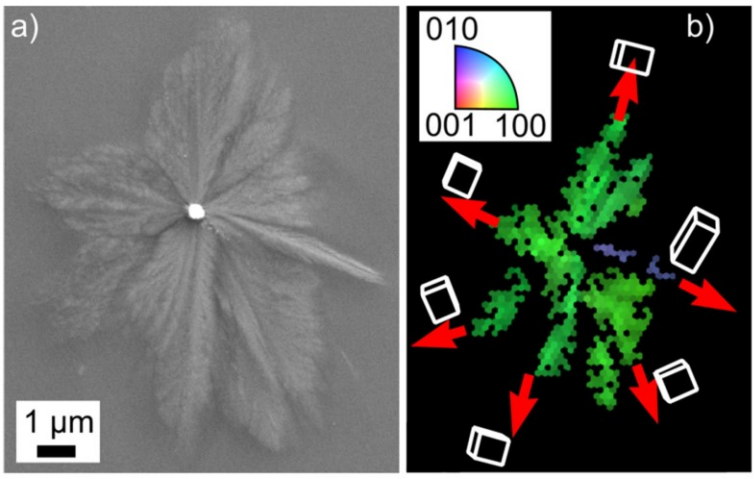

Figure 7 SEM micrograph of a sample with 50 ppm platinum thermally treated in a first step at 710 °C for 48 h and then at 780 °C for 30 min: **a** micrograph of a cut perpendicular to the surface, **b** combined image quality (IQ) + inverse pole figure (IPF) map with white-lined unit cells with *c*-axis direction (red lined) at certain crystal positions.

on colored gold nanoparticle layers deposited on glass surfaces [21].

Due to the extinction coefficient of platinum, the samples become darker with increasing platinum content. Nevertheless, the scattering intensity also increases with increasing platinum content and it can be concluded that the optical properties are influenced by metal absorption and the scattering behavior of the small platinum particles. Furthermore, if the platinum were homogeneously distributed as ions inside the glass, scattering would not occur. Hence, at least a part of the platinum is present as metallic particles inside the glasses.

Thermal analyses, kinetics of nucleation and crystal growth

Thermal analyses by DSC were proved to be a suitable tool for predicting the crystallization behavior of glasses from which the $Ba_{1-x}Sr_xZn_2Si_2O_7$ phase is formed [18, 19]. As Fig. 2 shows, even a concentration of 10 ppm of platinum is sufficient to affect the crystallization behavior significantly. The crystallization peak for a glass without platinum is observed at 948 °C, while for a sample with a platinum concentration of 10 ppm, the peak drops to 850 °C, i.e., a temperature nearly 98 K lower (see Fig. 3a. This indicates that already a small amount of platinum changes notably the crystallization tendency of the system. A further increase in the platinum concentration does not lead to a significant shift of the crystallization peak temperature. It varies only by 12 K for different platinum concentrations. This result is a little bit surprising but the effect is not due to a measuring effect (error) because it was observed for all supplied heating rates. An explanation can be given from the classical theory, the addition of noble metals to the glass systems leads to active centers for the nucleation/crystallization processes denoted as heterogeneous nucleation. This leads to a decrease in the specific surface of the nucleus. This explains the significant shift of crystallization peak when adding 10 ppm of Pt. Higher concentrations of platinum do not change significantly the crystallization peak, because at any platinum concentration the crystals start to grow at the same temperature. The time required until the growing crystals occupy the whole volume should hence only marginally increase with the platinum concentration. Unfortunately, comparisons with the DSC results of other glass systems from the literature where platinum was used as a nucleation agent cannot be made due to the lack of data. As seen in Table 2, T_g and T_m of the glasses are not affected significantly. The temperature difference T_{on}–T_g is frequently considered as a measure of the glass stability; the higher the difference, the more stable is the glass against devitrification during heating. The sample with 0 ppm platinum shows the highest value which should be attributed to the best resistance against devitrification.

The platinum concentration affects the intensity and the FWHM of the crystallization peak in the DSC profiles as seen in Fig. 3b, c. The FWHM is close to 30 K for the platinum-free glass and decreases to 10 K for the samples with higher platinum concentrations. In case of the peak intensity, exactly the opposite trend is observed. Numerous studies [24, 28, 29] published in the past proved that the change in the shape, the width and the intensity of the crystallization peak is usually an indication of a change in the crystallization mechanism. Broad crystallization peaks with low intensities are attributed to surface crystallization, while narrower peaks with higher intensity are an indication of volume crystallization [18, 24, 28, 29]. Hence, this can be considered as another indication that the platinum has a nucleating effect.

Two methods for the prediction of a crystallization mechanism were used and compared with previous results. The determination of the Avrami parameter is a well-known method, based on Eq. (1) [23, 24]. The Avrami parameter for the glass without platinum was determined at 920 °C and is equal to 1 which is an indication of surface crystallization and was confirmed by microstructural investigations in previous studies [18, 20]. The Avrami parameter was determined at 842 °C for glasses doped with 30–100 ppm platinum. For the glass with 10 ppm, a temperature of 837 °C was chosen, which was necessary because of the lower crystallization temperature of this system. The Avrami parameters for the samples with 10–50 ppm are equal to 3 which is an indication of volume crystallization and for the 100 ppm platinum it is equal to 4, which is correlated with 3D volume crystallization [18, 22, 23, 30]. The results were confirmed by a microstructural study as illustrated in Fig. 5, where all platinum containing samples show volume crystallization with the same crystal growth morphologies. The difference in the Avrami parameters but the lack of a change in the

morphology can be due to the fact that the Avrami parameter is dependent on the chosen temperature and can vary slightly. This was previously shown in a study by Pascual [24] for a glass with the composition 30 BaO·50 SiO_2·20 ZnO.

Furthermore, the different heating rates can be utilized for the calculation of the activation energies using the Kissinger [26] (see Eq. 2) as well as the Ozawa equation [22, 27] (see Eq. 3). Both methods are fairly similar and the obtained results differ within a range of only 6%. All calculated values are summarized in Table 3. According to Matusita [31], if volume crystallization occurs, additional parameters have to be taken into account which are denoted as "growth parameters" [24, 31]. They indicate the growth morphology and the mechanism, depending on the Avrami parameter, n. The value of m can be found in a table published by Donald [22]. Since this procedure is based on the Kissinger equation, in many sources, the equation is called the modified Kissinger equation. As seen in Table 3, the sample with 0 ppm platinum has an Avrami parameter = 1 which means $m = 1$ and, hence, the modified equation corresponds to the Kissinger equation [18, 23, 24]. For different platinum concentrations, a significant change in the values of the activation energies is determined but no clear trend can be observed.

In Fig. 4, another method for the determination of the crystallization tendency is presented. This method was developed by Ray et al. [32], and they proposed that the peak height and T_p may predict the crystallization behavior of a sample if measurements using different particle sizes are performed. If the peak intensity and the crystallization peak temperature decrease with increasing particle size, surface crystallization is predominant; however, if the peak intensity increases, volume crystallization is prevalent. This method was tested for the sample with 100 ppm platinum and particle size in the range from 25 to 500 µm. As shown in Fig. 4, both parameters increase with increasing particle size or with other words, the glass exhibits volume crystallization. In a previous study performed by Kracker et al. [20] for the glass system without platinum, the tendency was reversed and the peak intensity decreased with increasing particle size.

Microstructural analysis

The microstructure of all platinum containing glasses was investigated via SEM. As seen in Fig. 5, all samples exhibit the tendency to volume crystallization; nevertheless, the number of the crystals depends on the platinum concentration, if all samples are thermally treated at 720 °C for 100 h. The sample with the lowest platinum concentration of 10 ppm has the lowest number density of crystals and the highest concentration of glass phase. The mean size of the $Ba_{1-x}Sr_xZn_2Si_2O_7$ crystals is 41 µm. The statistical analysis was made from numerous SEM images, and only crystals with a platinum particle in the center were regarded. This way reduces the error which can occur during the determination of the length of the crystal from the SEM images. A small extend of crack formation is visible; most probably the origin of the cracks is near the center of the crystal where the platinum particle and the crystalline phase are in direct contact to each other. With increasing platinum concentrations, the concentration of the crystals increases and their mean size seems to decrease for the sample with 30 ppm platinum, and it is 31 µm. Statistical analyses of the particle sizes in samples with more than 50 ppm platinum are hard to

Table 3 Activation energies determined by the Kissinger plot, E_{ak}; by the Ozawa plot, E_{ao}; and by the modified Kissinger plot, E_{am}; furthermore, Avrami parameters, refractive indices, n_e and densities are given

Name (ppm)	E_{ak} (kJ mol^{-1})	E_{ao} (kJ mol^{-1})	E_{am} (kJ mol^{-1})	Avrami parameter	n_e	ρ (g/cm^3)
100*	285	304	399	4	1.6538	3.835
50	529	547	812	3	1.6542	3.845
30	469	488	722	3	1.6541	3.839
10	473	492	728	3	1.6543	3.835
0*	356	378	–	1	1.6599	3.832

*The values for these glasses are taken from Refs. [18, 19]

perform since the amount of glassy phase decreases significantly and individual crystals are hard to be found.

EDXS analyses were performed for the sample with 50 ppm platinum, thermally treated in the first step at 710 °C for 48 h and subsequently at 780 °C for 30 min. The crystal, shown in Fig. 6, is a typical example of a crystal within the $Ba_{1-x}Sr_xZn_2Si_2O_7$ solid solution series in the presence of platinum. The bright spherical particle in the center shows a clear enrichment of platinum as well as the absence of all other elements and hence it consists of metallic platinum. Furthermore, it seems to be the starting point of the crystal growth (see Fig. 6a). Besides, Si is slightly depleted in the crystals, i.e., enriched in the residual glassy phase (see Fig. 6c), while the opposite is observed for Ba and Zn.

The microstructure analysis with EBSD revealed that only the orthorhombic symmetry according to the ICSD file no. 429938 for $Ba_{0.6}Sr_{0.4}Zn_2Si_2O_7$ could be attributed to the diffraction patterns of the scan. This in agreement with a previously published study using X-ray diffraction in the same glass ceramic system [19]. Some very fine compartmented regions of the crystals could not reliably be indexed. Residual glass in between the crystals and possible orientation changes between the crystal parts lead to very low image quality and pattern superposition. Hence, the indexing results of those patterns did not fulfill the filter criteria and were excluded from the dataset. The patterns from the platinum particles are also of low IQ caused by the topography of the particles on the one hand and low crystal perfection by deformation, from polishing on the other hand (metallic platinum shows a plastic deformation behavior in comparison with the glass ceramics). Hence, they cannot be attributed to platinum or any other phase. The results of the EBSD measurements show a clear orientation of the *c*-axis [001] which is parallel to the fastest growing axis of the cut crystal. This is in agreement with recently published studies of surface crystallization in the $Ba_{1-x}Sr_xZn_2Si_2O_7$-system [20, 33].

Conclusion

Platinum seems to be a suitable nucleation agent for the $Ba_{1-x}Sr_xZn_2Si_2O_7$ phase. As proved by crystallization kinetics, even a small amount of platinum significantly changes the crystallization behavior of the system from sole surface crystallization to volume crystallization. A comparatively high platinum concentration of 100 ppm reduces significantly the size of the crystals and increases their number. Unfortunately, small crack formation still can be seen close to the origin of the crystals and further improvement has to be done in the future to ensure a fine-grained microstructure without substantial cracking.

Acknowledgements

This work was funded by the German Federal Ministry of Education and Research under the Grant Numbers 03VP01701 and 03VP01702.

References

[1] Bach H, Krause D (2005) Low thermal expansion glass ceramics, 2nd edn. Springer, New York

[2] Wang W, Huang R, Li W, Tan J, Zhao Y, Li S, Huang C, Li L (2014) Zero thermal expansion in $NaZn_{13}$-type $La(Fe,Si)_{13}$ compounds. Phys Chem Chem Phys 17:2352–2356

[3] Macdonald M, Badescu V (2014) The international handbook of space technology, 1st edn. Springer, Praxis

[4] Lind C, Wilkinson AP, Hu Z, Short S, Jorgensen JD (1998) Synthesis and properties of the negative thermal expansion material cubic $ZrMo_2O_8$. Chem Mater 10:2335–2337

[5] Tauch D, Rüssel C (2005) Glass-ceramics with zero thermal expansion in the system $BaO/Al_2O_3/B_2O_3$. J Non-Cryst Solids 351:2294–2298

[6] Yamai I, Oota T (1985) Low-thermal-expansion polycrystalline zirconyl phosphate ceramic. J Am Ceram Soc 68:273–278

[7] Müller G, Sternitzke M (1993) Computer modelling of structure and thermal expansion of β-quartz-and keatite-type aluminosilicates. J Mater Sci Lett 12:278–280

[8] McMillan PW (1979) Glass-ceramics, 2nd edn. Academic Press, London

[9] Browder JS, Ballard SS (1969) Low temperature thermal expansion measurements on optical materials. Appl Opt 8:793–798

[10] Kerstan M, Rüssel C (2011) Barium silicates as high thermal expansion seals for solid oxide fuel cells studied by high-temperature X-ray diffraction (HT-XRD). J Power Sour 196:7578–7584

[11] Thieme C, Rüssel C (2015) High thermal expansion in the solid solution series $BaM_{2-x}Ni_x Si_2O_7$ (M = Zn, Mg, Co)—the effect of Ni-concentration on phase transition and

expansion. J Mater Sci 50:3416–3424. https://doi.org/10.1007/s10853-015-8900-9

[12] Kerstan M, Thieme C, Grosch M, Müller M, Rüssel C (2013) $BaZn_2Si_2O_7$ and the solid solution series $BaZn_{2-x}Co_xSi_2O_7$ ($0 < x \leq 2$) as high temperature seals for solid oxide fuel cells studied by high-temperature X-ray diffraction and dilatometry. J Solid State Chem 207:55–60

[13] Kerstan M, Müller M, Rüssel C (2012) Thermal expansion of $Ba_2ZnSi_2O_7$, $BaZnSiO_4$ and the solid solution series $BaZn_{2-x}Mg_xSi_2O_7$ ($0 \leq x \leq 2$) studied by high-temperature X-ray diffraction and dilatometry. J Solid State Chem 188:84–91

[14] Thieme C, Rüssel C (2016) Negative thermal expansion in $Ba_{0.5}Sr_{0.5}Zn_2SiGeO_7$. Materials 9:631–636

[15] Thieme C, Rüssel C (2016) Very high or close to zero thermal expansion by the variation of the Sr/Ba ratio in $Ba_{1-x}Sr_xZn_2Si_2O_7$—solid solutions. Dalton Trans 45:4888–4895

[16] Thieme C, Görls H, Rüssel C (2015) $Ba_{1-x}Sr_xZn_2Si_2O_7$—a new family of materials with negative and very high thermal expansion. Sci Rep 5:18040

[17] Kracker M, Thieme C, Häßssler J, Rüssel C (2016) Sol-gel powder synthesis and preparation of ceramics with high- and low-temperature polymorphs of $Ba_{1-x}Sr_xZn_2Si_2O_7$ (x = 1 and 0.5): a novel approach to obtain zero thermal expansion. J Eur Ceram Soc 36:2097–2107

[18] Vladislavova L, Thieme C, Rüssel C (2017) The effect of ZrO_2 on the crystallization of a glass in the system BaO/SrO/ZnO/SiO_2: surface versus bulk crystallization. J Mater Sci 52:4052–4060. https://doi.org/10.1007/s10853-016-0667-0

[19] Vladislavova L, Thieme C, Zscheckel T, Patzig C, Höche T, Rüssel C (2017) Heterogeneous nucleation of $Ba_{1-x}Sr_xZn_2Si_2O_7$ from a BaO/SrO/ZnO/SiO_2 glass using platinum as nucleation agent. J Eur Ceram Soc 37:4801–4808

[20] Kracker M, Vladislavova L, Thieme C, Zscheckel T, Thieme K, Höche T, Rüssel C (2017) Surface crystallization of low thermal expansion $Ba_{0.5}Sr_{0.5}Zn_2Si_2O_7$ from an 8 BaO·8 SrO·34 ZnO·50 SiO_2 glass. RSC Adv 7:44834–44842

[21] Worsch C, Kracker M, Wisniewski W, Rüssel C (2012) Optical properties of self-assembled oriented island evolution of ultra-thin gold layers. Thin Solid Films 520:4941–4946

[22] Donald IW (2004) Crystallization kinetics of a lithium zinc silicate glass studied by DTA and DSC. J Non-Cryst Solids 345:120–126

[23] Guedes M, Ferro AC, Ferreira JMF (2001) Nucleation and crystal growth in commercial LAS compositions. J Eur Ceram Soc 21:1187–1194

[24] Pascual MJ, Lara C, Duran A (2006) Non-isothermal crystallisation kinetics of devitrifying RO–BaO–SiO_2 (R = Mg, Zn) glasses. Phys. Chem. Glas. Eur. J. Glass Sci. Technol. Part B 47:572–581

[25] Wurth R, Pascual MJ, Mather GC, Pablos-Martin A, Munoz F, Duran A, Cuello GJ, Rüssel C (2012) Crystallisation mechanism of a multicomponent lithium alumino-silicate glass. Mater Chem Phys 134:1001–1006

[26] Kissinger HE (1957) Reaction kinetics in differential thermal analysis. Anal Chem 29:1702–1706

[27] Ozawa TA (1976) Modified method for kinetic analysis of thermoanalytical data. J Therm Anal 9:69–373

[28] Massera J, Fagerlund S, Hupa L, Hupa M (2012) Crystallization mechanism of the bioactive glasses, 45S5 and S53P4. J Am Ceram Soc 95:607–613

[29] Ray CS, Day DE (1997) An analysis of nucleation-rate type of curves in glass as determined by differential thermal analysis. J Am Ceram Soc 80:3100–3108

[30] Arora A, Shaaban ER, Singh K, Pandey OP (2008) Non-isothermal crystallization kinetics of ZnO–BaO–B_2O_3–SiO_2 glass. J Non-Cryst Solids 354:3944–3951

[31] Matusita K, Sakka S (1980) Kinetic study of crystallization of glass by differential thermal analysis—criterion on application of Kissinger plot. J Non-Cryst Solids 38:741–746

[32] Ray CS, Yang Q, Huang W, Day DE (1996) Surface and internal crystallization in glasses as determined by differential thermal analysis. J Am Ceram Soc 79:3155–3160

[33] Thieme K, Zscheckel T, Thieme C, Höche T, Rüssel C (2017) On the search for nucleation agents in BaO–SrO–ZnO–SiO_2 glasses: the influence of P_2O_5. J Eur Ceram Soc 38:2017–2026. https://doi.org/10.1016/j.jeurceramsoc.2017.12.034

5.7 Crystallization of $Ba_{1-x}Sr_xZn_2Si_2O_7$ from the BaO/SrO/ZnO/SiO_2 Glass System: Different Platinum Concentrations and the Effect of Sb_2O_3 on Nucleation.

Liliya Vladislavova, Christian Thieme, Tilman Zscheckel, Thomas Höche, and Christian Rüssel

Submitted to the Ceramic International

Authors	Liliya Vladislavova	Christian Thieme	Tilman Zscheckel	Thomas Höche	Christian Rüssel
Conception of the research approach	X				X
Planning of examinations	X				X
Data collection	X		X		
Data analysis and interpretation	X	X	X		X
Writing the manuscript	X	X	X	X	X
Credits	1.0				

Elsevier Editorial System(tm) for Ceramics International

Manuscript Draft

Manuscript Number:

Title: Crystallization of Ba1-xSrxZn2Si2O7 from the BaO/SrO/ZnO/SiO2 Glass System: Effect of Platinum and Sb2O3 on Nucleation

Article Type: Full length article

Keywords: Glass-Ceramics; Crystallization; Nucleation; Strontium Barium Zinc Silicate

Corresponding Author: Miss Liliya Vladislavova, M.Sc.

Corresponding Author's Institution:

First Author: Liliya Vladislavova, M.Sc.

Order of Authors: Liliya Vladislavova, M.Sc.; Christian Thieme; Tilman Zscheckel; Thomas Höche; Christian Rüssel

Abstract: Glasses with the chemical composition 8 BaO·8 SrO·34 ZnO·49.5 SiO2·0.5 Sb2O3 with 50 and 100 ppm platinum were crystallized in a two-step treatment. The first step was performed slightly above the glass-transition temperature at temperatures in the range from 680 to 700 °C and the second at a temperature of 780 °C. In the first step, an increasing number of nuclei were formed, while in the second step, the growth of Ba1-xSrxZn2Si2O7 was observed. The latter phase has negative thermal expansion in a wide temperature range and is a promising candidate for the preparation of zero thermal-expansion glass ceramics. Scanning electron micrographs showed that Ba1-xSrxZn2Si2O7 crystals grow around platinum particles. These crystals are oriented with their c-axes parallel to their longest dimension, i.e., the growth direction. Besides, dendrite-like crystals with unique orientations aligned with their c-axes perpendicular to their primary growth direction are formed. It is shown that appropriately crystallized glasses exhibit a thermal expansion close to zero. The addition of antimony leads to a redox reaction of platinum ions with Sb3+ leading to metallic platinum. This results in an increasing number of platinum particles and hence nucleation sites during thermal treatment at temperatures slightly above Tg.

Suggested Reviewers: Bogdan Ranguelov
Institute of Physical Chemistry, Bulgarian Academy of Sciences, Bulgaria
rangelov@ipc.bas.bg

Tsuyoshi Honma
Nagaoka University of Technology, Japan
honma@mst.nagaokaut.ac.jp

Eduardo Bellini Ferreira
Engenharia de Materiais, Universidade de São Paulo, Brazil
ebferreira@sc.usp.br

Opposed Reviewers:

Cover Letter

Dear Editor,

We would like to submit a manuscript entitled:

"Crystallization of $Ba_{1-x}Sr_xZn_2Si_2O_7$ from the $BaO/SrO/ZnO/SiO_2$ Glass System: Effect of Platinum and Sb_2O_3 on Nucleation".

for publication in Ceramics International.

It was recently reported that the solid solution $Ba_{1-x}Sr_xZn_2Si_2O_7$ has zero to negative thermal expansion. In contrast to many other phases with negative thermal expansion, this phase can be crystallized from glasses and hence should be suitable for the preparation of cooktop panels, telescopes mirrors and other mass production materials, where the thermal expansion properties should be tailored exactly to zero. In order to make the $Ba_{1-x}Sr_xZn_2Si_2O_7$ phase applicable for industrial use, the nucleation and crystallization behavior should be well known.

In the present manuscript, the effect of different platinum concentrations in combination with Sb_2O_3 on the nucleation/crystallization process of the $BaO/SrO/ZnO/SiO_2$ glass system is reported. For the characterization of the glasses and glass-ceramics, intense studies on the crystallization kinetics were performed and Avrami parameters, as well as activation energies, were determined. The resulting microstructures were studied in detail using light scanning microscopy and a scanning electron microscope equipped with an EBSD detector. The addition of Sb_2O_3 to this system results in an increasing number of metallic platinum nanoparticles during thermal treatment at temperatures slightly above T_g. Furthermore, zero thermal expansion is obtained. The effect of small antimony concentrations is surprisingly large.

We hope that this manuscript is appropriate for publication in Ceramics International.

The submitted manuscript presents original research, which has not been published in any other journal. All authors read the manuscript and agree with its submission to Ceramics International

Sincerely,

Liliya Vladislavova

Crystallization of $Ba_{1-x}Sr_xZn_2Si_2O_7$ from the BaO/SrO/ZnO/SiO_2 Glass System: Effect of Platinum and Sb_2O_3 on Nucleation

Liliya Vladislavova[1], Christian Thieme[2], Tilman Zscheckel[1], Thomas Höche[2], and Christian Rüssel[1]

[1]Otto-Schott-Institut für Materialforschung, Chair of Glass Chemistry I, Jena University, Fraunhoferstr. 6, 07743 Jena, Germany

[2]Fraunhofer Institute for Microstructure of Materials and Systems IMWS, Walter-Hülse-Str. 1, 06120 Halle, Germany

Corresponding author: Liliya Vladislavova

email: vladislavova_1@abv.bg

telephone: +49 (0) 3641 948525

fax: +49 (0) 3641 948502

email of Christian Rüssel: ccr@uni-jena.de

email of Christian Thieme: christian.thieme@imws.fraunhofer.de

email of Tilman Zscheckel: tilman.zscheckel@uni-jena.de

Abstract

Glasses with the chemical composition 8 BaO·8 SrO·34 ZnO·49.5 SiO_2·0.5 Sb_2O_3 with 50 and 100 ppm platinum were crystallized in a two-step treatment. The first step was performed slightly above the glass-transition temperature at temperatures in the range from 680 to 700 °C and the second at a temperature of 780 °C. In the first step, an increasing number of nuclei were formed, while in the second step, the growth of $Ba_{1-x}Sr_xZn_2Si_2O_7$ was observed. The latter phase has negative thermal expansion in a wide temperature range and is a promising candidate for the preparation of zero thermal-expansion glass ceramics. Scanning electron micrographs showed that $Ba_{1-x}Sr_xZn_2Si_2O_7$ crystals grow around platinum particles. These crystals are oriented with their c-axes parallel to their longest dimension, i.e., the growth direction. Besides, dendrite-like crystals with unique orientations aligned with their c-axes perpendicular to their primary growth direction are formed. It is shown that appropriately crystallized glasses exhibit a thermal expansion close to zero. The addition of antimony leads to a redox reaction of platinum ions with Sb^{3+} leading to metallic platinum. This results in an increasing number of platinum particles and hence nucleation sites during thermal treatment at temperatures slightly above T_g.

Keywords: Glass-Ceramics, Crystallization, Nucleation, Strontium Barium Zinc Silicate

1. Introduction

Negative thermal expansion (NTE) at room temperature or elevated temperature is a scarcely observed effect because most materials expand upon heating. Among materials possessing a negative coefficient of thermal expansion (CTE) or close to zero-thermal expansion (ZTE), glass-ceramics are widely used in cook panels, gyroscopes and others. [1,2]. The most important of these glass ceramics and the only ones nowadays commercially available are alumosilicates, such as β-quartz, β-eucryptite, spodumene, or keatite [2–6]. All of them are predominantly based on lithium alumosilicates. The respective negative-thermal-expansion phases can be precipitated from glass, using an optimized temperature/time schedule [7]. The CTE, in most cases close to zero, is tailored by adjusting appropriate volume concentrations of the negative expansion phase, phases which exhibit positive thermal expansion, as well as the residual glass phase [2]. Besides the alumosilicate phases mentioned above, other phases, such as ZrW_2O_8, $ZrMo_2O_8$, and $BaAl_2B_2O_7$ have also been reported in the scientific literature [8,10]. Up to now, these materials are not produced in industry, due to a not sufficient chemical durability ($BaAl_2B_2O_7$) or, however, because the crystallization from glasses in quantities which allows adjusting zero thermal expansion is not possible [11]. This makes them difficult to fabricate as larger scale products.

Nowadays, materials with ZTE are widely applied, e.g. as cooktop panels, furnace windows, or as telescope mirror blanks. In the first two applications mentioned, the most important property is the resistivity to changing temperatures over a wide range [2,12]. For telescope mirror blanks, the predominant property is that they keep their shape with high accuracy in a temperature range from -40 to +80 °C. Another rapidly developing field is aerospace (laser gyroscopes) and the space programs funded by NASA, SpaceX, and others where ZTE materials find applications[13].

Recently, a new crystalline phase with negative thermal expansion was reported on: $Ba_{1-x}SrxZn_2Si_2O_7$ [14]. This compound and numerous other derived thereof are presently studied with high intensity. The pure phase $BaZn_2Si_2O_7$ occurs in two modifications, as a low and as a high temperature phase. The low temperature phase has the monoclinic space group *C2/c* and is stable up to 280 ºC. The mean CTE is about $17.6 \cdot 10^{-6}$ K^{-1} [15,16]. If Zn is partially or totally replaced by Co, Cu, Mn, Mg, or Ni, the transition low-temperature to high temperature phase can be shifted to a higher temperature of up to more than 800 °C [17]. In analogy, the substitution of Si against Ge also stabilises the low-temperature phase and shifts the phase transition to higher temperatures [18]. The pure high-temperature phase of $BaZn_2Si_2O_7$ shows a phase transition at 280 ºC which runs parallel to a volume expansion of around 2 % and a change from a monoclinic structure to an orthorhombic one with the space group $Ccm2_1$. The high temperature phase (HT phase) shows a low or partially negative CTE [15,16]. The substitution of more than 10 % Ba against Sr results in the formation of a new phase with a similar structure as the HT-phase of $BaZn_2Si_2O_7$ which, however, is already stable at room temperature [14]. The CTEs of the crystallographic axes were measured for different values of x within the solid solution $Ba_{1-x}Sr_xZn_2Si_2O_7$ and a large variety of temperatures using high-temperature powder diffraction and Rietveld refinement [19]. In analogy to lithium alumosilicates, this phase exhibits a high anisotropy in the CTEs which varies for different crystallographic directions in the range from below -30 (for the b axis) to above $+20 \cdot 10^{-6}$ K^{-1} (for the c axis) depending on the respective temperature range. This may lead to the formation of cracks and to less mechanically stable materials, which might be prevented by a homogeneous dispersion of tiny crystals [2]. However, it was shown that the preparation of crack-free sintered materials is enabled using a sol-gel method and a hot pressing procedure [20]. These materials exhibit low CTE. Sintering of glass powder and subsequent crystallization led to glass-ceramics with very different CTEs mainly depending on the used

grain size fraction. Nevertheless, it shows that $Ba_{1-x}Sr_xZn_2Si_2O_7$ solid solutions can easily be crystallized from silicate glasses in high volume concentrations. For this purpose, the microstructure has to be tailored by adjusting the glass composition and the temperature/time schedule. In most cases, surface crystallization of $Ba_{1-x}Sr_xZn_2Si_2O_7$ is predominant [21]. Volume crystallization can be achieved by adding nucleation agents, such as platinum [22], ZrO_2 [23] or a mixture of ZrO_2 and TiO_2 [24] to the glass composition. However, the number of crystals was fairly low and hence the sizes of those crystals fairly large, if oxides were used as nucleating agents.

Up to now, only platinum as nucleation agent shows promising results and predominant volume crystallization. This paper describes the effect of platinum in combination with Sb_2O_3 as a nucleating agent in the system BaO/SrO/ZnO/SiO_2.

2. Materials and methods

2.1 Glass preparation

The glass batch was prepared from the following raw materials: $BaCO_3$ (Merck, >98.5%), $SrCO_3$ (Ferak Berlin or VEB Laborchemie Apolda, > 99%), ZnO (Carl Roth GmbH + Co KG, >99%), SiO_2 (Carl Roth GmbH + Co KG, >99%), $PtCl_4$ (Merck, >57.5% Pt) and Sb_2O_3 (Merck, >98.5%). The $PtCl_4$ was dissolved in acetone and then given to the glass batch, thoroughly mixed, and subsequently dried. The batch (for 400 g glass) was melted in a platinum crucible using an induction furnace in air. For 1 h, a temperature in the range from 1300 to 1350 °C was supplied which was then risen to 1400 °C and kept for another 2 h. During this time, the melt was stirred with 60 min^{-1}. Then the stirrer was removed, and the glass was soaked for another 10 – 15 min. The glass was cast on a pre-heated steel mold and transferred to a muffle furnace preheated to a temperature of 680 °C. Then the furnace was switched off and the sample could cool down with a rate of approximately 3 K/min. The

chemical compositions of the respective samples are summarized in Table 1. The samples with 50 and 100 ppm platinum in the following are denoted as Pt 50 and Pt 100.

2.2 X-ray diffraction

To characterize the obtained glasses and crystallized materials, X-Ray Diffraction (XRD) was implemented using powdered samples and a Rigaku Miniflex 300 diffractometer with Ni-filtered Cu Kα radiation. The scanned 2θ-range was from 10° to 60° with a scan speed of 1 °/min.

2.3 Differential Scanning Calorimetry

Differential Scanning Calorimetry (DSC) was carried out using a Linseis DSC Pt 1600 which enabled the determination of characteristic temperatures such as glass transition temperature (T_g), onset of crystallization (T_{on}), offset of crystallization (T_{off}) and the crystallization maximum (T_p).

To minimize the effect of surface crystallization, glass powders with a mass of 0.15 g were given to a DSC platinum crucible, heated to the liquidus temperature, kept for 5 minutes and then cooled in air. Then, the measurement was performed in the DSC device using different heating rates (2, 5, 10, 15 and 20 K/min).

The order of reaction, (n), known as Avrami parameter was calculated by the method proposed by Ozawa [25–27]:

$$-n = \left| \frac{d\left[\ln(-\ln(1-x))\right]}{d(\ln \beta)} \right|_T \qquad \text{(Eq. 1)}$$

In Equation 1, n is the Avrami parameter, x = A_t/A, where A is the total area under the exothermal peak, A_t is the area under the exothermic peak up to a chosen temperature and β is the heating rate in [K/min].

The area under the crystallization peak for a chosen temperature was calculated for all supplied heating rates. The temperature varied depending on the glass composition and is usually determined by the rule that the A_t/A has to be in the range from $0.2 \leq x \leq 0.8$, which improves the accuracy of the method.

From DSC profiles, the variation of the peak crystallization temperature with different heating rates was determined and the activation energy was calculated using Kissinger equation [28–31]:

$$\ln\left[\frac{\beta}{T_p^2}\right] = \frac{-E_a}{RT_p} + const \qquad \text{(Eq.2)}$$

Where T_p is the temperature attributed to the maximum crystallization peak, E_a is the activation energy and R is the gas constant. The activation energy was also calculated using the Ozawa equation [28]:

$$\ln[\beta] = \frac{-E_a}{RT_p} + const \qquad \text{(Eq.3)}$$

After determining an Avrami coefficient according to Eq. 1 with values unequal to 1, the modified Kissinger equation (Matusita and Sakka method) can be used [28,29,32]:

$$\ln\left[\frac{\beta^n}{T_p^2}\right] = \frac{-mE_a}{RT_p} + const \qquad \text{(Eq.4)}$$

In Eq. 4, n is again the Avrami parameter and m is the dimensionality of crystal growth, which depends on the crystallization mechanism. The values of m were taken from ref [28].

2.4 Microstructural analysis

Light Scanning Microscopy (LSM)

Optical microscopy was carried out using a Laser Scanning Microscope (LSM) Axio Imager Z1m PASCAL5. The samples were heat treated in an external muffle furnace at different nucleation temperatures followed by a crystallization step. All samples were previously polished from both sides. For the determination of the nucleation rate and the crystal growth velocity, a z-stack was performed. Several images are recorded on the z-axis of the samples at a distance z and in a certain time interval. For determining the number of crystals and their length, the following equation was used [33,34]:

$$N_v = \frac{N}{A \cdot z \cdot n_e} \qquad \text{(Eq.5)}$$

in which N is the number of particles per unit area, A is the total area, z is the z-stack (depth of focus in z - direction) and n_e is the refractive index at a wavelength of 560 nm.

The software used for the determination of the number of crystals are ZEN 2012 and ImageJ.

Scanning Electron Microscopy (SEM)

Scanning Electron Microscopy (SEM) was used to study the crystal morphology using the microscopes JEOL JSM-7001F and JEOL JSM-6510 LV. For this purpose, the samples were cut and polished. For electron backscatter diffraction (EBSD), an additional final polishing step with colloidal silica was applied. A carbon coating was applied at a pressure of 10^{-3} Pa to avoid surface charging under the electron beam. The diffraction patterns were collected with a Digiview 3 EBSD-camera and later evaluated using the software packages TSL OIM Data

Collection 5.31 and TSL OIM Analysis 5.31. Only reliably indexed patterns were included to the mapping by applying a grain Confidence Index standardization clean up procedure with grain size =10 and grain tolerance angle = 3° to the dataset. Following this, a partition filter was used: Grain size = 10, Grain tolerance angle 3°, CI ≥0.2. The inverse pole figures (IPF) were referenced to the [001] direction (normal of the sample surface, same as image plane). The EDXS mapping and point measurements were collected at an acceleration voltage of 10 kV in order to increase the spatial resolution.

2.5 Viscosity measurements

A beam bending viscosity was determined by viscometer Bähr VIS 401 (viscosity range: 10^9 to $10^{12.5}$ dPa·s, heating rate: 10 K/min). The bended bars have a dimension of 5 x 5 x 50 and 5 x 4 x 50 mm^3. The data obtained from the two measurements were combined and fitted using the Vogel-Fulcher-Tammann equation (VFT-equation) [34]:

$$\log \eta = B + \frac{C}{T - T_0} \qquad \text{(Eq.6)}$$

2.6 Determination of refractive indices, densities and dilatometry

The densities were determined using a helium pycnometer Micromeritics AccuPyc 1330. The refractive indices were measured using a Pulfrich refractometer Carl Zeiss Jena PR2 were n_e is determent at 546 nm. The thermal expansion was analyzed using a NETZSCH Dil 402 PC dilatometer. The samples had a diameter of 8 mm and a length of 10 – 15 mm. The applied heating rate was 5 K/min up to 600 ºC and the curve was recorded also during cooling.

3. Results and Discussion

Figure 1 show XRD patterns for the two Pt containing glasses heat treated for 1 h at a temperature of 940 °C. This temperature was chosen to be above the exothermic DSC peaks shown in Fig. 2. In all patterns, the amorphous hump is no longer visible and all recorded patterns of the two compositions are similar and most of the peaks can be attributed to $Ba_{1-x}Sr_xZn_2Si_2O_7$. The respective theoretical peak positions of $Ba_{0.6}Sr_{0.4}Zn_2Si_2O_7$ (ICSD 429938) are displayed in the lower part of Fig. 1 and found in very good agreement with the experimental patterns recorded. In the XRD patterns of samples thermally treated at a temperature of 940 °C, an additional peak of minor intensity occurs at $2\theta = 21.8°$ (marked with a star). This peak is attributed to small quantities of crystalline cristobalite and might explain the second exothermic peak in the DSC profiles of Fig. 2. An additional peak of low intensity appears at $2\theta = 24.5°$. It is also attributable to the main peak of the $Ba_{1-x}Sr_xZn_2Si_2O_7$ solid solution but origins from a small intensity of CuK_β-radiation. It is not surprising that the main phase is $Ba_{1-x}Sr_xZn_2Si_2O_7$ because also in previously performed studies using other nucleation agents, this phase was found [23,24]. Since traces of cristobalite are only formed above 900 °C, cristobalite should not affect the CTE of the obtained materials crystallized at lower temperatures.

Figure 2 shows the DSC profiles of glasses with different platinum concentrations combined with antimony in comparison to the base glass without platinum; the supplied heating rate was 10 K/min. Adding different concentrations of platinum does not significantly change the glass transition temperature, T_g, of the glasses. The lowest T_g of 672 °C is observed in the base glass and the highest is 680 °C for the glass Pt 100. All three glasses exhibit a pronounced exothermic peak which is attributed to the crystallization of $Ba_{1-x}Sr_xZn_2Si_2O_7$. While this crystallization peak occurs at 948 °C for the base glass, it is observed at notably lower temperatures in the glasses with platinum, at 867 and 862 °C for Pt 50 and Pt 100,

respectively. In analogy, also the onset and offset temperatures of the crystallization peaks are strongly affected by the presence of platinum. The characteristic temperatures are summarized in Table 2 for different heating rates. The second crystallization peak with comparatively low intensity is observed for all glasses which agrees with the XRD results and is attributed to the formation of cristobalite. It should be mentioned that the crystallization of cristobalite has already been reported for similar systems. Adding 50 ppm platinum (Pt 50) to the base composition leads to a decrease in the onset of crystallization by 69 K and a decrease in the crystallization peak temperature of 81 K is observed. This is a significant effect and shows that even small amounts of platinum may govern the overall crystallization kinetic. This is in good agreement with a previous study were glasses without antimony, but different platinum concentrations were studied [22]. Adding Sb_2O_3 to the glass does not affect the onset or peak of crystallization. Both glasses have similar values for the difference between the onset and the glass transition temperature ($\Delta T=T_{on}-T_g$) which is considered to be the stability of glasses against devitrification. For the samples with Pt 50 and Pt 100, the differences ΔT are 168 and 171 °C respectively, however, we have to mention that the base glass has much higher values (245 °C) [23].

In Fig. 3, the results of DSC measurements for different heating rates of 2, 5, 10, 15, and 20 K/min are juxtaposed for both studied glasses. In Fig. 3a, the peak intensity is shown, which increases linearly with the heating rate. The peak heights are somewhat larger for the glass Pt 100. The temperatures attributed to the peak maximum increase with the heating rate and occur at up to 10 K lower temperatures for the glass Pt 100, i.e. for the glass with the higher Pt concentration. The dependence of the crystallization peak on the heating rate is a well-known phenomenon, related to the heat capacitance of the system and to the attributed time shift of the thermocouples, which is increasing with the heating rate [27]. The values for the full width at half maximum for all heating rates are almost the same (see Fig. 3b). This is not

the case for the glass Pt 50. In this case, scattering is observed for the heating rates 2 and 10 K/min. All results present in Fig 3 are an indication for a difference in the kinetics for the two glass systems; numerous studies published in the past proved that the change in the shape, width, and intensity of the crystallization peak are usually indications of a change in the crystallization mechanism [24,35,36]. Broad crystallization peaks with low intensities are attributed to surface crystallization while narrower peaks with higher intensity are an indication of volume crystallization[30,35,37]. This can be considered as another indication that the system has the tendency to volume crystallization. It can be seen, that there is a very slight difference in the peak temperature (Fig. 3c) in the two glass compositions since in the sample Pt 100, the peak temperature is observed at a lower temperature. In analogy, the peak intensities are also different. The sample Pt 50 has significantly lower intensity in comparison to the glass Pt 100.

In Fig. 4, Ozawa plots are shown for the glasses Pt 50 and Pt 100. In both cases, linear correlations according to Eq. 1 are observed. The Avrami parameters calculated from the slopes are 3.3 and 3.4 for the glasses Pt 50 and Pt 100, respectively. This is attributed to volume nucleation with three-dimensional crystal growth. It should be noted that the reference glass without platinum has an Avrami coefficient of around 1, which stands for sole surface crystallization [23,28]. This proves that the Avrami plots enable to distinguish between surface and bulk nucleation of the $Ba_{1-x}Sr_xZn_2Si_2O_7$ phase, as already evidenced in previous studies on this system which was also confirmed by microstructural investigation [22–24]. Since both glass systems have similar crystallization temperatures, the Avrami parameters were determined at a temperature of 842 °C.

Fig. 5 shows a Kissinger plot (see Eq. 2) and a plot of the modified Kissinger Equation (see Eq. 4), both plotted for the Pt 100 glass. From the slopes of the two plots, the activation energies were calculated to be 496 and 508 kJ/mol^{-1}, respectively. The results for both glass

systems are summarized in Table 3; not all of them are shown in graphical form. There is no significant difference in the activation energies determined by Kissinger (Eq.2) and Ozawa Equation (Eq. 3). The difference for both glasses is less than 6 percent, which is just a normal deviation. The modified Kissinger equation gives a better approximation if volume crystallization occurs, because additional constants, n and m are used. Then, the growth mechanism can be determined in detail and conclusions on a combination of surface and volume crystallization or only volume crystallization can be drawn. The activation energies for the glass Pt 100 are slightly higher than for the glass Pt 50.

The viscosity was determined using beam-bending viscometry. The results are graphically represented in Fig. 6, results obtained were fitted using Vogel-Fulcher-Tammann (VFT- Eq. 6) and only the fitting is graphically presented. The fitting parameters A, B, and T_0 of the VFT-equation are summarized in Table 4. The results are presented for the base glass (A) and the glasses Pt 50 and Pt 100 in the temperature range from 670 to 750 °C. The base glass has a higher viscosity in comparison to the glasses with platinum. The values of the two glasses with platinum are almost identical. This suggests that even small amounts of platinum and Sb_2O_3 can significantly change the viscosity of the glass, furthermore increasing the platinum concentration does not result in a significant effect.

The nucleation was studied using laser scanning microscopy. It is important to mention that the samples were thermally treated outside the microscope for better optimization and a polarization mode was used. In the micrographs (Figs. 7 a) to c)), the platinum particles can clearly be seen. The apparent colour in the optical micrograph of the glass matrix does not change with the distance from these platinum crystals.

Fig.7 a) presents an optical micrograph of a sample Pt 50 heat treated at 690 °C for 100 h and subsequently for 1 h at 780 °C. Around the platinum particles, large crystals supposedly

consisting of $Ba_{1-x}Sr_xZn_2Si_2O_7$ are observed. The number of these crystals is low, while their size is around 11 µm. In the center of the respective crystals, a small dark spot appears, which is metallic platinum [22]. In Fig. 7 b), a micrograph of the sample Pt 100 thermally treated at the same conditions as Fig. 7 a) is shown. As before, the dark spots in the middle of the crystals are metallic platinum, the size of the $Ba_{1-x}Sr_xZn_2Si_2O_7$ crystals is around 8 µm. Fig. 7 c) shows an optical micrograph of glass Pt 50 thermally treated at 710 °C for 48 h and subsequently at 780 °C for 1 h. Here the size of the crystals is around 23 µm; each of these crystals has a dark particle in its center. In this micrograph, also a second growth morphology appears which according to the X-ray patterns is also attributed to $Ba_{1-x}Sr_xZn_2Si_2O_7$.

Fig. 8 presents the number of crystals per volume as a function of time. In order to obtain the results, small pieces with a diameter of 8 mm and 3 mm height were nucleated for different periods of time in the range from 1 to 100 h at various temperatures near T_g of the glasses (680 - 700 °C) and subsequently crystallized at 780 °C for 30 min or 1 h. Furthermore, the samples were polished from two sides and inspected by LSM to enable the determination of the number of crystals, N_v using Eq. (5). In Fig. 8 a), the results for the glass Pt 50 are shown. A time lag is not observed and in the glasses without previous nucleation only a small quantity of crystals was found. The number of crystals is increasing with nucleation time up to 24 h. With further increasing nucleation times, a slight to notable decrease is observed. This effect is observed for any applied nucleation temperature. The number of formed crystals is also affected by the nucleation temperature. The lowest number is observed after nucleation at 700 °C. The largest number of crystals is observed after nucleation at 690 °C for nucleation times up to 24 h. For the glass Pt 100, the number of crystals is highest after nucleation at 680 °C and lowest after nucleation at 700 °C as shown in Fig. 8 b). The most significant difference between the two compositions, however, is that in the sample Pt 100, the number of crystals is almost five times larger than in the glass Pt 50. In both glasses, the number of

crystals is increasing up to 24 h independent of the applied nucleation temperature. With further increasing temperature, the number of crystals decreases again. This effect might be caused by Ostwald ripening. Another interesting feature is the lack of induction time which was frequently reported for other glass systems. The lack of induction time is due to a small amount of platinum particles which are already formed during cooling of the glass and which act as nucleation centers during crystallization. This phenomenon was reported and discussed in detail in Ref. [22]. From this observation, it is concluded that only a part of the platinum particles are formed during nucleation and some have already formed during cooling of the glass melt. Fig. 9 a) shows an SEM micrograph of a $Ba_{1-x}Sr_xZn_2Si_2O_7$ crystal with a small particle in its centre. The particle is facetted and around it, some cracks appear. The origin of the cracks seems to be located near the particle. The crack supposedly runs in an axial direction away from the centre first and then is deflected perpendicular to the long axis of the $Ba_{1-x}Sr_xZn_2Si_2O_7$ crystals. The elemental maps depicted in Fig. 9 b) show that the particles are strongly enriched in Pt and depleted in Si, Zn, and Ba. By contrast, the particles seem to be enriched in Sb. Point measurements were performed for 200 s on the residual glass, the crystal, and the central particle (see Fig. 9 c)).

The enrichment of Sb might either be real or an artefact. The latter might be due to an increased background of Bremsstrahlung. Since the excitation volume at 10 kV acceleration voltage has still a size of about 1 µm, the small Sb peak might be caused by peripheral excited material (crystal and residual glass) surrounding the sub-micrometre Pt-particle. Then also an increased Ba-signal should occur which, however, is not observed. The phase diagram Pt/Sb[38] has a deep eutectic at $Pt_{0.78}Sb_{0.22}$ attributed to a temperature of 633 °C. Hence, Pt and Sb should have a strongly negative mixing enthalpy. In metallic platinum, antimony is soluble, e.g. at a temperature of 755 °C around 7 wt% Sb can be dissolved. Therefore, it is assumed, that the particle contains a certain Sb-concentration.

Fig. 10 shows an SEM micrograph of a sample Pt 50 thermally treated at 710 °C for 48 h and subsequently at 780 °C for 1 h. Two crystals are shown and each of them exhibits two growth morphologies. On one side, crystals are grown from an apparent center, while at the other side, the different morphology appears similar as a dendritic growth. These structures were also characterized using EBSD. All reliably indexed Kikuchi patterns originate from the crystalline part of the microstructure and were attributed to the orthorhombic crystal phase $Ba_{0.6}Sr_{0.4}Zn_2Si_2O_7$ with the space group *Ccm2₁*, which is the desired crystal phase. At the bottom of Fig. 10, a combined Image Quality (IQ) + inverse pole figure (IPF)-map is shown.

While the crystals which run from the center have certain orientation gradients (changing colors), the dendrite-like crystals have a unique orientation (one color). This Figure also presents some white wired unit cells with marked (red arrows) c-axes direction which should be compared to the SEM micrograph displayed on top. While the crystals grown from the center are oriented with their c-axes parallel to their longest axis (the growth direction), the dendrite-like crystals are aligned with their c-axes perpendicular to their primary growth direction (and parallel to the longest axis of the secondary structures). In Fig. 11, dilatometric curves of the glasses Pt 50 and Pt 100 are shown. They have previously been thermally treated at 720 °C for 100 h. For the temperature range from 100 to 300 °C, the CTEs for the samples Pt 50 and Pt 100 are 0.98 and $-0.01 \cdot 10^{-6}$ K^{-1}. These results show that using platinum and Sb_2O_3 in combination can lead to a material with ZTE. This is a promising result for the development of suitable glass ceramics and for a better understanding of the $Ba_{1-x}Sr_xZn_2Si_2O_7$ phase. Further research regarding improvement of the microstructure must be done in the future.

5. Conclusions

Platinum and Sb_2O_3 proved to be suitable to achieve nucleation of the $Ba_{1-x}Sr_xZn_2Si_2O_7$ phase. It was shown by considering crystallization kinetics and the number of formed crystals as a function of time that volume crystallization is predominant for both glass compositions. Adding Sb_2O_3 to the systems leads to a dissolution of metallic platinum in the glass melt and to the formation of platinum particles during thermal treatment at temperatures slightly above T_g. Here, the number of crystals increases up to 24 h of thermal treatment. The crystals formed have a platinum particle in their center. Furthermore, adding Sb_2O_3 and platinum to the glass system leads to a second morphology of the $Ba_{1-x}Sr_xZn_2Si_2O_7$ crystals: dendrite-like crystals were aligned with their c axes perpendicular to their primary growth direction and do not show cracks. The combination of platinum and Sb_2O_3 enables the preparation of a ZTE material which is shown by dilatometry measurements.

Acknowledgment

This work was funded by the German Federal Ministry of Education and Research under the grant numbers 03VP01701 and 03VP01702.

References

1 J. Evans, T. Mary, A. Sleight, Negative thermal expansion materials, Phys. B Condens. Matter, 241 (1997) 311–316.

2 H. Bach, D. Krause, Low Thermal Expansion Glass Ceramics, 2 nd edn. Springer, New York. (2005).

3 D. Tauch, C. Rüssel, Glass-Ceramics with Zero Thermal Expansion in the System $BaO/Al_2O_3/B_2O_3$, J. Non-Cryst. Solids. 351 (2005) 2294-2298.

4 G. Müller, M.Sternitzke, Computer modelling of structure and thermal expansion of β-quartz-and keatite-type aluminosilicates, J. Mater. Sci. Lett. 12 (1993) 278–280.

5 J. Moya, A. Verduch, Hortal M. Thermal expantion of β-eucryptite solid solution. Trans. Brit. Ceram. Soc. (1974) 177–178.

6 H. Scheidler, E. Rodek, Li_2O-Al_2O_3-SiO_2 glass-ceramics, Am. Ceram. Soc. Bull. 68 (1989) 1926–1930.

7 P. McMillan, Glass-ceramics, 2 nd edn. Academic Press, London. (1979).

8 C. Lind, A. Wilkinson, Z. Hu, S. Short, J. Jorgensen, Synthesis and properties of the negative thermal expansion material cubic $ZrMo_2O_8$, Chem. Mater., 10 (1998) 2335–2337.

9 R. Hovhannisyan, Rafaelites–new kinds of glass ceramics with low thermal expansion and low melting temperatures on the basis of alkaline earth aluminium borates. Glass Technol., 44 (2003) 96–100.

10 I. Yamai, T. Oota, Low- Thermal- Expansion Polycrystalline Zirconyl Phosphate Ceramic J. Am. Ceram. Soc. 68 (1985) 273–278.

11 D. Tauch, C. Rüssel, Thermal expansion of glass–ceramics in the system $BaO/Al_2O_3/B_2O_3$, J. Non-Cryst. Solids, 351 (2005) 3483–3489.

12 E. Zanotto, Bright future for glass-ceramics, Am. Ceram. Soc. Bull., 89 (2010) 19–27.

13 M. Macdonald, V. Badescu, The International Handbook of Space Technology 1 st edn. Springer, Praxis. (2014).

14 C. Thieme, H. Görls, C. Rüssel, $Ba_{1-x}Sr_xZn_2Si_2O_7$-A new family of materials with negative and very high thermal expansion, Sci. Rep. 5 (2015) 18040.

15 J. Lin, H. Lu, J. Du, M. Su, C. Loong, J. Richardson, Phase transition and crystal structures of $BaZn_2Si_2O_7$, J. Phys. Chem. Solids. 60 (1999) 975–983.

16 M, Kerstan, M. Müller, C.Rüssel. Thermal expansion of $Ba_2ZnSi_2O_7$, $BaZnSiO_4$ and the solid solution series $BaZn_{2-x}Mg_xSi_2O_7$ ($0 \leq x \leq 2$) studied by high-temperature X-ray diffraction and dilatometry, J. Solid State Chem.188 (2012) 84–91.

17 C. Thieme, T. Waurischk, S. Heitmann, C. Rüssel, New Family of Materials with Negative Coefficients of Thermal Expansion: The Effect of MgO, CoO, MnO, NiO, or CuO on the Phase Stability and Thermal Expansion of Solid Solution Phases Derived from $BaZn_2Si_2O_7$, Inorg. Chem. 55 (2016) 76–4484.

18 C. Thieme, C. Rüssel, Negative Thermal Expansion in $Ba_{0.5}Sr_{0.5}Zn_2SiGeO_7$, Materials.9 (2016) 631- 636.

19 C. Thieme, C. Rüssel, Very high or close to zero thermal expansion by the variation of the Sr/Ba ratio in $Ba_{1-x}Sr_xZn_2Si_2O_7$, Solid solutions, Dalton Trans.45 (2016) 4888–4895.

20 M. Kracker, C. Thieme, J. Häßler, C.Rüssel, Sol-gel powder synthesis and preparation of ceramics with high- and low-temperature polymorphs of $Ba_{1-x}Sr_xZn_2Si_2O_7$ (x =1 and 0.5):

A novel approach to obtain zero thermal expansion, J. Eur. Ceram. Soc. 36 (2016) 2097–2107.

21 M. Kracker, L. Vladislavova, C. Thieme, C. Zscheckel, K. Thieme, T. Höche, C. Rüssel. Surface crystallization of low thermal expansion $Ba_{0.5}Sr_{0.5}Zn_2Si_2O_7$ from an 8 BaO·8 SrO·34 ZnO·50 SiO_2 glass, RSC Adv. 7 (2017) 44834–44842.

22 L. Vladislavova, C. Thieme, T. Zscheckel, C. Patzig, T. Höche, C. Rüssel, Heterogeneous nucleation of $Ba_{1-x}Sr_xZn_2Si_2O_7$ from a BaO/SrO/ZnO/SiO_2 glass using platinum as nucleation agent, J. Eur. Ceram. Soc. 37 (2017) 4801-4808.

23 L. Vladislavova, C. Thieme, C. Rüssel, The effect of ZrO_2 on the crystallization of a glass in the system BaO/SrO/ZnO/SiO_2: surface versus bulk crystallization. J. Mater. Sci. 52 (2017) 4052-4060.

24 L. Vladislavova, M. Kracker, T. Zscheckel, C. Thieme, C. Rüssel, Crystallisation of $Ba_{1-x}Sr_xZn_2Si_2O_7$ from BaO/SrO/ZnO/SiO_2 glass with different ZrO_2 and TiO_2 concentrations, Solid State Sci.78 (2018) 107-115.

25 M. Ghasemzadeh, A. Nemati, A.Nozad, Z. Hamnabard, S. Baghshahi, Crystallization kinetic of glass-ceramics by differential thermal analysis, Ceram.-Silikaty, 55 (2011) 188–194.

26 T. Ozawa, Modified Method for Kinetic Analysis of Thermoanalytical Data. J. Therm. Anal., 9 (1976) 69–373.

27 M. Guedes, A. Ferro, J. Ferreira, Nucleation and crystal growth in commercial LAS compositions, J. Eur. Ceram. Soc. 21 (2001) 1187–1194.

28 I. Donald, Crystallization kinetics of a lithium zinc silicate glass studied by DTA and DSC, J. Non-Cryst. Solids. 345 (2004) 120–126.

29 R. Wurth, M. Pascual, G. Mather, A. Pablos-Martin, F. Munoz, A. Duran, G. Cuello, C. Rüssel, Crystallisation mechanism of a multicomponent lithium alumino-silicate glass. Mater. Chem. Phys.134 (2012) 1001–1006.

30 A. Arora, E. Shaaban, K. Singh, O. Pandey, Non-isothermal crystallization kinetics of ZnO–BaO–B_2O_3–SiO_2 glass, J. Non-Cryst. Solids. 354 (2008) 3944–3951.

31 H. Kissinger, Reaction Kinetics in Differential Thermal Analysis, Anal. Chem.29 (1957) 1702-1706.

32 K. Matusita, S. Sakka, Kinetic study of crystallization of glass by differential thermal analysis—criterion on application of Kissinger plot. J. Non-Cryst. Solids. 38 (1980) 741–746.

33 P. James, Kinetics of crystal nucleation in silicate glasses. J. Non-Cryst. Solids, 73 (1985) 517–540.

34 K. Thieme, T. Zscheckel, C. Thieme, T. Höche, C. Rüssel, On the search for nucleation agents in BaO-SrO-ZnO-SiO_2 glasses: The influence of P_2O_5, J. Eur. Ceram. Soc 38 (2017) 2017-2026.

35 J. Massera, S. Fagerlund, L. Hupa, M. Hupa, Crystallization mechanism of the bioactive glasses, 45S5 and S53P4. J. Am. Ceram. Soc. 95 (2012) 607–613.

36 C. Ray, Q. Yang, W. Huang, E. Day, Surface and internal crystallization in glasses as determined by differential thermal analysis. J. Am. Ceram. Soc.79 (1996) 3155–3160.

37 K. Narayan, K. Kelton, and C. Ray, Effect of Pt doping on nucleation and crystallization in $Li_2O{\cdot}2SiO_2$ glass: experimental measurements and computer modeling. J. Non-Cryst. Solids, 195 (1996) 148–157.

38 T. Massalski, J. Murray, L Benett, H. Baker, Binary Alloy Phase Diagrams. Am. Soc. Metals. Metals Park, OH, (1986).

Table.1 Chemical compositions of the studied samples (in mol %)

Sample	Chemical composition in mol%					
	BaO	SrO	ZnO	SiO_2	Sb_2O_3	$PtCl_4$
Pt 50	8	8	34	49.50	0.5	0.005
Pt 100	8	8	34	49.49	0.5	0.01
Base glass (A*)	8	8	34	50	-	-

*ref [23]

Table 2: Results from the DSC-profiles of the samples Pt 50 and Pt 100. β: heating rate, T_g: glass transition temperature, T_{on}: onset of the crystallization peak, T_{off}: offset of the crystallization peak, T_p: temperature of the crystallization peak; and T_{on}-T_g.

	β (K/min)	T_g (°C)	T_{on} (°C)	T_{off} (°C)	T_p (°C)	T_{on}-T_g (K)
Pt 50	2	-	810	845	831	-
	5	674	845	869	860	171
	10	679	847	880	867	168
	15	679	867	888	879	188
	20	680	872	896	887	192
Pt 100	2	-	819	837	830	-
	5	679	836	854	847	157
	10	680	851	869	862	171
	15	681	860	879	871	179
	20	683	867	885	877	184

Table 3: E_{ak}: activation energies, determined by the Kissinger plot; E_{ao}: activation energy determined by the Ozawa plot; E_{am}: activation energy, determined by modified Kissinger plot, ρ: the density and n_e: the refractive index at a wavelength of 560 nm of the respective glasses.

Name	E_{ak} [kJ mol^{-1}]	E_{ao} [kJ mol^{-1}]	E_{am} [kJ mol^{-1}]	ρ [g/cm^3]	n_e
Pt 50	432	451	445	3.870	1.6605
Pt 100	496	515	508	3.868	1.6607

Table.4 Results of fitting the viscosity data to the VFT-equation.

Name	**A [dPa·s]**	**B [°C]**	**T_0 [°C]**
A	0.486±0.015	150.452±8.578	436.867±8.578
Pt 50	0.402±0.031	210.264±20.996	375.423±16.511
Pt 100	0.490±0.016	148.227±9.060	434.715±8.330

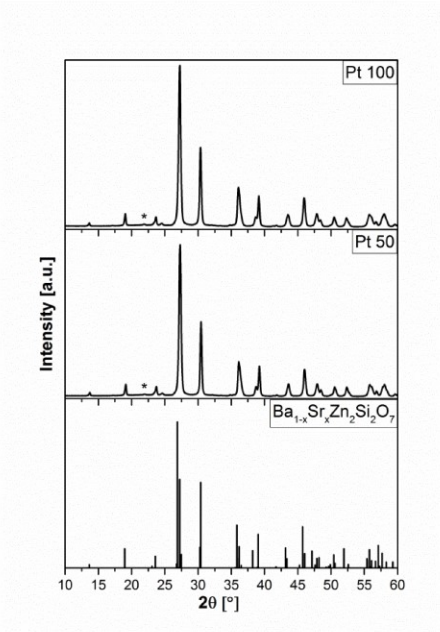

Fig. 1 X-ray diffraction patterns of glasses with different Pt concentrations and Sb_2O_3 crystallized at 940 °C for 1 h.

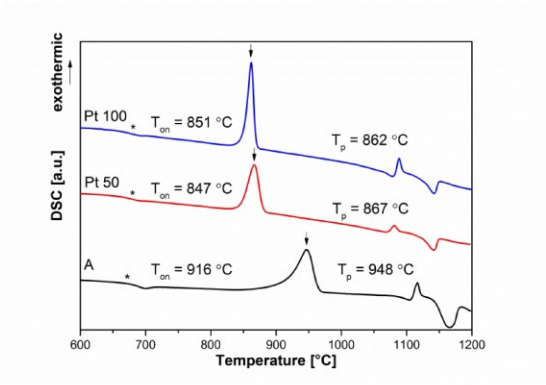

Fig. 2 DSC profiles of glasses with different platinum concentrations using a heating rate of 10 K/min. The stars mark the glass transition temperatures.

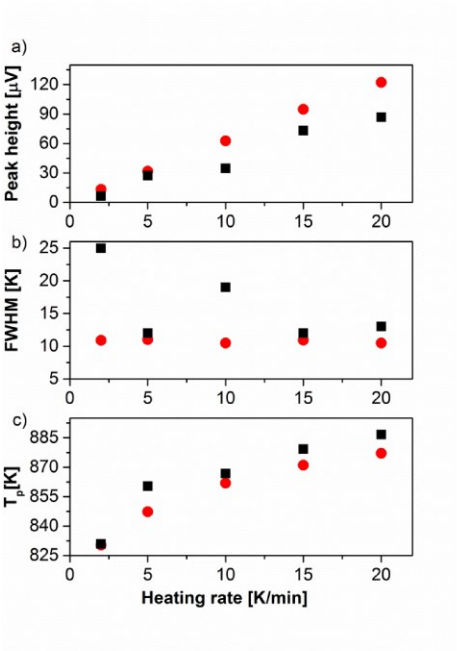

Fig. 3 Evaluation of the exothermic effects observed in the DSC measurements as a function of the heating rate for the glass Pt 50 (■) and Pt 100 (●): a) the intensity of the peaks; b) full with at the half maximum; c) temperature of the crystallization peak;

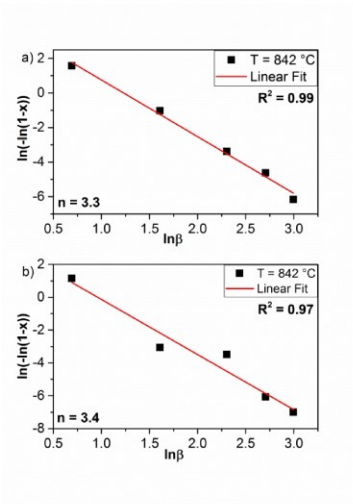

Fig. 4 Ozawa plot of (ln-(ln(1-x))) versus lnβ used to calculate the Avrami parameter n: a) sample Pt 50 at 842 °C; b) sample Pt 100 at 842 °C.

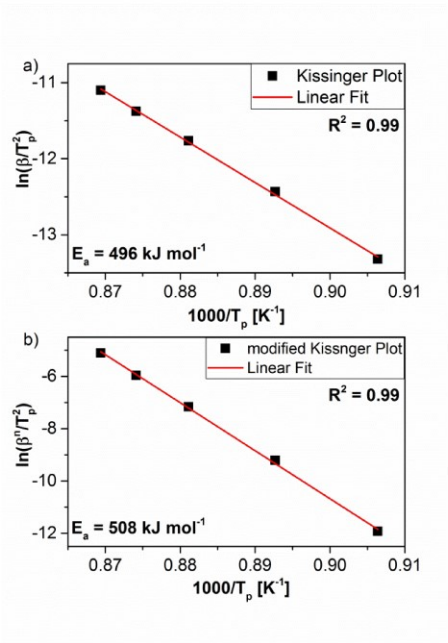

Fig. 5 Graphical presentation of the activation energy for the sample with Pt 100 applying: a) Kissinger plot (see Eq. 2); b) modified Kissinger plot (see Eq. 4).

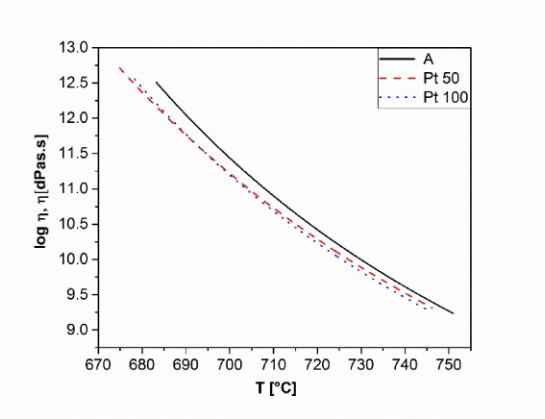

Fig. 6 Viscosities in the temperature range from 670 to 750 °C plotted with the VFT-equation from beam bending viscometer.

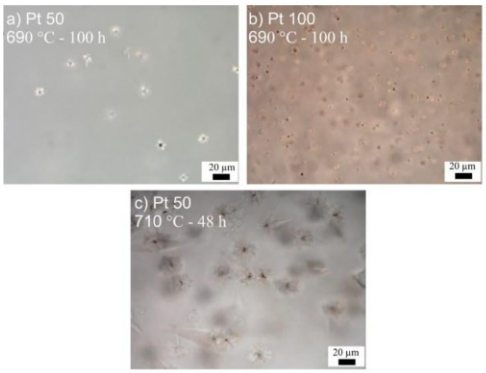

Fig. 7 Optical micrograph recorded with a laser scanning microscope: a) sample Pt 50 thermally treated at 690 °C for 100 h; b) sample Pt 100 thermally treated at 690 °C for 100 h; c) sample Pt 50, nucleated at 710 °C for 48 h; all samples have an additional crystallization step for 1 h at 780 °C.

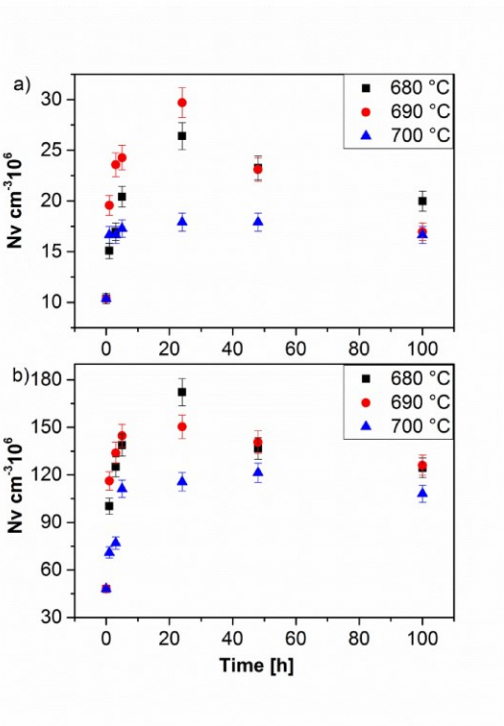

Fig. 8 Number of crystals per unit volume as a function of for different nucleation temperatures; a) sample Pt 50; b) sample Pt 100.

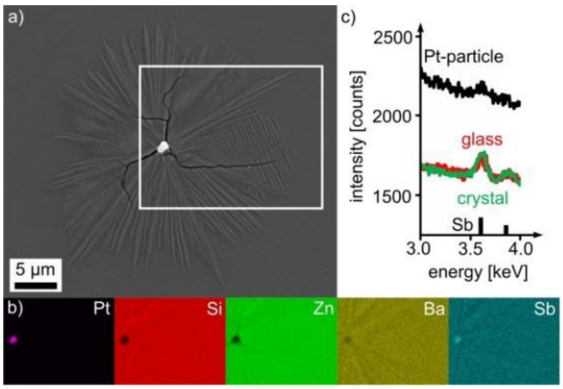

Fig. 9 Cross section of a sample Pt 50 thermally treated in a first step at 710 °C for 48 h and then at 780 °C for 1 h: a) SEM micrograph with a Pt particle in the middle and two different $Ba_{1-x}Sr_xZn_2Si_2O_7$ crystals; b) elemental mapping of the highlighted region including Pt, Si, Zn, Ba and Sb; c) spectra of point measurements around the theoretical Sb peak, recorded at 10 kV for 200 s.

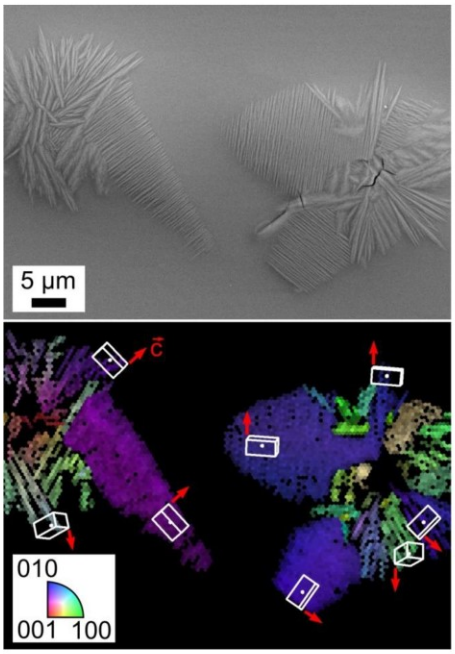

Fig. 10 SEM micrograph of a sample Pt 50 thermally treated in a first step at 710 °C for 48 h and then at 780 °C for 1 h: a) micrograph of a cut perpendicular to the surface (volume observation), b) EBSD results: combined Image Quality (IQ) + inverse pole figure (IPF)-map of $Ba_{0.6}Sr_{0.4}Zn2Si_2O_7$ with white lined unit cells and highlighted c-axis directions (red lined) at certain crystal positions.

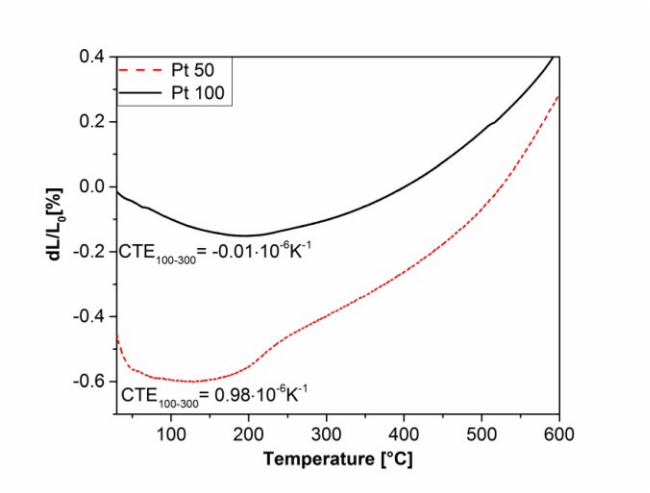

Fig. 11 Dilatometric measurements of thermally treated samples Pt 50 and Pt 100 at 720 °C for 100 h.

6 Discussion

6.1 Importance of raw materials, the solubility of nucleation agents in the base glass system and glass colourations.

This dissertation is focused on finding the proper nucleation agent/agents and optimising the microstructure of the obtained glass-ceramics. During the first experimental study on the topic, ZrO_2 was chosen as nucleation agent. ZrO_2 was proven to be an efficient nucleation agent in other glass systems with low thermal expansion such as lithium alumosilicates and other commercial glass-ceramics. Besides, ZrO_2 is widely available at relatively low cost [1,63], especially in comparison to noble metals. The main study on this topic can be found in **paper 5.1** were different concentration of ZrO_2 in the $BaO/SrO/ZnO/SiO_2$ system are investigated [27]. The maximum solubility of ZrO_2 in this system is 6 mol%, the glasses are completely transparent, and no visible colouration is observed. An interesting phenomenon concerning the ZrO_2 was that the solubility of ZrO_2 was depended on the used raw material. The ZrO_2 produced by the Japanese company Tosoh (chemically pure > 99 %) had a solubility of 6 mol% under the conditions supplied. However, when a raw material produced by the German company Carl Roth GmbH (chemically pure > 99 %,) was used, the solubility of the ZrO_2 drops to 5 mol %. Further analyses show that the particle size for the ZrO_2 produced by the two companies are different. For Carl Roth GmbH the mean particle size is 6-10 µm and Tosoh have a mean particle size of 0.47 µm. It is clear that the smaller particle size makes it easier for the ZrO_2 to be completely dissolved during melting. The melting temperature of ZrO_2 is very high (2715 °C) and a smaller particle size is beneficial for the preparation of homogeneous melts [1,6]. The, coarser powder would require higher melting temperatures or longer melting times. This leads to the important conclusion that the raw materials may have a significant role on the

obtained glasses, which can affect their solubility and hence affect the reproducibility of all results.

Since the solubility of the ZrO_2 was reached but volume crystallization was not observed in a sufficient extend, another approached was considered. It is well known from the literature that ZrO_2 and TiO_2 in combination act as nucleation agents and are also widely used for producing low thermal expansion materials. Nucleation is usually triggered by the formation of $ZrTiO_4$ nanocrystals which precipitated in the glasses and act as a substrate for the desired phase (this was discussed in **Chapter 4.3**). TiO_2 is known as a conditional glass former and may decrease the overall viscosity of the glass system [63,65]. Different ZrO_2/TiO_2 ratios were supplied as shown in **Table 1** of **paper 5.5** [26]. The solubility of TiO_2 in the base glass is somewhat below 8 mol% before spontaneous surface crystallization occurs. Adding TiO_2 in combination with ZrO_2 increases the solubility of ZrO_2 up to 7 mol% if combined with 1 mol% TiO_2. Introducing TiO_2 in the glass leads to a yellow coloration which strongly increases with the TiO_2 concentration. The intensity of the color changes to light brown if 5 mol% TiO_2 are added, nevertheless these glasses remain transparent. These optical phenomena have already been observed in other glass systems when adding TiO_2 and are well described [3,63]. Most technical raw materials have up to 1 mol% impurities in different concentrations which depend on the type of the used raw materials. In this case, the coloration is triggered by the presence of Fe ions which contribute to the absorption in the UV and visible range spectrum. The mechanism is explained by the presence of Ti^{4+} which forms a charge transfer complex with Fe^{3+}. This charge transfer complex is (Fe^{3+}-O-Ti^{4+}) and the resulting coloration is frequently denoted as ilmenite coloration. The use of both ZrO_2 and TiO_2 as additives lead to volume crystallization in one of the glass systems (Z7T1), however, surface crystallization was still predominant, and the volume fraction of crystals was still too low.

Since combing the oxides did not result in a sufficient extend of volume crystallization for the $Ba_{1-x}Sr_xZn_2Si_2O_7$ phase, another approached was applied. In many glass systems, the addition of noble metals was reported to give good results when used as nucleation agents, however, they are usually not widely applied due to the higher cost, however, they are effective in very low quantity [16,51,66]. As such a nucleating agent, Pt was chosen in the present work. Two main approaches for adding the $PtCl_4$ to the glass batch were tested. The glass batch containing all components except $PtCl_4$ was melted as usual (**papers 5.1**, **5.3** and **5.5**). Then, the cooled glass was powered to a grain size smaller than 315 μm, mixed with a solution of acetone and $PtCl_4$ concentrations in the range from 50 to 100 ppm. The mixture was dried in a furnace for 20 min at 120 °C and melted again for 30 min at 1400 °C during stirring. The obtained glass was transparent and colorless. From further studies (SEM, X-ray diffraction and crystallization studies) no evidence of Pt or $PtCl_4$ was found, which lead to the conclusion that this method for adding Pt is not efficient. The second method which was implemented and later used as the main procedure for melting Pt-containing glass was reported in the papers (**5.2, 5.4, 5.6 and 5.7**). In this case, the batch is mixed with $PtCl_4$ dissolved in 400 ml acetone. This leads to glasses which are transparent with greyish coloration. As seen in **Figure 1** of **paper 5.6,** the colours of the glasses are strictly dependent on the Pt concentration. Similar results were reported by Rindone when he studies the light scattering effect of platinum in lead glasses [66,67]. A possible explanation for that can be given by decomposition reactions of the $PtCl_4$ (given below).

$$PtCl_4 = PtCl_2 + Cl_2 \qquad \text{(Eq. 6.1)}$$

$$PtCl_2 = Pt + Cl_2 \qquad \text{(Eq. 6.2)}$$

According to Eq. 6.1, platinum is kept in ionic form and the glasses have a yellow coloration. However yellow coloration is not observed in the $BaO/SrO/ZnO/SiO_2$ system when $PtCl_4$ is

added to the batch. This means that reaction Eq. 6.2 takes place and the reduction to metallic Pt occurs. The small Pt particles in the glass have sizes in the 0.5 to 2 µm range and the glasses appear as grey. Eq. 6.2 also explains why the intensity of the coloration is dependent on the Pt concentration. Furthermore, X-Ray diffraction proves the presence of metallic Pt which can be seen in **Figure 3 in paper 5.2**.

6.2 Kinetics of nucleation and crystallization

Determining the kinetics of nucleation and crystallization is usually a long and complicated process. Using DSC can help to get a first idea of the crystallization behaviour of a certain system (**Chapter 4**). This is possible by determining the characteristic temperatures: glass transition temperature (T_g), the onset of the crystallization peak (T_{on}), offset of the crystallization peak, (T_{off}) peak of crystallization (T_p). Using this parameter and employing Eq. 4.1, the Ozawa method for calculating the Avrami parameter, and how this can be used for predicting the crystallization tendency of a glass ceramic will further be discussed [15,43,57–61,68,69].

The base glass system from which the $Ba_{1-x}Sr_xZn_2Si_2O_7$ phase can be crystallized is $BaO/SrO/ZnO/SiO_2$. Unfortunately, as mentioned previously, this system exhibits solely surface crystallization [27,54]. The glass system was reported for the first time in **paper 5.1** and further investigated in **paper 5.3**. The characteristic temperatures obtained from DSC are summarised in **Table 2** of **paper 5.1**; T_g = 672 °C and the T_p = 948 ° C. The peak is rather broad with T_{on} at 916 °C and T_{off} at 969 °C. The overall low peak intensities and the high values of FWHM are graphically shown in **Figure 3 of paper 5.6**.

Adding different nucleation agents such as ZrO_2 and TiO_2 affects T_g depending on their respective concentrations, while Pt did not affect T_g, slight variations within the limits of error are seen. Adding ZrO_2 slowly increases T_g of the glasses and a maximum value

(697 °C) was recorded for sample 6Z. This is an increase of 25 K, which is explained by the increased viscosity of the glass melt. The effect is well known and previously reported for other systems, this means if ZrO_2 is present, more energy must be introduced before nucleation can start [6,53,63]. Decrease of T_g can be achieved by adding TiO_2 as shown in **Table 2 of paper 5.5**. The lowest T_g (667 °C) was obtained for sample T5. Even considering the limits of error in the DSC measurement (± 3 K), the addition of TiO_2 leads to a decrease in T_g, also when ZrO_2 is present, and is systematically decreasing with the TiO_2 concentration for sample Z6T2 the T_g = 689 °C, which is a decrease of 8 K in comparison to sample Z6. This trend is seen for all glass compositions reported in **Table 1 of paper 5.5**. The reduction of T_g can be explained by reduction of the viscosity in the glass. Typically, TiO_2 is incorporated in highly alkaline earth containing compositions as network modifier which take part in the glass formation and explains the reduction of T_g [52,63,65]. Although the glass was doped with different Pt concentrations (from 10 to 100 ppm) significant changes in T_g of the glasses were not observed. (**Table 2 of paper 5.6**). It must be mentioned that slight fluctuation of 3 K is present, which however, is within the limits of error of the measurement and a correlation with the Pt concentration is not observed. In the literature, no hint at a change of T_g with the addition of Pt was found. This fact leads to the suggestion that Pt does not affect the T_g of the glasses. This can be partially explained by the low concentration, which is not sufficient to affect the viscosity.

The peak of crystallization in the DSC profile plays an important part in determining the activation energies and can give an indication of the crystallization tendency of the system using different approaches. In this study more than one heating rate was used to ensure statistical accuracy for the determination of Avrami parameters and the activation energies. Nevertheless, in the following discussion only values recorded for a heating rate 10 K/min will be considered. The peak of crystallization for the base glass is 948 °C and adding ZrO_2 leads to an increase in

T_p to 977 and 985 °C for Z3 and Z6, respectively. If TiO_2 is added to the base glass composition, T_p is dropping to 925 °C which is the lowest reported crystallization peak temperature, if oxides are used as nucleation agents. The combination of ZrO_2 and TiO_2 increases the crystallization peak temperature up to 980 °C for the sample Z6T2. This increase is correlated to an increase due to ZrO_2; an exception for this is sample Z7T1 where T_p drops to 954 °C. However, this is not very surprising regarding the fact that in this system besides surface crystallization also volume crystallization takes place. A significant reduction of T_p was seen if small amounts of Pt were added to the system as shown in **Figure 2 of paper 5.6** where a DSC result for the base glass and different Pt concentrations is presented. Even 10 ppm of Pt reduced T_p by almost 100 K in comparison to the base glass.

In **Chapter 4,** the Avrami parameter was introduced, which can be used as a prediction tool for determining the crystallization behavior on the system. By applying Eq. 4.1 and different heating rates, the Avrami parameters were successfully calculated for all glass compositions and the results are published in the **papers 5.1, 5.2, 5.4-5.7.** In the case when the Avrami parameter was n = 1, which corresponds to surface crystallization, was obtained for low ZrO_2 concentrations (< 6 mol%), the result can be seen in the **papers 5.1 and 5.5,** this is valid for samples (Z0, Z3, Z5, Z5T3 and Z5T3) [26,27,57,59]. After a microstructural analysis in all samples mentioned above except Z5T5 and T5, surface crystallization was confirmed. In the cases of Z5T5 and T5, very low numbers (2-3) of volume crystals were detected during the microstructural studies. However, an explanation for this can be that the small amount of volume crystals might be caused by the formation of bubbles or impurities from the raw materials, which do not affect the overall kinetics of the crystallization processes and cannot be predicted by Eq. 4.1. In the systems where volume and surface crystallization were detected (Z6 and Z7T1) the parameter n was approximately 2; the results were confirmed by the microstructural studies [57]. Adding platinum in small concentrations, even 10 ppm resulted in

n = 3 which indicated volume crystallization and was confirmed by microstructural studies (**papers 5.2, 5.4, 5.6 and 5.7**). When 100 ppm of Pt was added to the composition, an Avrami parameter n equal to 4 was calculated which corresponds to a 3D volume crystallization. It should be noted that a corresponding change in the microstructure was not observed. An explanation for that is that the Avrami parameter depends on the chosen temperature and may vary slightly. This was previously shown in a study by M.-J. Pascual for a glass with the composition 30 $BaO \cdot 50\ SiO_2 \cdot 20\ ZnO$ [15,43]. This was also proven in **Figure 35.3, paper 5.4** where the Avrami parameter is potted against the temperature; here the change of the values of the parameter is well visible. Despite the slight variation independent on the chosen temperature, determining the Avrami parameter using Eq. 4.1 gives a good approximation for crystallization tendency of the $Ba_{1-x}Sr_xZn_2Si_2O_7$ phase.

Furthermore, different heating rates can be utilized for the calculation of the activation energies using the Kissinger [15,57,61] (see Eq. 4.2) as well as the Ozawa Equation [57,58,69] (see Eq. 4.3). Both methods are similar, and the obtained results differ within a range of only 6 %. The equations can be used when surface crystallization is the predominant mechanism of crystallization and the results can be seen in **papers 5.1, 5.2, 5.5-5.7**. According to the equation of Matusita, also known as the modified Kissinger equation (Eq. 4.4), if volume crystallization occurs, an additional parameter (parameter m) has to be taken into account which is denoted as "growth parameter" [4,57,62]. This parameter indicates the growth morphology and the mechanism, depending on the Avrami parameter, n. The value of m can be found in a Table 4.1 which was originally published by Donald [57].

6.3 Nucleation and crystallization

One of the main concerns, when additives are introduced in the base system, is whether they also lead to the crystallization of other crystalline phases or only the desire one. [6,66,70] For

this purpose, XRD studies were performed at several stages of crystallization: in the as melted glass, after nucleation, where a temperature of T_g up to T_g +40 K was chosen and after full crystallization. For the cases when ZrO_2 and TiO_2 oxides were used, the glasses were amorphous after melting and no traces of ZrO_2, TiO_2 or $ZrTiO_4$ were found in the glasses. However, this was not the case if Pt was introduced into the system. If a slow scan with 0.1 °/min was performed, the main peak of metallic Pt at $2\theta = 39.7°$ can be detected even for a Pt concentration as low as 30 ppm. The assumption that the Pt particles are formed during cooling of the glass is also supported by the TEM measurement shown in **Figure 10 of paper 5.2** for a glass sample with 100 ppm Pt. The Pt peak is no longer visible, when the $Ba_{1-x}Sr_xZn_2Si_2O_7$ starts to crystallize. This is shown in the XRD-pattern presented in **Figure 3 of paper 5.2** for a sample containing 100 ppm Pt nucleated at different temperatures. When additives such as ZrO_2, TiO_2, $PtCl_4$ or Sb_2O_3 are added, the main crystalline phase is the $Ba_{1-x}Sr_xZn_2Si_2O_7$ solid solution and small amounts of willemite (Zn_2SiO_4) and cristobalite are found, however this is expected because they can easily crystallize from the base system. It has to be mentioned that cristobalite is only formed at temperatures above 1000 °C which is above the working range of a cook top of around 600 °C so it should not affect the application of the material. Other additives such as P_2O_5, for example, lead to the formation of additional unknown phases at a temperature as low as 850 °C; also in the case of Al_2O_3 additions, additional unknow phases are formed [70,71].

Finding proper nucleation agents for the $Ba_{1-x}Sr_xZn_2Si_2O_7$ system where the quantity and size of the crystals can be controlled by the time/temperature schedule, was a tedious task [27,54,70]. Since the selected oxides did not achieve the desired effect, noble metals were the next step. When Pt was added to the system, the number of nuclei was only dependent on the used Pt quantity which was proved by SEM investigations (see **Figure 5 of paper 5.6**) where glasses with different platinum concentrations were thermally treated at 720 °C for 100 h.

However, if both Pt and Sb_2O_3 were used, the formation of new crystals is observed during thermal treatment. The result is published and shown in **Figure 8 of paper 5.7** where the number of crystals versus time is presented. In glasses with different Pt concentrations, the number of crystals increases up to a heat treatment time of 24 h independent of the applied nucleation temperature. With further increasing temperature, the number of crystals decreases again. This effect might be caused by Ostwald ripening. Another interesting feature is the lack of induction time which is in contrast to reports on other glass systems. The lack of induction time is due to a small number of Pt particles which have already been formed during cooling of the glass and which act as nucleation centres during crystallization [6,51,72]. The optimum nucleation temperature where the number of crystals is highest, depends on the Pt concentration, 690 and 680 °C for 50 and 100 ppm Pt, respectively. This means that Pt is a good nucleation agent, which can be supported by Sb_2O_3 additions and furthermore, the number and the size of the crystals can be controlled by the nucleation time and temperature, which is a key component for obtaining a tailored microstructure.

6.4 Microstructure

The microstructure is one of the most important parameters of materials with low thermal expansion. Small cracks in the microstructure can grow when multiple heating/cooling cycles are implied and lead to a destruction of the already built up materials. Example for that is the cooking panel which must withstand for many years of use and also should not be damaged by rapid cooling, for example, by a spill of water [1,6]. In Chapters 4.2 and 4.3, the importance of the Avrami parameter and the ability to prediction the crystallization behaviour of the $Ba_{1-x}Sr_xZn_2Si_2O_7$ phase is discussed. However, no matter how accurately the Avrami parameter predicts the crystallization mechanism, the microstructure of the $Ba_{1-x}Sr_xZn_2Si_2O_7$ phase containing glass ceramics should be studied, also with respect to their tendency to crack formation. This is possible through SEM, TEM or LSM analyses. It should also be mentioned

that the Avrami parameter cannot give 100 % certainty, this is why most authors advise to perform additional microstructure studies [15,26,58,67,72].

It was already discussed that most of the oxides do not work as effective nucleation agents and only high oxide concentrations will trigger volume nucleation (see **papers 5.1 and 5.5** [26,27]). The first time where volume crystallization was active in the base systems is shown in **Figure 6 of paper 5.1**; it was the sample Z6 thermally treated at 720 °C for 48 h and subsequently at 840 °C for 1 h. The LSM gives a good indication of the fact that volume crystallization is present, however, only a small amount of crystals is seen. SEM analyses on the same sample show that surface crystallization is the predominant crystallization mechanism (see **Figure 8 of paper 5.1**). This result is in good agreement with the obtained Avrami parameter, (see **Figure 5b of paper 5.1**), which is equal to 2 and corresponds to volume and surface crystallization. A crystal formed in the volume of the same glass composition was studied and presented in **Figure 7 of paper 5.1**. This micrograph also shows multiple crack formation. This is most probably caused by the sizes of the crystal (e.g. 182 µm) and their low quantity which is not sufficient to overcome the anisotropy in the coefficients of thermal expansion of the system. All other glass systems presented in **Table 1 of paper 5.1** show only surface crystallization, which is in a good agreement with the obtained Avrami parameters graphically presented in **Figure 5** of the same paper and discussed in **chapter 6.2**.

The results summarizing the microstructures if ZrO_2 and TiO_2 are used as nucleation agents are shown in **paper 5.5**. According to the Avrami parameters, the only glass composition of those shown in **Table 1 of paper 5.5**, from which volume crystallization occurs is Z7T1. This is in good agreement with **Figure 7** of **paper 5.5** which shows such a sample thermally treated at 750 °C for 48 h and at 840 °C for 45 min: 3 crystals are found in the volume. In this glass system, the crystals have a mean size of 87 µm, which is a significant reduction in comparison to sample Z6 where the mean size was 182 µm. This reduction of almost 100 µm and the

increasing number of crystals shows that adding TiO_2 is favorable for the volume crystallization. This is caused by two factors: (i) the reduction in the viscosity and (ii) a change in the solubility of ZrO_2, so more of this nucleation agent can be added [6,53]. However, some inconsistencies regarding the Avrami parameter were also observed because some few volume crystals were found in samples T5 and Z5T5, the reasons for these inconsistencies are explained in Chapter 6.2. In all other glass systems, only surface crystallization was found.

The morphology of the crystals obtained by using only ZrO_2 as a nucleating agent has a core in the middle from which a radial growth of the crystalline phase starts. The crystals seem to have a high aspect ratio and most probably grow with the morphology of thin sheets. However, this did not explain the interesting phenomena observed for sample Z7T1 thermally treated at 750 °C for 48 h and subsequently at 840 °C for 45 min, as shown in **Figure 9a of paper 5.5.** There the circular cracks are formed at two locations around the crystal. This gave rise to further investigations with EBSD shown in the same Figure **(Figure 9b, bottom)**. This Figure shows a combined Image Quality (IQ) and inverse pole figure (IPF) map for all recorded patterns which are attributed to the orthorhombic structure of the $Ba_{0.6}Sr_{0.4}Zn_2Si_2O_7$ phase. The colour code of the inverse pole figure describes the crystal direction which shows a gradual change of the orientation from the centre of the structure to the edge. The white unit cells and the corresponding c-axis directions help to read the map. Typically, the dimensions of these cells are a = 12.98, b = 7.71, and c = 6.59 Å. The c-axes [001] develop from perpendicular to the cut plane in the centre to almost parallel to the cut plane and parallel to the long axis of the substructures with increasing distance from the centre. The courses of the cracks are highlighted with blue lines and are perpendicular to the c-axes of the broken crystals. Similar results are reported for the surface crystallization where the crack formation is also perpendicular to the c-axes and can be seen in **Figure 8 of paper 5.3** for the base glass thermally treated for 1.5 h at 790 °C and **Figure 8 of paper 5.5**. for the sample Z6T2 thermally treated at 710 °C for 48 h

and subsequently at 840 °C for 45 min. The result show that the crack formation is caused by the phase itself and is not affected by the type of crystallization (surface or volume) as well as if another component is added to the base glass composition. As this does not depend on the glass composition and is connected to the phase structure the following conclusion can be drawn: the c-axis is perpendicular to the cracks which indicates that they are caused by the anisotropy of the CTE. The c-axis shows the highest positive value and, hence, contracts strongest during cooling, while the b-axis expands strongly and the a-axis contracts slightly. Therefore, cracks perpendicular to the c-axis seem to be a logical consequence, because the crystals get under tensile stresses during cooling.

Since the studied oxides did not induce sufficient extend of volume crystallization, even at the point where the limit of solubility in the system has been reached, another approach was used. It is well known that noble metals can be used in small quantity and induce volume crystallization. Noble metals such as gold, silver or platinum may be added to the base system, however, in this dissertation, the main focus of discussion will be the Pt [50,66,71,72]. The glass composition to which Pt was added is found in **Table 1 and the papers 5.2, 5.6 and 5.7.** The effect of other components such as ZrO_2 and Sb_2O_3 have also a notable impact on the microstructure. All glasses where Pt is added even in very small concentrations of 10 ppm exhibit volume crystallization as the predominant mechanism. When only Pt is used in different concentration as reported in **paper 5.6,** the volume crystal concentration depends more strongly on the Pt concentration. This is seen very well in **Figure 5 of paper 5.6** where samples with different Pt concentrations were heat-treated at 720 °C for 100 h; a comprehensive explanation is also given in Subchapter 6.3. The Pt particle acts as a substrate from where the $Ba_{1-x}Sr_xZn_2Si_2O_7$ phase starts to grow.

Good example of typical crystal precipitation when only Pt is present in the system is shown in **Figure 6 of paper 5.6.** The sample shown there has 50 ppm Pt and is thermally treated for

48 h at 710 °C and for 30 min at 780°C; the bright spherical particle in the center shows an enrichment of Pt according to the EDX measurement. Enrichments of Zn and Ba are seen at the locations of the crystal which is not surprising. The EBDS analysis performed at the same sample seen in **Figure 7 of paper 5.6** shows the orientation of the crystal of the orthorhombic structure of the $Ba_{1-x}Sr_xZn_2Si_2O_7$ phase (ICSD 429938). The color code of the inverse pole figure describes the crystal direction perpendicular to the sample surface. Most parts of the crystal show different absolute orientations, but the a-axes [100] are almost perpendicular to the sample surface (green dots). Patterns obtained from the platinum particles possess a low IQ caused by the topography of the particles and furthermore by a low crystal perfection which is caused by deformation e.g. from polishing (metallic platinum shows a plastic deformation behavior in comparison to the glass ceramics). Hence, the EBSD patters cannot be attributed to platinum or to any other phase. The results of the EBSD-measurements show a clear orientation of the c-axis [001] which is parallel to the fastest growing axis of the cut crystal. This agrees with the results described above for the base glass and the ZrO_2/TiO_2 containing glasses. Crack formation is still present in the crystal even if the crystal size is less than 40 µm (the size depends on the Pt concentration and the heat treatment procedure). The origin of the cracks is near the Pt particle and should also be caused by the different CTE between the Pt and the crystalline phase. The morphology of the crystals is different from that of the oxide containing glasses. The crystals start growing from the Pt particle and have one main growth direction. This direction is attributed to a higher crystal growth velocity in comparison to the surrounding/thickening part of the crystals. By comparison, in sample Z6Pt, volume crystallization is the main crystallization mechanism, but the morphology is similar to the oxide containing glasses. This can be seen in **Figure 35.4 of paper 5.4** for the sample nucleated at 720 °C for 48 h and thermally treated at 780 °C for 5 h. In this case, a bright spherical crystal attributed to a Pt particle is observed surrounded by spherical crystals corresponding to the

$Ba_{1-x}Sr_xZn_2Si_2O_7$ phase. This means that the morphology of the $Ba_{1-x}Sr_xZn_2Si_2O_7$ phase is dependent on the additive to the base glass system.

As previously discussed in **Chapter 6.1**, the oxidation state is of extreme importance, i.e. whether ionic Pt or metallic Pt occurs. The Sb_2O_3 is a well know agent which might induce a reducing effect during cooling of the glass or during thermal treatment at temperatures slightly above T_g. However, adding a combination of Sb_2O_3 and Pt (see **Table 1 of paper 5.7**) affects significantly the microstructure of the obtained materials. As seen, from the LSM images in **Figure 7** and the SEM image in **Figure 9** (both published in **paper 5.7**) the shape of the Pt particles changes. Some of them still have spherical form but many also have irregular shapes like rods and triangles. This and the EDX of sample Pt 50 thermally treated at 710 °C for 48 h and at 780 °C for 1 h (**Figure 9 of paper 5.7**) lead to some interesting conclusion. In the EDX mapping, we see that the bright particle in the center of the crystal is not only enriched in Pt as previously described, but also in Sb. Although clearly seen in **Figure 9b**, the enrichment of Sb might either be real or an artefact. There are two possibilities that the signal is not real due to an increased background of Bremsstrahlung. Since the excitation volume at 10 kV acceleration voltage has still a size of about 1 µm, the small Sb peak might be caused by peripheral excited material (crystal and residual glass) surrounding the sub-micrometer Pt-particle. However, then also an increased Ba-signal should occur, which is not observed. The other possibility is the formation of an alloy of Pt and Sb. The phase diagram Pt/Sb has a deep eutectic minimum at $Pt_{0.78}Sb_{0.22}$ attributed to a temperature of 633 °C. Hence, Pt and Sb should have a strongly negative mixing enthalpy. In metallic platinum, antimony is soluble, e.g. at a temperature of 755 °C around 7 wt% Sb can be dissolved. Therefore, it is assumed, that the particle contains a certain Sb-concentration.

Another interesting effect caused by Sb_2O_3 is the appearance of two growth morphologies which are attributed to the orthorhombic structure of the $Ba_{1-x}Sr_xZn_2Si_2O_7$ phase

(ICSD 429938) [20]. On one side, crystals are grown from an apparent center, while at the other side, the different morphology appears similar as a dendritic growth. This is presented in **Figure 10 of paper 5.7** for the sample with Pt 50 thermally treated at 710 °C for 48 h and subsequently crystallized at 780 °C for 1 h. These structures were also characterized using EBSD. While the crystals which run from the center have certain orientation gradients (changing colors), the dendrite-like crystals have a unique orientation (one color). While the crystals grown from the center are oriented with their c-axes parallel to their longest axis (the growth direction), the dendrite-like crystals are aligned with their c-axes perpendicular to their primary growth direction (and parallel to the longest axis of the secondary structures). The dendritic structure is less prone to cracking and can grow up to 100 µm and crack formation will still not occur. This and the fact that zero thermal expansion was reached as seen in **Figure 11 of paper 6.7** and the dilatometric measurements of samples Pt 50 and Pt 100 thermally treated at 720 °C for 100 h. This observation suggested that a further adjustment must be made on the composition of the glass system and their applied heat treatment schedule in order to optimize the final product. Below, in Table 6.1, some suggestion of possible new compositions which should lead to improvement of the microstructure based on the results and the conclusions form this dissertation are shown.

Table.6.1 New possible chemical compositions in mol% for further improvement of the microstructure.

Number	Chemical composition in mol%							
	BaO	SrO	ZnO	SiO_2	$PtCl_4$	ZrO_2	TiO_2	Sb_2O_3
1	7.5	7.5	34.0	50.28	0.02	0	0	1
2	7.5	7.5	34.0	42.48	0.02	6.5	1	1
3	7.5	7.5	34.0	42.49	0.01	6.5	1	1

7. Conclusion

The base glass composition $BaO/SrO/ZnO/SiO_2$ is a suitable candidate for the crystallization of the $Ba_{1-x}Sr_xZn_2Si_2O_7$ phase and can be well combined with other nucleation agents or additives such as ZrO_2, TiO_2, Pt and Sb_2O_3. The base glass system without additives has the tendency to sole surface crystallization and due to the high anisotropy of the crystal structure, the obtained materials are destroyed by the tension stress formed during cooling inside the glass-ceramic. This was proven by the SEM analysis in combination with EBSD. The results show that the origin of the cracks is perpendicular to the c-axis of the $Ba_{1-x}Sr_xZn_2Si_2O_7$ crystal. This axis has a strongly positive CTE and hence strongly contracts during cooling of the material.

The kinetic parameters of all glasses were determined using DSC. Important highlights are the determination of the activation energies and Avarami parameter, which was found using the Ozawa equation. The Avrami parameter proves to be a quite suitable for the prediction of the crystallization tendency for the $Ba_{1-x}Sr_xZn_2Si_2O_7$ phase. All results were cross referenced with a microstructural study to confirm the predicted results.

Adding nucleation agents such as ZrO_2 and TiO_2 did not give sufficient, result in a satisfactory extend of volume crystallization. The latter is only observed at high concentration and even then the surface crystallization is the predominant mechanism. Only two glass systems when oxides are used as nucleation agents (Z6 and Z7T1) led to volume crystallization with a mean crystal size of 180 µm and 80 µm, respectively. However, this size is still too large and the number of crystals too low to overcome the anisotropy of the system and to produce crack free glass ceramics. Adding Pt to the system led to an increasing number of volume crystals with a relatively small size of around 20 µm. Nevertheless, these nucleation agents have a significant drawback as the number of Pt particle does not depend on the heat treatment schedule but on

the added Pt concentration. The formation of metallic Pt was detected by XRD, SEM and TEM. In agreement with the literature, the working theory is that the metallic Pt is formed during the cooling of the glass and is caused by a redox reaction. Adding antimony in oxidizing atmosphere to the systems in the presence of different Pt concentration leads to a dissolution of metallic platinum in the glass melt and to the formation of platinum particles during thermal treatment at temperatures slightly above T_g. Here, the number of crystals increases up to 24 h of thermal treatment. The combination of platinum and Sb_2O_3 enables the preparation of a ZTE material which is shown by dilatometric measurements.

References

[1] H. Bach, D. Krause, Low Thermal Expansion Glass Ceramics. 2nd edn. Springer, New York.(2005)

[2] G.D. Barrera, J.A.O. Bruno, T.H.K. Barron, N.L. Allan, Negative thermal expansion, J. Phys. Condens. Matter. 17 (2005) R217-R252.

[3] H. Scheidler, E. Rodek, Li_2O-Al_2O_3-SiO_2 glass-ceramics, Am. Ceram. Soc. Bull. 68 (1989) 1926–1930.

[4] J. Massera, S. Fagerlund, L. Hupa, M. Hupa, Crystallization mechanism of the bioactive glasses, 45S5 and S53P4, J. Am. Ceram. Soc. 95 (2012) 607–613.

[5] J.F. MacDowell, Aluminoborate Glass-Ceramics with Low Thermal Expansivity, J. Am. Ceram. Soc. 73 (1990) 2287–2292.

[6] P.W. McMillan, Glass-ceramics, 2nd edn. Academic Press, London. (1979).

[7] J.S. Browder, S.S. Ballard, Low Temperature Thermal Expansion Measurements on Optical Materials, Appl. Opt. 8 (1969) 793–798.

[8] M. Macdonald, V. Badescu. The International Handbook of Space Technology 1st edn. Springer, Berlin, Praxis. (2014).

[9] W. Wang, R. Huang, W. Li, J. Tan, Y. Zhao, S. Li, C. Huang, L. Li, Zero thermal expansion in NaZn13-type La(Fe,Si)13 compounds, Phys. Chem. 17 (2014) 2352–2356.

[10] D. Tauch, C. Rüssel, Glass-Ceramics with Zero Thermal Expansion in the System $BaO/Al_2O_3/B_2O_3$, J. Non-Cryst. Solids 351 (2005) 2294-2298.

[11] K. Takenaka, Negative thermal expansion materials: technological key for control of thermal expansion, Sci. Technol. Adv. Mater. 13 (2012) 013001

[12] C. Thieme, C. Rüssel Very high or close to zero thermal expansion by the variation of the Sr/Ba ratio in $Ba_{1-x}Sr_xZn_2Si_2O_7$ - solid solutions, Dalton Trans. 45 (2016) 4888–4895.

[13] G. Müller, M. Sternitzke, Computer modelling of structure and thermal expansion of β-quartz-and keatite-type aluminosilicates, J. Mater. Sci. Lett. 12 (1993) 278–280.

[14] M. Sternitzke, G. Müller, Crystal structure and thermal expansion of quartz-type aluminosilicates, J. Mater. Sci. 26 (1991) 3051–3056.

[15] R. Wurth, M.J. Pascual, G.C. Mather, A. Pablos-Martin, F. Munoz, A. Duran, G.J. Cuello, C. Rüssel, Crystallisation mechanism of a multicomponent lithium alumino-silicate glass, Mater. Chem. Phys. 134 (2012) 1001–1006.

[16] S.D. Stookey, Catalyzed crystallization of glass in theory and practice, Ind. Eng. Chem. 51 (1959) 805–808.

[17] D. Tauch, C. Rüssel, Thermal expansion of glass–ceramics in the system $BaO/Al_2O_3/B_2O_3$, J. Non-Cryst. Solids. 351 (2005) 3483–3489.

[18] I. Yamai, T. Oota, Low Thermal Expansion Polycrystalline Zirconyl Phosphate Ceramic, J. Am. Ceram. Soc. 68 (1985) 273–278.

[19] C. Lind, A.P. Wilkinson, Z. Hu, S. Short, J.D. Jorgensen, Synthesis and properties of the negative thermal expansion material cubic $ZrMo_2O_8$, Chem. Mater. 10 (1998) 2335–2337.

[20] C. Thieme, H. Görls, C. Rüssel, $Ba_{1-x}Sr_xZn_2Si_2O_7$-A new family of materials with negative and very high thermal expansion, Sci. Rep. 5 (2015) 18040.

[21] M. Kerstan, C. Rüssel, Barium silicates as high thermal expansion seals for solid oxide fuel cells studied by high-temperature X-ray diffraction (HT-XRD), J. Power Sources. 196 (2011) 7578–7584.

[22] C. Thieme, T. Waurischk, C. Lin, C. Rüssel, Lilac ceramic pigments based on $Ba_{0.5}Sr_{0.5}Zn_{2-x}Ni_xSi_2O_7$ solid solutions, Ceram. Int. 11 (2016) 13035–13040

[23] J.H. Lin, G.X. Lu, J. Du, M.Z. Su, C.-K. Loong, J.W. Richardson, Phase transition and crystal structures of $BaZn_2Si_2O_7$, J. Phys. Chem. Solids. 60 (1999) 975–983.

[24] L. Vladislavova, C. Thieme, T. Zscheckel, C. Patzig, T. Höche, C. Rüssel, Heterogeneous nucleation of $Ba_{1-x}Sr_xZn_2Si_2O_7$ from a BaO/SrO/ZnO/SiO_2 glass using platinum as nucleation agent, J. Eur. Ceram. Soc. (2017) 4801-4808.

[25] L. Vladislavova, M. Kracker, T. Zscheckel, C. Thieme, C. Rüssel, Crystallisation of $Ba_{1-x}Sr_xZn_2Si_2O_7$ from BaO/SrO/ZnO/SiO_2 glass with different ZrO_2 and TiO_2 concentrations, Solid State Sci. (2018) 107-115.

[26] L. Vladislavova, C. Thieme, C. Rüssel, The effect of ZrO_2 on the crystaallization of a glass in the system BaO/SrO/ZnO/SiO_2: surface versus bulk crystallization, J. Mater. Sci 52. (2016) 4052-4060.

[27] W.D. Callister Jr, Materials Science and Engineering, John Wiley & Sons, Inc, London N. Y. (2007).

[28] C.B. Carter, M.G. Norton, Ceramic materials: science and engineering, Springer Science & Business Media, London N.Y (2007).

[29] A.X. Lu, Z.B. Ke, Z.H. Xiao, X.F. Zhang, X.Y. Li, Effect of heat-treatment condition on crystallization behavior and thermal expansion coefficient of Li_2O–ZnO–Al_2O_3–SiO_2–P_2O_5 glass–ceramics, J. Non-Cryst. Solids. 353 (2007) 2692–2697.

[30] G.K. White, R.B. Roberts, Thermal expansion of willemite, Zn_2SiO_4, Aust. J. Phys. 41 (1988) 791–798.

[31] W. Wisniewski, C. Thieme, R. Müller, S. Reinsch, S. Groß-Barsnick, C. Rüssel, Oriented Surface Nucleation and Crystal Growth in a 18 BaO 22 CaO·60 SiO_2 mol% Glass Used for SOFC Seals, CrystEngComm.20 (2018) 787-795.

[32] F. Träger, Springer handbook of lasers and optics, Springer Science & Business Media London, N.Y. (2012).

[33] B.K. Jasthi, W.J. Arbegast, S.M. Howard, Thermal expansion coefficient and mechanical properties of friction stir welded invar (Fe-36% Ni), J. Mater. Eng. Perform. 18 (2009) 925–934.

[34] K. De Buysser, P. Lommens, C. De Meyer, E. Bruneel, S. Hoste, I. Van Driessche, ZrO_2-ZrW_2O_8 composites with tailor-made thermal expansion, Ceram.-Silik. 48 (2004) 139–144.

[35] J.N. Grima, V. Zammit, R. Gatt, Negative Thermal Expansion, Journal of the Malta Chamber of Scientists 11 (2006) 17-29.

[36] M.G. Tucker, A.L. Goodwin, M.T. Dove, D.A. Keen, S.A. Wells, J.S. Evans, Negative thermal expansion in ZrW_2O_8: Mechanisms, rigid unit modes, and neutron total scattering, Phys. Rev. Lett. 95 (2005) 255501.

[37] K.D. Hammonds, M.T. Dove, A.P. Giddy, V. Heine, B. Winkler, Rigid-unit phonon modes and structural phase transitions in framework silicates, Am. Mineral. 81 (1996) 1057–1079.

[38] J.S.O. Evans, T.A. Mary, A.W. Sleight, Negative thermal expansion materials, Phys. B Condens. Matter. 241–243 (1997) 311–316.

[39] C. Thieme, Dissertation, Crystalline Phases and Ceramic Materials with High and Low Coefficients of Thermal Expansion Based on Alkaline Earth Zinc Silicates, (2015) Jena University, Germany.

[40] C. Thieme, G.B. Souza, C. Rüssel, Glass-Ceramics in the System BaO–SrO–ZnO–SiO_2 with Adjustable Coefficients of Thermal Expansion, J. Am. Ceram. Soc. 99 (2016). 3097-3103.

[41] M.J. Pascual, C. Lara, A. Duran, Non-isothermal crystallisation kinetics of devitrifying RO–BaO–SiO_2 (R= Mg, Zn) glasses, Phys. Chem. Glass: Eur. J. Glass Sci. Technol. Part B. 47 (2006) 572–581.

[42] M. Kerstan, M. Müller, C. Rüssel, Thermal expansion of $Ba_2ZnSi_2O_7$, $BaZnSiO_4$ and the solid solution series $BaZn_{2-x}Mg_xSi_2O_7$ ($0 \leq x \leq 2$) studied by high-temperature X-ray diffraction and dilatometry, J. Solid State Chem. 188 (2012) 84–91.

[43] M. Kerstan, C. Thieme, M. Grosch, M. Müller, C. Rüssel, $BaZn_2Si_2O_7$ and the solid solution series $BaZn_{2-x}Co_xSi_2O_7$ ($0 < x \leq 2$) as high temperature seals for solid oxide fuel cells studied by high-temperature X-ray diffraction and dilatometry, J. Solid State Chem. 207 (2013) 55–60.

[44] C. Thieme, C. Rüssel, High thermal expansion in the solid solution series $BaM_{2-x}Ni_xSi_2O_7$ (M= Zn, Mg, Co)-the effect of Ni-concentration on phase transition and expansion, J. Mater. Sci. 50 (2015) 3416–3424.

[45] C. Thieme, T. Waurischk, S. Heitmann, C. Rüessel, New Family of Materials with Negative Coefficients of Thermal Expansion: The Effect of MgO, CoO, MnO, NiO, or CuO on the Phase Stability and Thermal Expansion of Solid Solution Phases Derived from $BaZn_2Si_2O_7$, Inorg. Chem. 55 (2016)

[46] C. Rüssel, C. Thieme, Negative Thermal Expansion in $Ba_{0.5}Sr_{0.5}Zn_2SiGeO_7$, Materials. 9 (2016) 631.

[47] M. Kracker, C. Thieme, J. Haessler, C. Rüssel, Sol-gel powder synthesis and preparation of ceramics with high- and low-temperature polymorphs of $Ba_xSr_{1-x}Zn_2Si_2O_7$ (x=1 and 0.5): A novel approach to obtain zero thermal expansion, J. Eur. Ceram. Soc. 36 (2016) 2097–2107.

[48] J.M. Rincón, Principles of nucleation and controlled crystallization of glasses, Polym.-Plast. Technol. Eng. 31 (1992) 309–357.

[49] G.E. Rindome, Further Studies of the Crystallization of a Lithium Silicate Glass, J. Am. Ceram. Soc. 45 (1962) 7–12.

[50] K. Thieme, C. Rüssel, Nucleation inhibitors—the effect of small concentrations of Al_2O_3, La_2O_3 or TiO_2 on nucleation and crystallization of lithium disilicate, J. Eur. Ceram. Soc. 34 (2014) 3969–3979.

[51] K. Thieme, C. Rüssel, Nucleation and growth kinetics and phase analysis in zirconia-containing lithium disilicate glass, J. Mater. Sci. 50 (2015) 1488–1499.

[52] M. Kracker, L. Vladislavova, C. Thieme, T. Zscheckel, K. Thieme, T. Höche, C. Rüssel, Surface crystallization of low thermal expansion $Ba_{0.5}Sr_{0.5}Zn_2Si_2O_7$ from an 8 BaO·8 SrO·34 ZnO·50 SiO_2 glass, RSC Adv. 7 (2017) 44834–44842.

[53] S. Krüger, J. Deubener, Heterogeneous surface nucleation of lithium disilicate glass: An isothermal DSC study, J. Non-Cryst. Solids. 417–418 (2015) 45–51.

[54] E.D. Zanotto, Bright future for glass-ceramics, Am. Ceram. Soc. Bull. 89 (2010) 19–27.

[55] I.W. Donald, Crystallization kinetics of a lithium zinc silicate glass studied by DTA and DSC, J. Non-Cryst. Solids. 345 (2004) 120–126.

[56] T. Ozawa, A modified method for kinetic analysis of thermoanalytical data, J. Therm. Anal. 9 (1976) 369–373..

[57] A. Arora, E.R. Shaaban, K. Singh, O.P. Pandey, Non-isothermal crystallization kinetics of ZnO–BaO–B_2O_3–SiO_2 glass, J. Non-Cryst. Solids. 354 (2008) 3944–3951.

[58] M. Guedes, A.C. Ferro, J.M.F. Ferreira, Nucleation and crystal growth in commercial LAS compositions, J. Eur. Ceram. Soc. 21 (2001) 1187–1194.

[59] H. E. Kissinger, Reaction Kinetics in Differential Thermal Analysis. Anal Chem 29 (1957) 1702-1706.

[60] K. Matusita, S. Sakka, Y. Matsui, Determination of the activation energy for crystal growth by differential thermal analysis, J. Mater. Sci. 10 (1975) 961–966.

[61] M. Chavoutier, D. Caurant, O. Majérus, R. Boulesteix, P. Loiseau, C. Jousseaume, E. Brunet, E. Lecomte, Effect of TiO_2 content on the crystallization and the color of (ZrO_2, TiO_2)-doped Li_2O–Al_2O_3–SiO_2 glasses, J. Non-Cryst. Solids. 384 (2014) 15–24.

[62] M. Lopes, J.E. Shelby, Introduction to Glass Science and Technology, The Royal Society of Chemistry, Location (2005).

[63] W. Zdaniewski, DTA and X-Ray Analysis Study of Nucleation and Crystallization of MgO-Al_2O_3-SiO_2 Glasses Containing ZrO_2, TiO_2, and CeO_2, J. Am. Ceram. Soc. 58 (1975) 163–169.

[64] G.E. Rindone, Influence of platinum nucleation on crystallization of a lithium silicate glass, J. Am. Ceram. Soc. 41 (1958) 41–42.

[65] L. Vladislavova, M. Kracker, T. Zscheckel, C. Thieme, C. Rüssel, The effect of different platinum concentrations as nucleation agent in the BaO/SrO/ZnO/SiO_2 glass system, J. Mater. Sci. 53 (2018) 11204–11215.

[66] J. Augis, J. Bennett, Calculation of the Avrami parameters for heterogeneous solid state reactions using a modification of the Kissinger method, J. Therm. Anal. Calorim. 13 (1978) 283–292.

[67] M. Ghasemzadeh, A. Nemati, A. Nozad, Z. Hamnabard, S. Baghshahi, Ccrystallization kinetics of glass-ceramics by differential thermal analysis, Ceram.-Silik. 55 (2011) 188–194.

[68] K. Thieme, T. Zscheckel, C. Thieme, T. Höche, C. Rüssel, On the search for nucleation agents in BaO-SrO-ZnO-SiO_2 glasses: The influence of P_2O_5, J. Eur. Ceram. Soc. 38 (2017). 2017-2026.

[69] C. Thieme, M. Kracker, A. Erlebach, C. Patzig, M. Sierka, T. Höche, C. Rüssel, Effect of Al_2O_3 on phase formation and thermal expansion of a BaO-SrO-ZnO-SiO_2 glass ceramic, Ceram. Int. 44 (2018) 2098–2108.

[70] L. Cormier, Nucleation in Glasses – New Experimental Findings and Recent Theories, Procedia Mater. Sci. 7 (2014) 60–71.

[71] K.L. Narayan, K.F. Kelton, C.S. Ray, Effect of Pt doping on nucleation and crystallization in $Li_2O{\cdot}2SiO_2$ glass: experimental measurements and computer modeling, J. Non-Cryst. Solids. 195 (1996) 148–157.

[72] G.E. Rindone, J.L. Rhoads, The Colors of Platinum, Palladium, and Rhodium in Simple Glasses, J. Am. Ceram. Soc. 39 (1956) 173–180.

Abstract

This work is dedicated to the search for proper nucleation agents for the base glass in the system $BaO/SrO/ZnO/SiO_2$ from which the recently discovered $Ba_{1-x}Sr_xZn_2Si_2O_7$ phase can crystallize in bulk. The $Ba_{1-x}Sr_xZn_2Si_2O_7$ phase exhibits close to zero thermal expansion and can be easily crystallized from appropriate glass compositions. Glass ceramics with negative or zero thermal expansion are suitable candidates for numerous applications, such as cooking panels, telescope mirrors and optical applications or components. Unfortunately, the $BaO/SrO/ZnO/SiO_2$ glass system exhibits sole surface crystallization which leads to the formation of cracks during cooling and finally to the destruction of the produced materials. Finding a proper nucleation agent, which enables the crystallization in the volume in a high quantity and with small crystallite sizes, which can be controlled, is a key step for the implementation of the new phase for industrial use. This work is focused on the effect of different nucleation agents and additives to the base glass $BaO/SrO/ZnO/SiO_2/N$ (N = ZrO_2, TiO_2, Pt, Sb_2O_3) and the resulting microstructures. In this dissertation also, the kinetic parameters such as the activation energy and the Avrami parameter as well as the characteristic temperatures are reported.

Kinetics parameters, as well as the characteristic temperatures, were determined by using differential scanning calorimetry (DSC). The Avrami parameters (n) determined by applying the Ozawa equation proved to enable an accurate prediction of the crystallization mechanism and the crystallization tendency of the $Ba_{1-x}Sr_xZn_2Si_2O_7$ phase. This enabled to clearly distinguish between a surface (n = 1), combined surface and volume (n = 2) and volume crystallization (n = 3). This helps for faster assessment of the effect of certain nucleation agents and their concentrations, which was e.g. well-illustrated for different ZrO_2 concentrations. In analogy, a comparison of the calculated activation energies was made by using Kissinger equation, Ozawa equation and modified Kissinger equation.

In a first step, ZrO_2 and ZrO_2/TiO_2 were added to the base glass system, since they act as effective nucleation agents in other glass systems with low thermal expansion, such as lithium alumosilicates. However, in the studied system, they did not work as sufficient nucleation agent and trigger volume crystallization only at high concentrations: 6 mol% ZrO_2 and combination of both 7 mol% ZrO_2 and 1 mol% TiO_2. Nevertheless, the predominant crystallization mechanism in this system was the surface crystallization and the quantity of volume crystals is too small to prevent crack formation induced from the anisotropy of the crystal phase.

Adding noble metal was the next step, which leads to a significant improvement in the size and quantity of the crystals in the volume. Even small amounts of Pt such as 10 ppm may trigger volume crystallization. This was predicted by the Avrami parameter (n =3) and further confirmed by scanning electron microscopy (SEM). The concentration of Pt enables to control the number and size of the crystals. This is due to the presence of metallic Pt particles inside the glass, which are formed during the cooling of the glass and are affected by a reduction process.

Adding Sb_2O_3 and Pt in combination changes the reduction process in the glass and ionic Pt was formed at high temperature. This, for the first time, enabled a controlled volume crystallization of the $Ba_{1-x}Sr_xZn_2Si_2O_7$ phase. The number of crystals increases for up to 24 h of heat treatment, while further treatment decreases the number of crystals again. The morphology of all obtained glass ceramics was studied using SEM in combination with electron backscatter diffraction (EBSD). These studies showed a strong correlation between the crystallographic direction and the crack formation of the crystal phase and the strong anisotropy of the coefficient of thermal expansion. The cracks are perpendicular to the c -axis, which shows the highest coefficients of thermal expansion and, hence, contracts strongest during cooling, while the b-axis expands and the a-axis contracts slightly.

Zusammenfassung

Diese Arbeit beschäftigt sich mit der Suche nach geeigneten Keimbildnern für ein $BaO/SrO/ZnO/SiO_2$ Grundglas, aus welchem die erst seit kurzem bekannte Phase $Ba_{1-x}Sr_xZn_2Si_2O_7$ im Volumen kristallisieren kann. Die $Ba_{1-x}Sr_xZn_2Si_2O_7$ Phase hat einen thermischen Ausdehnungskoeffizienten nahe Null und kann aus geeigneten Glaszusammensetzungen leicht kristallisiert werden. Glaskeramiken mit einem thermischen Ausdehnungskoeffizienten, der negativ ist oder bei nahe null liegt, sind für verschiedene Anwendungen geeignet, zum Beispiel Glaskeramikkochfelder, Teleskopspiegel oder andere optische Komponenten und Anwendungen. Leider zeigt das $BaO/SrO/ZnO/SiO_2$ Grundglas nur Oberflächenkristallisation, was beim Abkühlen zu Rissen und schließlich der Zerstörung des produzierten Materials führt. Für die industrielle Nutzung der neuen Phase ist es daher ein notwendiger Schritt, Keimbildner zu finden, die im Volumen die Ausscheidung kleiner Kristallite kontrollierbarer Größe ermöglichen. Diese Arbeit konzentriert sich auf die Effekte verschiedener Keimbildner und Zusatzstoffe zum $BaO/SrO/ZnO/SiO_2/N$ ($N = ZrO_2$, TiO_2, Pt, Sb_2O_3) Grundglas und den daraus resultierenden Mikrostrukturen. In dieser Dissertation wird außerdem über kinetische Parameter wie die Aktivierungsenergie und Avrami Parameter sowie die charakteristischen Temperaturen berichtet.

Kinetische Parameter und charakteristische Temperaturen wurden über dynamische Differenzthermoanalyse (DTA) ermittelt. Die über die Ozawa Gleichung bestimmten Avrami Parameter (n) lassen sich für eine genaue Bestimmung der Kristallisationsmechanismen und Kristallisationstendenzen der $Ba_{1-x}Sr_xZn_2Si_2O_7$ Phase nutzen. Hierdurch ist es möglich, klar zwischen Oberflächen- (n=1), kombinierter Oberflächen- und Volumen- (n=2) und Volumenkristallisation (n=3) zu unterscheiden. Das hilft, den Einfluss von Keimbildnern und ihrer Konzentrationen schneller einzuschätzen, was zum Beispiel für verschiedene ZrO_2 Konzentrationen sehr gut gezeigt werden konnte. Analog wurden die mittels Kissinger

Gleichung, Ozawa Gleichung und modifizierter Kissinger Gleichung berechneten Aktivierungsenergien verglichen.

Im ersten Schritt wurden ZrO_2 und ZrO_2/TiO_2 zum Grundglas hinzugefügt, da sie in anderen Glassystemen mit niedriger thermischer Dehnung wie Lithiumalumosilicaten als effektive Keimbildner bekannt sind. Im hier untersuchten System bewirken diese Stoffe allerdings keine hinreichende Keimbildung und Volumenkristallisation tritt erst bei hohen Konzentrationen: 6 mol% ZrO_2 oder einer Kombination von 7 mol% ZrO_2 und 1 mol% TiO_2 ein. Auch in diesem Fall ist jedoch die Oberflächenkristallisation der dominante. Kristallisationsmechanismus und die Anzahl der Volumenkristalle ist zu klein um durch die Anisotropie der kristallinen Phase induzierte Risse zu verhindern.

Im zweiten Schritt wurden Edelmetalle hinzugefügt, was zu einer deutlichen Verbesserung der Anzahl und Größe der Kristalle im Volumen führte. Selbst kleine Mengen Pt wie 10 ppm können schon Volumenkristallisation bewirken. Dies wurde über die Avrami Parameter vorhergesagt und mittels Raster Elektronen Mikroskopie (REM) bestätigt. Die Pt Konzentration erlaubt die Anzahl und Größe der Kristalle einzustellen. Dies kann damit erklärt werden, dass beim Abkühlen metallische Pt Partikel im Glas bilden und durch einen Reduktionsprozess beeinflusst werden. Die Zugabe von Sb_2O_3 kombiniert mit Pt verändert den Reduktionsprozess im Glas und führt zur Entstehung von oxidierten Pt Spezies bei hohen Temperaturen. Dies erlaubte zum ersten Mal, die Volumenkristallisation der $Ba_{1-x}Sr_xZn_2Si_2O_7$ Phase zu kontrollieren. In den ersten 24 Stunden der Temperaturbehandlung steigt die Anzahl der Kristalle, danach nimmt sie wieder ab. Die Morphologie aller in Rahmen der Arbeit hergestellten Glaskeramiken wurde mittels REM und Elektronenrückstreubeugung (ESBD) untersucht. In diesen Untersuchungen zeigte sich eine starke Korrelation zwischen kristallographischer Richtung und Rissbildung der kristallinen Phase and der starken Anisotropie des thermischen Ausdehnungskoeffizienten. Die Risse verlaufen senkrecht zur C-

Achse, welche den höchsten thermische Ausdehnungskoeffizienten besitzt und daher am stärksten beim Abkühlen kontrahiert, während sich die b-Achse ausdehnt und die a-Achse nur leicht kontrahiert.

Publications:

On the dissertation topic

1. **L. Vladislavova**, C. Thieme, C. Rüssel, The effect of ZrO_2 on the crystallization of a glass in the system BaO/SrO/ZnO/SiO_2: surface versus bulk crystallization, J. Mater. Sci. 52 (2017) 4052-4060.

2. **L. Vladislavova**, C. Thieme, T. Zscheckel, C. Patzig, T. Höche, C. Rüssel, Heterogeneous nucleation of $Ba_{1-x}Sr_xZn_2Si_2O_7$ from a BaO/SrO/ZnO/SiO_2 glass using platinum as nucleation agent, J. Eur. Ceram. Soc.37 (2017) 4801-4808

3. M. Kracker, **L. Vladislavova**, C. Thieme, T. Zscheckel, K. Thieme, T. Höche, C. Rüssel, Surface crystallization of low thermal expansion $Ba_{0.5}Sr_{0.5}Zn_2Si_2O_7$ from an 8 BaO·8 SrO·34 ZnO·50 SiO_2 glass, RSC Adv. 7 (2017) 44834–44842.

4. **L. Vladislavova**, C. Thieme, T. Zscheckel, C. Patzig, T. Höche, C. Rüssel, BaO/SrO/ZnO/SiO_2 Glass System: Influence of Different Nucleation Agents: Bulk Versus Surface Crystallisation, NATO Science for Peace and Security Series - B: Physics and Biology, Volume Advanced Nanotechnologies for Detection and Defense against CBRN Agents Springer-Verlag, (2018) 361-366

5. **L. Vladislavova**, M. Kracker, T. Zschecke, C. Thieme and C. Rüssel, The effect of different platinum concentrations as nucleation agent in the BaO/SrO/ZnO/SiO_2 glass system, J. Mater. Sci. 53 (2018) 11204-11215

6. **L. Vladislavova**, M. Kracker, T. Zscheckel, C. Thieme, C. Rüssel, Crystallisation of $Ba_{1-x}Sr_xZn_2Si_2O_7$ from BaO/SrO/ZnO/SiO_2 glass with different ZrO_2 and TiO_2 concentrations, Solid State Sci.78 (2018)- 107-115

7. **L. Vladislavova**, C. Thieme, T. Zscheckel, T. Höche, and C. Rüssel, Crystallization of $Ba_{1-x}SrxZn_2Si_2O_7$ from the BaO/SrO/ZnO/SiO_2 Glass System: Effect of Platinum and Sb_2O_3 on Nucleation, Ceram Int - submitted

---

8. R. Harizanova, **L.Vladislavova**, C. Bocker, G. Avdeev, C. Rüssel, Sr-Substituted Barium Titanate Glass Ceramics from Oxide Glasses As Potential Material for Sensor Preparation, NATO Science for Peace and Security Series - B: Physics and Biology, Volume Advanced Nanotechnologies for Detection and Defense against CBRN Agents Springer-Verlag, (2018) 349-359

9. R. Harizanova, M. Abrashevb I. Avramova, **L. Vladislavova**, C. Bocker, G. Tsutsumanova, G. Avdeeve, C. Rüssel, Phase composition identification and microstructure of $BaTiO_3$-containing sodium-aluminoborosilicate glass-ceramics, Solid State Sci. 52 (2016) 49–56.

10. R. Harizanova, A. Mazhdrakova, **L. Vladislavova**, C. Bocker, G. Avdeev, G. Tsutsumanova, I. Gugov, C. Rüssel, Crystallization behaviour of the systems

$Na_2O/BaO/TiO_2/SiO_2/B_2O_3/Al_2O_3$ and $Na_2O/BaO/TiO_2/SiO_2/B_2O_3/Fe_2O_3/Al_2O_3$, J. Chem. Tech. Metall. 50 (2015) 375-380

11**. L. Vladislavova**, R. Harizanova, C. Bocker, G. Avdeev, G. Tsutsumanova, I. Gugov, C. Rüssel, $BaTiO_3$-Based Glass-Ceramics: Microstructure and Phase Composition, NATO Science for Peace and Security Series A: Chemistry and Biology (2014) 381-386.

12. R. Harizanova, **L. Vladislavova**, C. Bocker, C. Rüssel, I. Gugov, Phase composition and microstructure of sodium-alumoborosilicate glasses and glass-ceramics in the system $Na_2O/BaO/TiO_2/Al_2O_3/B_2O_3/SiO_2/Fe_2O_3$, Bulg. Chem. Comm.46 (2014) 56 – 61.

13. R. Harizanova, **L. Vladislavova**, A. Mazhdrakova C. Bocker, G. Avdeev, G. Tsutsumanova, I. Gugov, C. Rüssel, Crystallization of Barium Titanate in oxide glasses, Advances in Natural Science: Theory and Applications 3 (2014) 21-27.

14 R. Harizanova, A. Mazhdrakova, **L. Vladislavova**, C. Bocker, G. Avdeev, M. Abrashev, I. Gugov, C. Rüssel, Synthesis of nano- and submicron-sized crystals for the preparation of oxide glass-ceramics with advanced magnetic and dielectric properties, NATO Science for Peace and Security Series - A: Chemistry and Biology, Volume: Nanoscience advances in CBRN agents detection, Information and energy security, Eds.: P. Petkov, Dumitru Tsiulyanu, Wilhelm Kulisch, Cyril Popov, Springer-Verlag, 2014, 359-369

15. **L. Vladislavova**, R. Harizanova, S. Vasilev, I. Gugov, Synthesis, Phase composition and microstructure of glasses and glass-ceramics in the system $Na_2O/BaO/TiO_2/B_2O_3/SiO_2/Fe_2O_3$, Advances in Natural Science: Theory and Applications 1 (2012) 89-94.

Presentation and posters

L. Vladislavova, R. Harizanova, I. Gugov, Microstructure and magnetic properties of silicate glasses containing (Fe, Mn)-based nanocrystals, VIII Scientific poster session, UCTM Sofia, Bulgaria 18.05.2011 – **Poster**

L. Vladislavova, R. Harizanova, S. Vasilev, I. Gugov Inverse sodium-borate glasses with high concentrations of alkaline earth and 3d-transition metal oxides: Phase formation and microstructure, Third National Crystallographic Symposium, October 3–5, 2011, Sofia, Bulgaria – **Poster**

L. Vladislavova, R. Harizanova, S. Vasilev, I. Gugov, Synthesis, phase composition and microstructure of glasses and glass-ceramics in the system $Na_2O/BaO/TiO_2/B_2O_3/SiO_2/Fe_2O_3$, International Workshop on Oxide and Non-oxide Materials for Optoelectronics, 21-22.12.2012, Sofia – **Poster**

L. Vladislavova, R. Harizanova, S. Vasilev, I. Gugov, Glasses and glass-ceramics in the system $Na_2O/BaO/TiO_2/B_2O_3/Fe_2O_3$: phase formation and microstructure, International Workshop on Oxide and Non-oxide Materials for Optoelectronics, 21-22.12.2012, Sofia – **Poster**

L. Vladislavova, R. Harizanova, I. Gugov, Crystallisation of barium titanate in inverse sodium-alumo-borosilicate glasses, IX Scientific poster session, UCTM Sofia, Bulgaria, 18.05 2012. – **Poster**

R. Harizanova, **L. Vladislavova**, I. Gugov, S. Vasilev, Crystallization behaviour and microstructure of the glass-ceramics from the system $Na_2O/TiO_2/BaO/B_2O_3/Fe_2O_3$, XXII Congress of Chemists and Technologists of Macedonia, Ohrid, 5-9 September 2012- **Poster**

R. Harizanova, **L.Vladislavova**, C. Bocker, G. Avdeev, C. Rüssel, I. Gugov, Crystallization and dielectric properties of barium titanate precipitated in inverse sodium-aluminoborosilicate glasses whit high concentration of iron oxide, 5th Szeged International Workshop on Advances in Nanoscience 2012 (SIWAN5), 24–27th October, 2012, Szeged, Hungary – **Poster**

L. Vladislavova, R. Harizanova, G. Avdeev, I. Gugov – Crystallization of barium titanate in inverse sodium-alumoborosilicate glasses with high concentration of 3d-transition metals, IV'NCS, November 1–3, 2012, Sofia, Bulgaria– **Poster**

L. Vladislavova, L. Reehten, J. Slowik, R. Harizanova, C. Bocker, G. Avdeev, C. Rüssel and I. Gugov, Crystallization of barium titanate in sodium-aluminoborosilicate invert glasses, X Scientific poster session, UCTM Sofia, Bulgaria May 2013, Sofia, Bulgaria - **Poster**

L. Vladislavova, J. Slowik, L. Reehten, R. Harizanova, C. Bocker, G. Avdeev, C. Rüssel and I. Gugov, Dielectric Properties of Barium Titanate Crystallized in Invert Sodium-aluminosilicate Glass, Anniversary Scientific Conference with International Participation "60 Years UCTM", 3-6.06.2013, UCTM Sofia, Bulgaria -**Poster**

R. Harizanova, **L. Vladislavova**, C. Bocker, G. Avdeev, I. Gugov and C. Rüssel, Synthesis and Crystal growth of $BaTiO_3$ obtained in sodium-aluminoborosilicate glasses, 15th International Conference for Nanotechnology, 21-23.11.2013, TU-Sofia, Bulgaria – **Poster**

R. Harizanova, **L.Vladislavova**, A. Mazhdrakova, C. Bocker, G. Avdeev, G. Tsutsumanova, I. Gugov, C. Rüssel, Crystallization of $BaTiO_3$ in oxide glasses, ICONMO2, 19-22.12.2013, Borovets, Bulgaria – **Poster**.

L. Vladislavova, R. Harizanova, C. Bocker, G. Avdeev, M. Abrashev, I. Gugov, C. Rüssel, Synthesis and microstructure of oxide glasses, glass-ceramics with applications in electronics, VII - Spring Seminar PhD students and young scientists from Bulgarian Academy of Sciences "Interdisciplinary chemistry" 25-27 April 2014, Vitosha Mountain, Bulgaria - **Talk**

L. Vladislavova, R. Harizanova, C. Bocker, G. Avdeev, G. Tsutsumanova, I. Gugov, C. Rüssel, $BaTiO_3$-based glass-ceramics: microstructure and phase composition - International Workshop "Nanoscience Advances in CBRN Agents Detection, Information and Energy Security", 29.05-05.06.2014, Sozopol, Bulgaria- **Elevator speech and poster**

L. Vladislavova, R. Harizanova, C. Bocker, G. Avdeev, M. Abrashev, I. Gugov, C. Rüssel, $BaTiO_3$ crystallization from multicomponent oxide glasses - phase composition and microstructure investigation, Vth National Crystallographic Symposium NCS2014, 25-27.09.2014 Sofia, Bulgaria – **Poster**

L. Vladislavova, C. Thieme, C. Rüssel, and Crystallization of glasses in the system $BaO/SrO/ZnO/SiO_2/ZrO_2/TiO_2$ Thüringer Werkstofftag 2016, 06.04.2016 Ilmenau, Germany- **Poster**

L. Vladislavova, C. Thieme, C. Rüssel, Surface and internal crystallization in glass ceramics with a low thermal expansion phase, VIth National Crystallographic Symposium 2016, 05-07.10.2016 Sofia, Bulgaria - **Talk.**

L. Vladislavova, C. Thieme, T. Zscheckel, C. Rüssel, Volume crystallization of the low thermal expansion phase $Ba_{1-x}Sr_xZn_2Si_2O_7$ from glasses in the system $BaO/SrO/ZnO/SiO_2$, Thüringen Werkstofftag 2017, 30.03.2017 Jena, Germany- **Elevator speech and poster**

L. Vladislavova, C. Thieme, C. Rüssel, Influence of different platinum concentrations in the $BaO/SrO/ZnO/SiO_2$ glass system, 12th International Symposium on Crystallization in Glasses and Liquids, 10-12.09.2017 Segovia, Spain - **Poster**

L. Vladislavova, C. Thieme, T. Zscheckel, C. Patzig, T. Höche, C. Rüssel, $BaO/SrO/ZnO/SiO_2$ glass system: Influence of different nucleation agent: bulk versus surface crystallization, Advanced Technologies for Detection and Defence Against CBRN Agents, 12-20.09.2017, Sozopol, Bulgaria – **Talk**

L. Vladislavova, C. Thieme, C. Rüssel, Differences in the crystallization behaviour of the $Ba_{0.6}Sr_{0.4}Zn_2Si_2O_7$ phase in the presence of oxides and noble metals, International Autumn

School on Fundamental and Electron Crystallography, 08-13.10.2017 Sofia, Bulgaria – **Participant and poster**.

L. Vladislavova, M. Kracker, T. Zscheckel, C. Thieme, C. Rüssel, Influence of different ZrO_2 and TiO_2 concentrations as a nucleation agents in the $BaO/SrO/ZnO/SiO_2$ glass system, Thüringen Werkstofftag 2018, 16.03.2018 Weimar, Germany- **Elevator pitch and poster**

Curriculum Vitae

Personal Information

Name: Liliya Vladislavova

Date of birth: 15.08.1990

Place of birth: Sofia

E-Mail: Vladislavova_l@abv.bg

Academic Career

10/2017	International Autumn School on Fundamental and Electron Crystallography
09/2015 - 10/2015	International School on Introduction in the Rietveld Structure Refinement, Sofia
Since 09/2015	**Ph.D. student** at the Otto-Schott-Institute of Materials Research, Friedrich-Schiller-University Jena, Germany with the topic" Nucleation agents in the glass system $BaO/SrO/ZnO/SiO_2$"
10/2013 – 07/2015	Master's thesis at the University of chemical technology and metallurgy – Sofia, Bulgaria with the topic" Microstructure and phase formation in compound sodium-aluminoborosilicate glasses"
09/2009 – 09/2013	Bachelor's thesis at the University of chemical technology and metallurgy – Sofia, Bulgaria with the topic" Синтез и микроструктура на оксидни стъкла и стъклокерамики с приложение в електрониката"
09/2017	Pro Chance 2017 Grant "12th International Symposium on Crystallization in Glasses and Liquids", Spain

02/2015 – 05/ 2015	**Erasmus grants**
06/2013 – 08/2013	at the Otto-Schott-Institute of Materials Research, Friedrich-Schiller-University Jena, German
07/2012 – 09/2012	
11/2013 – 12/2013	Industrial Internship at Weiss Profil in the field of PVC and Aluminium Systems Solutions
Since 09/2015	Studies of Materials Science at the Friedrich-Schiller-University Jena, Germany
10/2013 - 07/2015	Studies of Materials Science at the University of chemical technology and metallurgy – Sofia, Bulgaria
09/2009 – 09/2013	Studies of Chemical engineering at the University of chemical technology and metallurgy – Sofia, Bulgaria

School

09/2005 – 05/2009	Academician Nikola Obreshkov – Sofia, Bulgaria
09/1997 – 07/2001	Tsar Simeon I – Sofia, Bulgaria

Jena, 05.07.2018 /Liliya Vladislavova/

Acknowledgements

Firstly, I would like to express my sincere gratitude to my advisor Prof. Christian Rüssel for the continuous support of my PhD for his patience, motivation, and advises. His guidance helped me in the time of research and writing of this thesis.

Besides my advisor, I would like to thank my colleagues Otto Schott Institute of Materials Research (OSIM) at the Friedrich Schiller University of Jena for their insightful comments and encouragement, but also for the hard question which provokes me to widen my research from various perspectives. To Dr. Chistian Thieme and Dr.Tilman Zscheckel for the help during the preparation of the manuscripts. I also would like to say special thank you to my colleagues and friends Guilherme Nunes Braga Maurício de Macedo, Dr. Caio Barca Bragatto and Dr. Bruno Poletto Rodrigues, which push me to be better not only as a scientist but also as a person. I also want to express my gradated to Mr. Thomas Kittel for the light microscopy study and to Mrs. Gabriele Möller und Mr. Rainer Weiß for the preparation of the samples.

I would also like to express my gratitude to Prof. Thomas. Höche and Dr. Chistian Patzig from Fraunhofer Institute for Microstructure of Materials and Systems in Halle.

My sincere thanks also go to Prof. Ruzha Harizanova, not only for the support and guidance during my Bachelor and Master thesis but also for risking with me and introducing to the science world. I am extremely grateful for all the discussion and advises with I resaved during the years and the years to come. I also would like to say thank you to all members of the Department of Physics at University of Chemical Technology and Metallurgy.

I want to also thanks to my family and friends from Germany and Bulgaria for their support and patience which kept me going. To my friend Ina Ivanova, Silvia Lazova and my cousin Simeon Todorov for always being there for me, to Dr. Marek Patschger and Prof. Ruzha

Harizanova for believing in me and talking me out of quitting my PhD and going back home and to Jannik Trapp for the German translation and his support.

Специални Благодарности за баща ми Венцислав Владиславов и сестра ми Милена Владиславова благодаря Ви за всичко което сте направили за мен.

Erklärung zu den Eigenanteilen und Zweitpublikationsrechten

Für alle in dieser kumulativen Dissertation verwendeten Manuskripte liegen die notwendigen Genehmigungen der Verlage (”Reprint permissions“) für die Zweitpublikation vor. Die Koautoren der in dieser kumulativen Dissertation verwendeten Manuskripte sind sowohl über die Nutzung, als auch über die angegebenen Eigenanteile der weiteren Doktoranden/Doktorandinnen als Koautoren an den Publikationen und Zweitpublikationsrechten bei einer kumulativen Dissertation informiert und stimmen dem zu.

Jena, 05.07.2018 Liliya Vladislavova

Ich bin mit der Abfassung der Dissertation als publikationsbasiert, d. h. kumulativ, einverstanden und bestätige die vorstehenden Angaben. Eine entsprechend begründete Befürwortung mit Angabe des wissenschaftlichen Anteils des Doktoranden an den verwendeten Publikationen werde ich parallel an den Rat der Chemisch-Geowissenschaftlichen Fakultät richten.

Jena, 05.07.18 Prof. Christian Rüssel

Selbstständigkeitserklärung

Ich erkläre, dass ich die vorliegende Arbeit selbstständig und unter Verwendung der angegebenen Hilfsmittel, persönlichen Mitteilungen und Quellen angefertigt habe.

Jena, 05.07.18 Liliya Vladislavova